



Tobias Thaler, BSc

Design of a facility for testing evaporator concepts for compact heat exchangers

Master Thesis

to achieve the degree of a

“Diplom-Ingenieur“

Master program Process Engineering

submitted at the

Graz University of Technology

Supervisor:

Ao. Univ.-Prof.i.R. Dipl.-Ing. Dr.techn. Hans Schnitzer

Institute of Process and Particle Engineering

Bao Nam Dang, MSc

AEE INTEC

Graz, September 2016

English version:

STATUTORY DECLARATION

I declare that I have authored this thesis independently, that I have not used other than the declared sources / resources, and that I have explicitly marked all material which has been quoted either literally or by content from the used sources. The text document uploaded in the TUGRAZonline is identically to the Master Thesis in its present form.

Graz, 16th of September 2016



.....

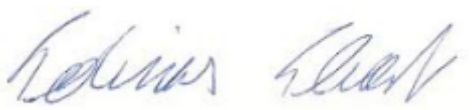
Tobias Thaler, BSc

German Version:

EIDESSTÄTTLICHE ERKLÄRUNG

Ich erkläre an Eides statt, dass ich die vorliegende Arbeit selbstständig verfasst, andere als die angegebenen Quellen/Hilfsmittel nicht benutzt, und die den benutzten Quellen wörtlich und inhaltlich entnommenen Stellen als solche kenntlich gemacht habe. Das in TUGRAZonline hochgeladene Textdokument ist mit der vorliegenden Masterarbeit identisch.

Graz, am 16. September 2016



.....

Tobias Thaler, BSc

Acknowledgement

At this point I would like to thank all those who supported and motivated me during the preparation of this thesis.

First, my thanks go to Hans Schnitzer and Bao Nam Dang, who supervised and inspected my Master's thesis. For helpful suggestions and constructive criticism in the preparation of this work I would like to thank them especially.

I would also like to thank the employees of AEE INTEC and especially Waldemar Wagner and Reinhard Pertschy who helped me with a lot of patience, interest and helpfulness. I would like to thank for the numerous interesting debates and ideas that have made a major contribution to this thesis.

A special thanks to my friends Christoph Rohringer, Bernhard Maunz and Aaron Woblistin for who I am particularly grateful for the strong emotional support over the duration of my entire studies.

Finally, I would like to thank my family and my girlfriend Anja Nigsch, which not only made my study possible additionally they have been with me whenever I have needed them.

Master Thesis
of
Tobias Thaler BSc

Task:

The EU funded project CREATE has the goal to develop and to demonstrate an innovative sorption heat exchanger. One of the key components in this facility is the evaporator/condenser. Sorption heat exchangers are operated at low pressure conditions at about 20 mbar. As there has not been much research in the field of evaporation/condensing for low pressure systems it is hard to predict their behavior.

The task in this Master Thesis is to derive the design and further on construct of a test facility so that evaporation/condensing processes with water at low pressure conditions can be investigated.

Abstract

This master thesis describes the process of development of a test rig for evaporation at low pressure conditions from the designing till the evaluation of the first tests. Based on the theoretical foundations derived in this thesis the design and the dimensions were evaluated and implemented in a CAD program. The model of the CAD program has been used as a basis for the orders of all the consisting parts. After the test rig has been built and taken into operation the automation protocol was implemented to run tests by dictated conditions. In the end several tests have been performed to proof the functionality of this facility. At last the tests performed within this master thesis were compared to the theoretical approach used to define the dimensions of this facility.

Zusammenfassung

Diese Masterarbeit beschreibt den Prozess der Entwicklung eines Teststands für Verdampfung unter Niederdruckbedingungen ausgehend vom Design bis hin zur ersten Testreihe nach der Inbetriebnahme. Basierend auf theoretischen Grundlagen wurde das Design entwickelt, die Dimensionen abgeleitet und in ein CAD Programm übernommen. Das CAD Programm lieferte die Grundlage für die Bestellung der einzelnen Komponenten. Nachdem der Teststand aufgebaut und in Betrieb genommen worden ist, wurde ein Automatisierungsprotokoll geschrieben welches es ermöglicht verschieden Testbedingungen kontrolliert zu untersuchen. Am Schluss wurden einige Tests durchgeführt welche mit dem Theoretischen Modell zur Dimensionierung der Anlage verglichen worden sind.

Content

| | | |
|-------|---|----|
| 1 | Introduction | 1 |
| 1.1 | Problem definition | 2 |
| 1.2 | Research issue and objective | 4 |
| 1.3 | Structure | 4 |
| 2 | Theoretical foundations of evaporation/condensing | 5 |
| 2.1 | Evaporation..... | 5 |
| 2.1.1 | Pool boiling..... | 5 |
| 2.1.2 | Capillary evaporation | 8 |
| 2.1.3 | Falling film evaporation | 10 |
| 2.1.4 | Previous Works | 14 |
| 3 | Concept and design | 15 |
| 3.1 | Evaluation method | 15 |
| 3.2 | Heat transfer | 16 |
| 3.2.1 | Outer heat transfer coefficient α_o | 16 |
| 3.2.2 | Inner heat transfer coefficient α_i | 18 |
| 3.3 | Design..... | 20 |
| 3.3.1 | Main chamber | 22 |
| 3.3.2 | Reservoir..... | 26 |
| 3.3.3 | Plate heat exchanger | 31 |
| 3.3.4 | Hot and cold water supply line | 32 |
| 3.3.5 | Heat loss calculation for insulation | 33 |
| 3.3.6 | Measurement and Control..... | 34 |
| 3.4 | Construction of the test rig | 43 |
| 3.5 | Design for testing Condensing..... | 44 |
| 4 | Commissioning..... | 45 |
| 4.1 | Level Measurement calibration | 45 |
| 4.2 | Leakage | 46 |
| 5 | Experimental procedure | 48 |
| 5.1 | Preparations | 48 |
| 5.2 | Dependencies of the variables among each other | 48 |
| 5.3 | Automation..... | 51 |
| 5.4 | Evaluation | 53 |
| 6 | Experimental results..... | 55 |
| 6.1 | Tube bundle and distributor | 55 |
| 6.2 | Falling film evaporation | 56 |
| 6.2.1 | First test to declare the proper function of the test rig | 56 |

| | | |
|-------|--|----|
| 6.2.2 | Test series..... | 63 |
| 6.3 | Evaluation..... | 70 |
| 6.4 | Comparison of the theoretical calculation to the experiment..... | 72 |
| 7 | Summary..... | 76 |
| 8 | Appendix..... | 77 |
| 8.1 | Measurement and control..... | 77 |
| 8.1.1 | Sensors..... | 77 |
| 8.1.2 | Valves..... | 78 |
| 8.1.3 | Level Indicator and mass balance..... | 78 |
| 8.1.4 | Heat meter..... | 79 |
| 8.1.5 | Splitter..... | 79 |
| 8.1.6 | Pump..... | 80 |
| 8.2 | Symbol directory..... | 81 |
| 8.3 | List of Equations..... | 83 |
| 8.3.1 | Heat loss calculation..... | 83 |
| 8.3.2 | Pump calculation..... | 84 |
| 8.4 | Allocation of the variables to determine the performance..... | 85 |
| 8.5 | Illustrations of the several test rig components..... | 86 |
| 8.6 | Dimensioning of the tube bundle..... | 89 |
| 8.7 | Comparison of the theoretical calculations to the experimental evaluated tests | 90 |
| 8.8 | Image Index..... | 91 |
| 8.9 | List of Tables..... | 93 |
| 8.10 | Bibliography..... | 94 |

1 Introduction

Solar thermal energy is an upcoming technology and its storage has gotten more important over the past few years. A widely known storage concept is water which is heated up by solar radiation preferably in the summer and afterwards used in the winter where the energy is needed. The downside of such a system is the low energy density of water (60 kWh/m^3) that would claim a huge amount of space to satisfy the required energy demand. Furthermore such systems have a relative high heat loss over time. [1]

An innovative new concept to store energy is called the closed sorption heat storage. The solar radiation heats a tank filled with solid particles, causing those particles to dry out. If the energy demand is required vapour has to be adsorbed by those particles to set the energy free. A big advantage of such storage systems is the high energy density (180 kWh/m^3) of those particles and the minimal heat loss compared to water storage concept. [2]

One of the key components in this closed sorption storage system is the evaporator/condenser and its task will be stated in the next chapter.

1.1 Problem definition

The main part of the closed sorption process is the fixed bed heat exchanger. It is filled with solid particles. Those particles can be dried (desorbed) to charge up by storing heat energy or humidified (adsorbed) to release the heat energy.

To desorb the particles they are heated by an external heat source, mostly delivered by solar radiation. The vapour, which is set free by desorption of the drying particles, is condensed by a low temperature source and stored in a water tank as displayed in Figure 1.

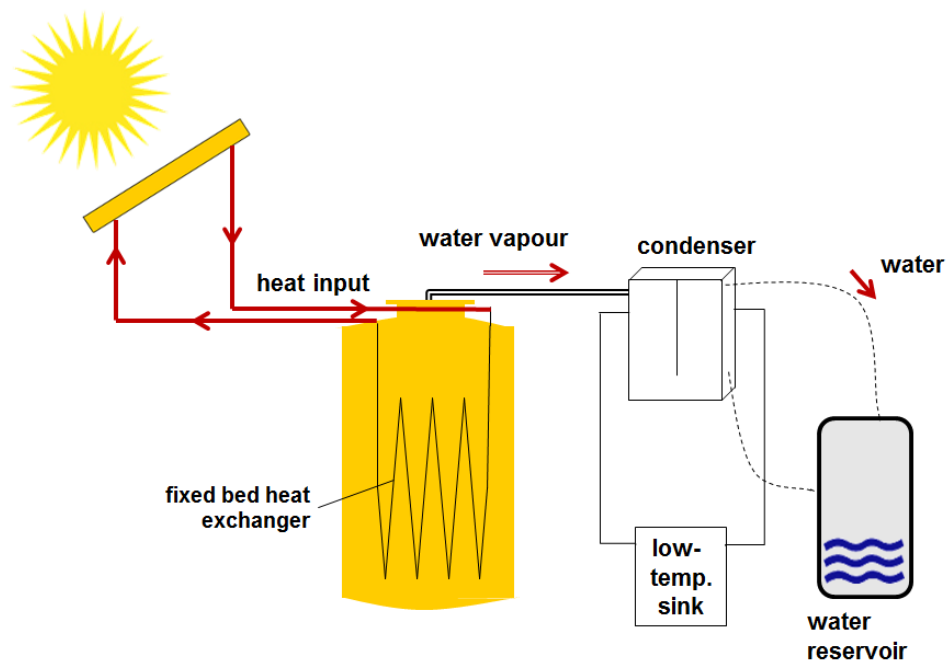


Figure 1: Desorption (charging) process of a closed sorption storage system [3]

If the energy is required the water will be evaporated by the low temperature heat source which is further on adsorbed by the particles (Figure 2).

By using low temperature heat sources, as groundwater with approximately 20 °C, to evaporate/condense the water in this facility, it has to be operated at a pressure range of about 10 – 20 mbar.

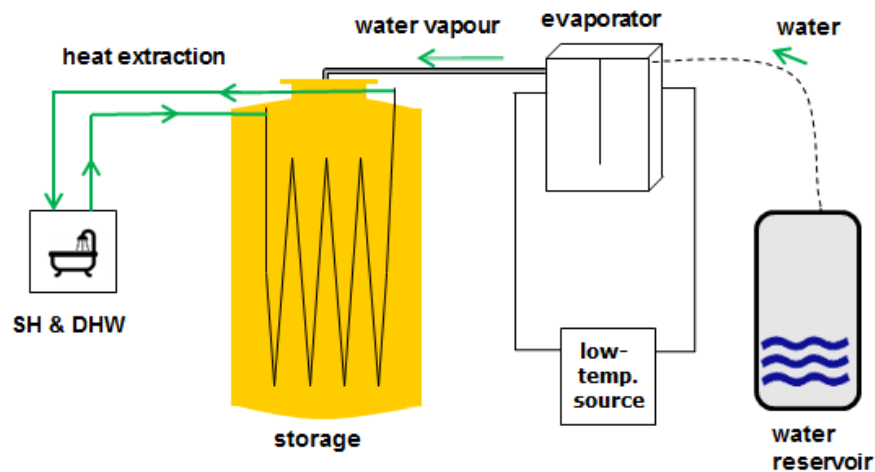


Figure 2: Adsorption (discharging) process of a closed sorption heat storage system [3]

Different concepts of sorption processes use different types of evaporators/condensers. As they were not compared with each other a huge potential is estimated by investigating this step of the sorption process.

For example the COMTES project uses a plate heat exchanger used as an evaporator/condenser [3].

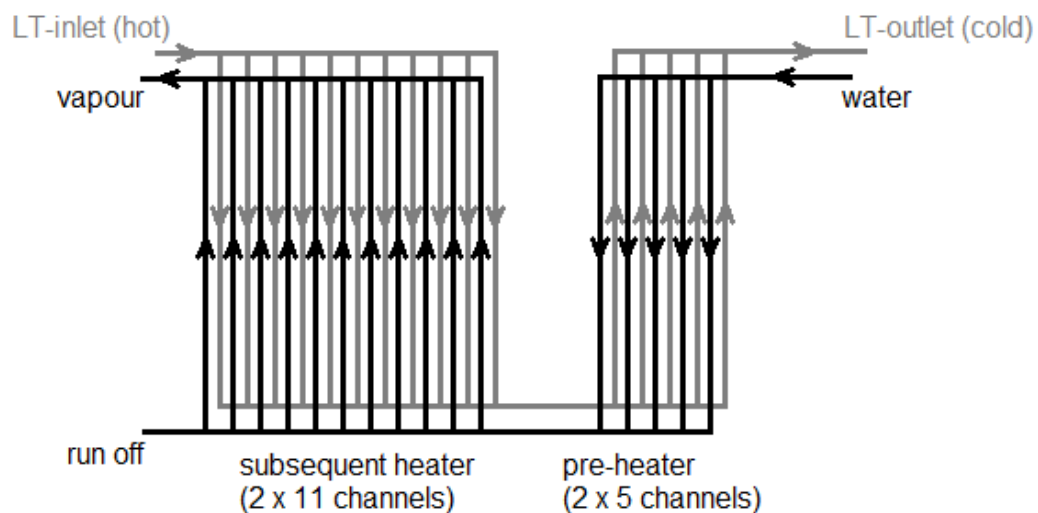


Figure 3: Scheme of evaporator and condenser [3]

A schema of the plate heat exchanger is shown in Figure 3. The liquid water enters the heat exchanger on the right side and is preheated by the low temperature heat

source and afterwards partially evaporated in the subsequent heater area. While the vapour leaves through the upper left exit the non-evaporated water leaves through the bottom left exit.

As plate heat exchangers are neither intended to evaporate nor to condense, a huge potential of improvement is estimated by changing the state of the art for this part of the facility.

1.2 Research issue and objective

The lack of knowledge to describe evaporation methods makes it hard to predict the behavior of certain conditions. There are already several researches about those processes but none of them describe the conditions of a heat sorption storage facility at 20 mbar or below.

The objective in this master thesis is to derive the design followed by the construction of a test facility so that evaporation processes with water at low pressure conditions can be investigated.

1.3 Structure

After describing promising approaches for evaporation concepts the design of the test rig is adjusted to the concept with the highest potential. The mathematical design is provided by literature and on their basis the design specification for the test chamber can be approximated. With the built test rig, several concepts can and will be investigated and afterwards evaluated and compared to each other.

2 Theoretical foundations of evaporation/condensing

Based on this chapter the further investigation of the test facility will be analyzed. This knowledge is needed to cover and understand the evaporation process in the following test facility.

2.1 Evaporation

To evaporate liquid water three concepts are appropriate for the proposed test rig. Those concepts were already investigated but not specifically for the field of interest which are at 20 mbar absolute pressure.

The concepts are pool boiling, capillary evaporation and falling film evaporation. All of them differ in their efficiency and furthermore not all of them provide a sufficient condensing. Those concepts will be explained in the following paragraphs.

2.1.1 Pool boiling

Pool boiling is performed by directly heating the liquid with a warmer surface without any interference of an external stream flow. There are several ways to design such a concept, but most of them deal with plain surfaces or tubes that are located throughout the fluid. Besides the design, the boiling regime has a huge impact on the heat flux. In Figure 4 the heat transfer coefficient and the heat flux are plotted over the temperature difference of the heating surface and the saturation temperature of the fluid. The pool boiling principle is described in Figure 4.

From the operating point "A" to be "B", displayed in Figure 4, the heat flux is transferred by free convection due to the small temperature difference from the wall to the fluid. Within this spectrum no bubbles are occurring on the wall. With increasing the wall temperature bubbles are formed on the surface. More frequent the higher the difference between the temperatures of the wall to the fluid. The bubbles promote the turbulence and therefore the transferred heat flux.

At a certain point the heat flux density decreases as too many bubbles occur on the surface while forming a vapour film between the liquid and the wall (film boiling). The heat in that case is essentially transferred by radiation. Technically film boiling jumps from C to E in order to transmit the current heat flux which increases the wall temperature from 100 °C to 900 °C (for atmospheric condition) leading to a destruction of most devices. [4]

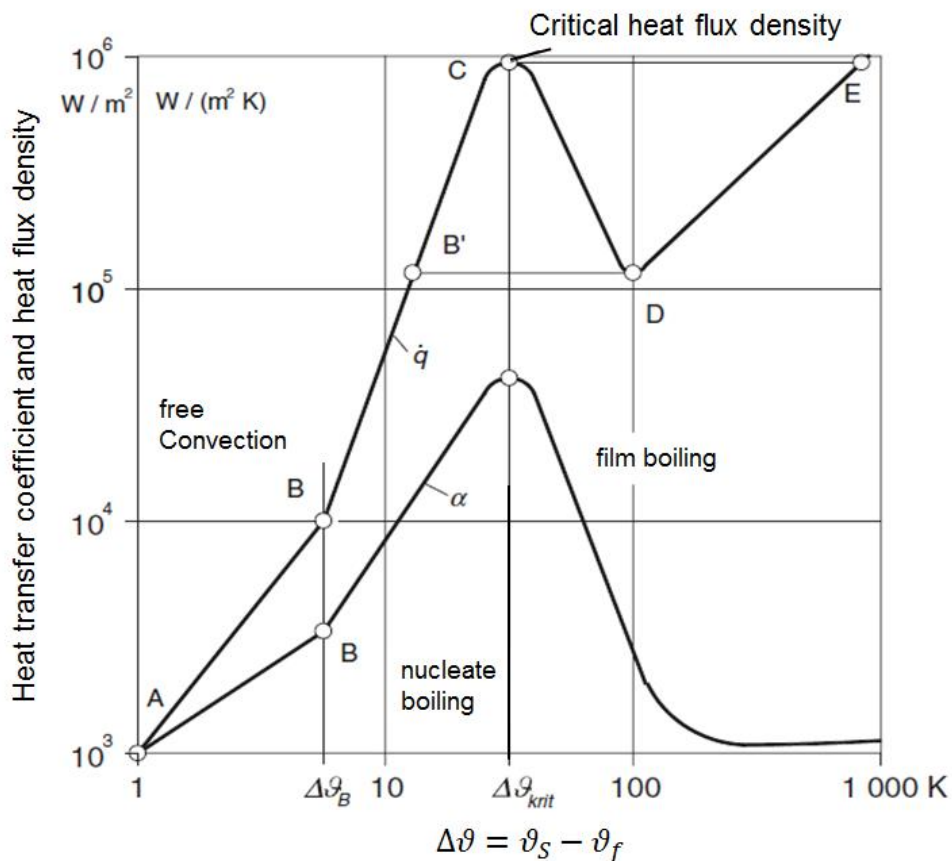


Figure 4: Evaporation heat flux of water at 1 bar pressure [4], edited by Author

While nucleate boiling provides the highest heat flux it can be improved by adjusting the height of the liquid level above the heating surface. The best effects are realized by reducing the water film above the warm surface to a minimum. An example: Increasing the liquid level by 10 mm increases the pressure by 1 mbar, which leads to a higher saturation temperature. Based on this correlation pool boiling cannot be constructed into height to save space but rather need to be built into length and width.

Further on, the heat flux can be improved by the size and ratio in which the droplets occur on the surface. F. Giraud et al [5] made an experiment which shows precisely how the bubbles form on a hot surface. Basically the lifetime of such a droplet passes as described in the following paragraph:

Gases and vapour are trapped in the micro area which infects the liquid and forms a new droplet. Therefore bubbles occur generally on the same spot. Those bubbles grow until their buoyancy and the dynamic forces overwhelm the adhesions force.

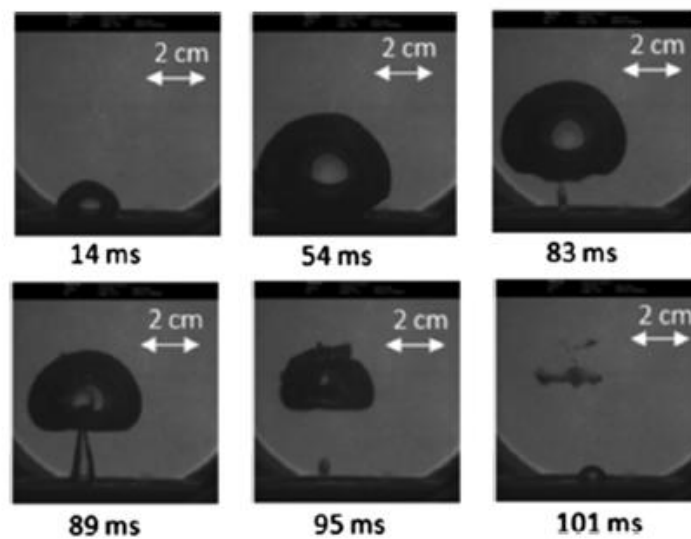


Figure 5: Bubble growth with liquid and vapor jets following the bubble departure ($P_v = 1.2 \text{ kPa}$, $T_l = 10 \text{ }^\circ\text{C}$, $h_l = 200 \text{ mm}$, $q = 22.6 \text{ W/cm}^2$). [5], edited by Author

In general the droplets appear on areas where nucleation is favored, for example in wells of the micro area where seeds can dispose. [5]

Seeds can be formed homogenous as a spontaneous growth of a vapor bubble in a metastable liquid or heterogeneous as a nucleation on particles or on entrapped in-condensable gases. [6]

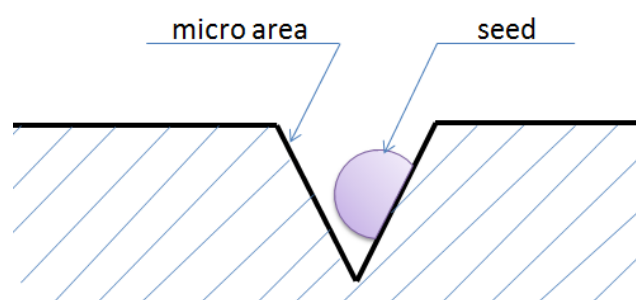


Figure 6: Example of a micro area with a seed inside

To increase the frequency and the size of the bubbles the spots where the droplets emerge has to be increased. An easy and efficient way to increase those spots is to roughen the surface so that more micro areas with seeds can support the nucleation. A better solution is by adding fins to the surface which can improve the heat flux up to five times according to M. A. Chan et al [7].

As all those improvements are already well studied there are some problems that occur by evaporating at low pressure atmospheres. The downside of low pressure evaporation is that the size of the droplets increases with the decrease of the surrounding pressure. The decrease of the surrounding pressure also causes a higher temperature difference between the wall and the fluid in order to reach the nucleate boiling regime. [6]

2.1.2 Capillary evaporation

Capillary evaporation takes place directly between the liquid and the heating surface but the dynamics causing this phase change are different compared to the pool boiling. While the solid surface emerges out of the liquid the capillary force coats the hot surface illustrated in Figure 7. The formed thin film of liquid will then be evaporated. A big advantage compared to the pool boiling is the guaranteed thin liquid film due to the capillary forces causing a higher heat flux. [8]

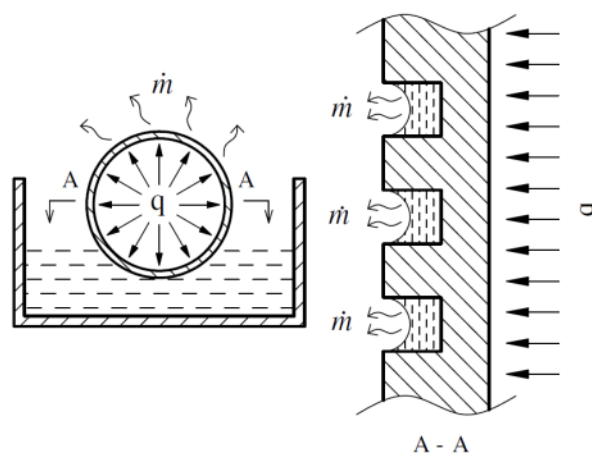


Figure 7: Capillary-assisted evaporation principle [8], edited by Author

To improve the effects of the capillary forces the layout of this concept is very important. In most of the cases where capillary evaporation was tested the layouts were either a finned tube or a lamella.

The mechanism of the capillary evaporation on a finned tube is shown in Figure 8.

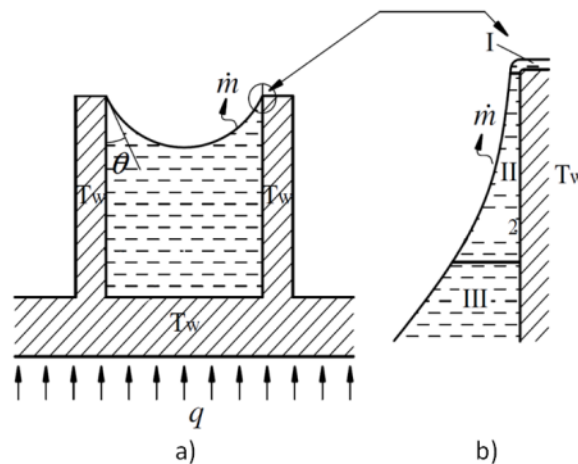


Figure 8: The schematic of capillary-assisted evaporation along a circumferential rectangular micro-groove and the extended meniscus: (a) \perp -directional cross-section, and (b) the extended meniscus. [8], simplified by Author

Due to capillary forces the liquid moves towards the apex of the groove, the liquid film becomes thinner. The extended meniscus can be classified into three sections: the non-evaporating adsorbed film section I, the evaporating thin film section II and the inner meniscus III, marked in Figure 8 [8].

- Section I

The section on the top of the apex is too thin. Therefore, the water is held in place on the wall by adsorption forces. This strongly inhibits the evaporation process.

- Section II

In section II, the liquid film is thin enough to significantly reduce the thermal resistance without being influenced by the adsorption forces. This results in very good heat transfer conditions for this area and causes the majority of the heat to be transferred there.

- Section III

The liquid film in this area is too thick to profit from the capillary force effects.

In addition to the layout the location of the tube relative to the liquid plays a major role. A study in unsteady conditions has shown that the heat flux increases with the decrease of the water surface. The highest impact on capillary evaporation was investigated while the surface was placed barely above the fluid level as seen in Figure 9. [9]

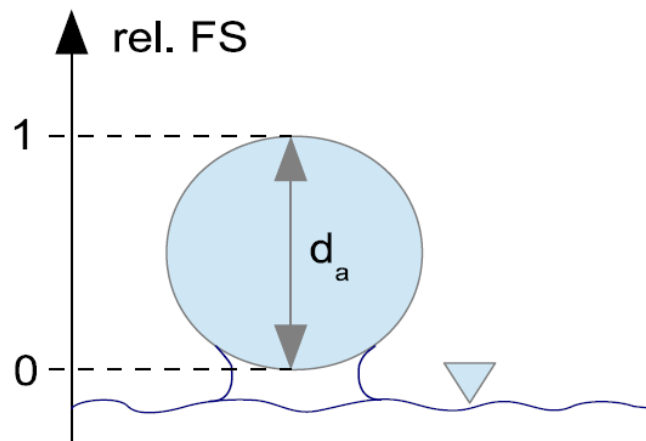


Figure 9: Wetting of a surface about the water surface [9]

The downside of this optimized liquid level is that a pump is needed to adjust the surface of the liquid while it is evaporated.

2.1.3 Falling film evaporation

On the contrary to the other concepts the falling film evaporation is based on a gravitational forced stream flow. The liquid enters on top of the facility and sprinkles downwards the heated surface. While there are many concepts of how the surface can be constructed this work will focus only on horizontal tubes.

The heat flux depends significantly on the flow type of the falling film. Therefore it is important to quantify those types. In the work of Hu X and Jacobi A.M. [10] they distinguish between six different types.

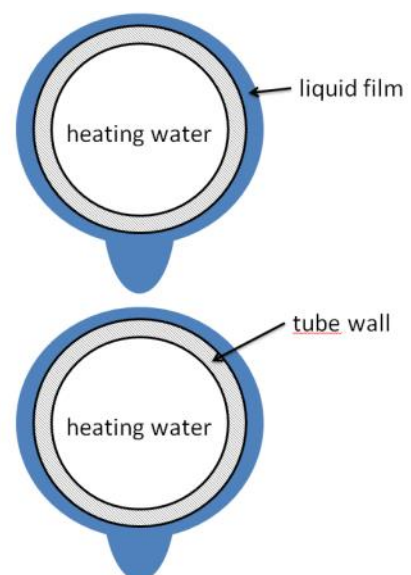


Figure 10: Falling film tube bundle

Shown in Figure 11 the falling film on horizontal tubes can occur as droplet mode, jet mode and sheet mode or as a mixture of droplet/jet and jet/sheet. The mode appearing depends on the distance between the pipes, the specific values and significantly on the volumetric flow which can be manipulated easily rather than the other parameters. In order to achieve a good heat flux the irrigation has to be optimized. The heat flux and therefore the irrigation has to be high enough to coat the whole tubes as dry surface areas lead to a lower heat transfer coefficient, but low enough to prevent the film thickness to get bigger than needed as thicker film leads to a smaller heat transfer coefficient. [11], [12].

In the following paragraphs the modes will be explained in detail:

a) Droplet mode:

The regime is in droplet mode when there are only liquid droplets distinctive between the tubes.

b) Droplet-jet mode:

This intermediate regime is designated when at least one stable jet exists additionally to the droplets. It is also possible that the jet moves sideways along the tube. As long as it is continuously stable it is called a jet.

c/d) inline-jet mode/staggered jet mode

Those two regimes differ only whether the jets are inline from tube to tube or not. Depending on the flow rate the jets appear to be offset with a higher flow rate.

e) jet-sheet mode

The intermediate regime, jet-sheet, occurs when both a jet and a continuously liquid sheet appears between two tubes. The sheet forms of two jets that merge together.

f) Sheet mode

This regime occurs when the fluid flows uniformly between the tubes as a continuous sheet.

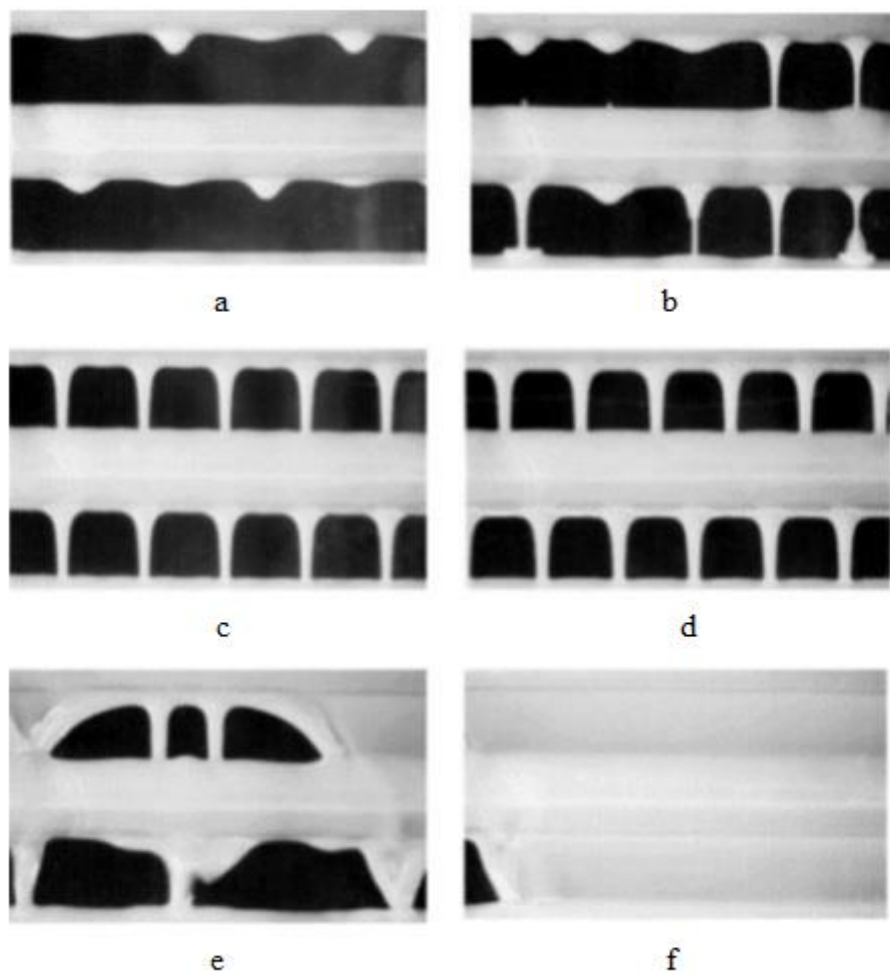


Figure 11: Falling-film flow modes: (a) droplet mode, (b) droplet-jet mode, (c) inline jet mode, (d) staggered jet mode, (e) jet-sheet mode, and (f) sheet mode [10]

The outer heat transfer coefficient can be improved by changing the pattern of the tube. Wei Li et al. [13] have tested some different shapes for cylindrical tubes (Figure 12) and compared the results to a tube with a smooth surface.

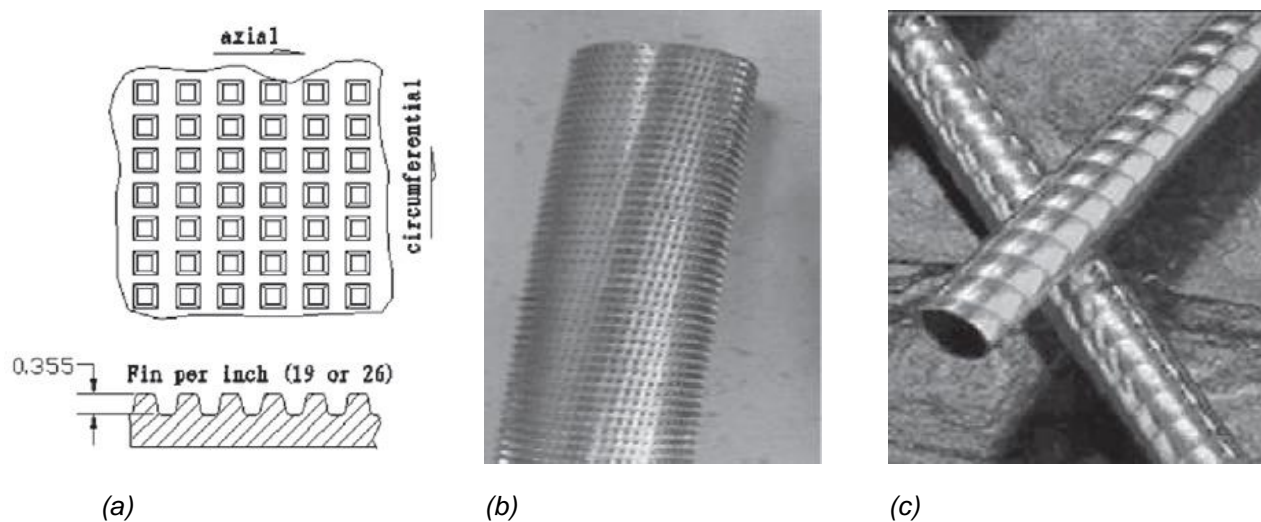


Figure 12: Experimental setup and the enhanced tubes. (a) fins on Turbo-CAB tubes, (b) Turbo-CAB-19 fpi, and (c) Korodense. [13]

The heat transfer coefficient for the CAB-26fpi¹ is about three times the heat transfer coefficient of the smooth tube, based on irrigation density of $Re_r = 40$. The improvement is caused by the pattern supporting a better moistening. Different types of patterns have a different impact due to the heat transfer coefficient as shown in Figure 13. [13]

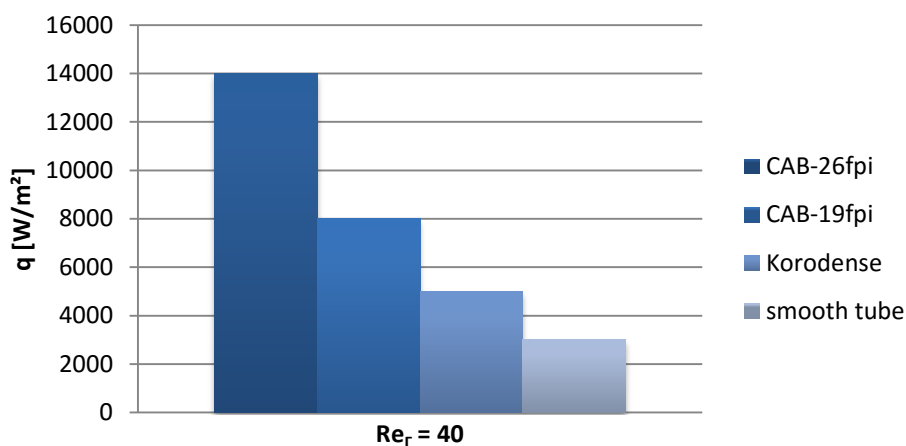


Figure 13: Heat transfer coefficients of different tube types on the basis of [13]

¹ fpi = fins per inch

2.1.4 Previous Works

Previous work has shown that pool boiling provides the lowest heat transfer coefficient within a range of 2880 to 5880 W/m²K [7] even with enhanced surfaces. Additionally, the heat transfer coefficient decreases with the decrease of the ambient pressure because of the high temperature difference needed between the heating surface and the fluid caused by the hydrostatic pressure of the liquid level. Even if the saturation temperature is smaller, the heat flux suffers not only from the temperature difference but also from the increasing bubble size at low pressure conditions.

Both the capillary evaporation and the falling film evaporation provide a better heat flux. The heat transfer coefficients for both concepts are nearly the same, while the capillary evaporation concept can reach an outer heat transfer coefficient up to 13800 W/m²K [5], the falling film evaporation concept can reach up to 14000 W/m²K [13] by taking the optimizations described in the previous chapters and the enhanced surfaces into account.

Within this thesis a test rig will be constructed capable of testing all the mentioned concepts. As the falling film evaporation requires the biggest amount of space, this test rig will be dimensioned based on the falling film concept.

3 Concept and design

The test rig shall be able to evaluate the heat flux in a multitude of variations depending on the operation conditions based on the three concepts introduced in chapter 2. Considering the following evaluation methods and the heat transfer correlations the first approximation of a total heat flux of about five kW were intended, based on the power of the plate heat exchanger in the COMTES project. Those design specifications developed in chapter 3.3.

3.1 Evaluation method

The determination of the evaporation performance is done by energy balances for either the outer stream of the falling film (FF) or the inner tube flow (TF).

Leading to the heat flux for the heating stream inside the tubes:

$$\dot{Q}_{TF} = \dot{m}_{TF} * cp_{TF} * (T_{TF,In} - T_{TF,Out}) \quad (3.1)$$

And on the other side of the tube to estimate the heat flux of the evaporated water in the falling film:

$$\dot{Q}_{FF} = \dot{m}_{FF} * \Delta h_{FF} \quad (3.2)$$

Without any losses the heat fluxes should be identical.

$$\dot{Q}_{TF} = \dot{Q}_{FF} = \dot{Q} \quad (3.3)$$

Furthermore the vapour has to be condensed before it gets circulated back into the evaporator. The equations for condensing are similar to those of evaporation, with the difference that the heat flux is negative due to the discharged heat.

While the variables of the inner tube flow can be measured easily, the evaporated falling film mass has to be measured with a liquid level sensor and additionally a mass balance in order to exclude uncertainties that could occur by one of those measurement devices. [14]

3.2 Heat transfer

The following paragraphs will deal with the theoretical approaches which were made to determinate the inner and outer heat transfer coefficient of a tube. These are necessary to approximate the heat flux for the upcoming test facility [14].

The two heat transfer coefficients can further on be combined to the heat transfer resistance.

$$k_o = \left(\frac{1}{\alpha_o} + \frac{d_o}{2 * \lambda_{tube}} * \ln\left(\frac{d_o}{d_i}\right) + \frac{d_o}{d_i * \alpha_i} \right)^{-1} \quad (3.4)$$

If the surface is given the heat flux can be calculated as followed:

$$\dot{Q} = k_o * A_o * \Delta T_{ln} \quad (3.5)$$

Note that the heat transfer resistance and the surface are based on the outer diameter. The logarithmic temperature difference is defined as:

$$\Delta T_{ln} = \frac{\Delta T_{In} - \Delta T_{Out}}{\ln \frac{\Delta T_{In}}{\Delta T_{Out}}} \quad (3.6)$$

While:

$$\Delta T_{In} = T_{TF,In} - T_{FF,Mean} ; \Delta T_{Out} = T_{TF,Out} - T_{FF,Mean} \quad (3.7)$$

3.2.1 Outer heat transfer coefficient α_o

Before investigating the different approaches the irrigation density (Re_F) has to be mentioned since all of the upcoming theories refer to this number. Additionally approaches due to the film thickness and the falling film pattern can be assumed by analyzing the irrigation number.

3.2.1.1 Irrigation Density

The irrigation Density (Re_F) is an indicator to classify the behavior of the flow in a falling film and is calculated as follows [12]:

$$Re_{\Gamma} = \frac{4 * \Gamma_{FF}}{\mu_{FF}} \quad (3.8)$$

Where Γ_{FF} is the flow rate of the liquid on one side of the tube per unit length of tube in kg/ms. Consequently, the total flow rate on both sides is two times Γ_{FF} .

$$\Gamma_{FF} = \frac{\dot{m}_{FF}}{2 * l} \quad (3.9)$$

\dot{m}_{FF} is the total mass flow that has to be divided by the columns of irrigated pipes and twice their length.

As already mentioned in 2.1.3 the irrigation has to be high enough to coat the whole tube but low enough to prevent the film becoming thicker bigger than needed. [14]

3.2.1.2 Theoretical approach by Lorenz and Yung

The theoretical approach by Lorenz and Yung explained in the Engineering Data Book III of Wolverine Tube Inc. [12] has been chosen as it combines three concepts relevant for the evaporation in a falling film regime. Those three heating modes that could appear during the falling film evaporation: a sub cooled film over the length L_{dev} , evaporation of a saturated film over the remaining length and nucleate boiling in the film over the entire perimeter. Those three combined result in the mean heat transfer coefficient.

$$\alpha_o = \alpha_{nb} + \alpha_{dev} * \frac{L_{dev}}{L} + \alpha_{lam} * \left(1 - \frac{L_{dev}}{L}\right) \quad (3.10)$$

With the lengths defined as followed:

$$L = \pi * d_o \quad (3.11)$$

$$L_{dev} = \frac{\Gamma^{\frac{4}{3}}}{4 * \pi * \rho * a} * \sqrt{\frac{3 * \mu}{g * \rho^2}} \quad (3.12)$$

α_{nb} is the nucleate boiling coefficient which was assumed to be zero due to the small impact of the nucleate boiling in the falling film compared to the others, α_{dev} is the convective film heat transfer in the thermally developing region of length L_{dev} ,

$$\alpha_{\Gamma,dev} = 0,375 * cp_l * \left(\frac{\Gamma_l}{L_{dev}} \right) \quad (3.13)$$

and α_{lam} is the convective film coefficient in the fully developed region given by the equations of Chun and Seban explained in the Engineering Data Book III of Wolverine Tube Inc [12].

$$\alpha_{\Gamma,lam} = 0,821 * \left(\frac{\mu_l^2}{g * \rho_l^2 * \lambda_l^3} \right)^{-0,33} * Re_{\Gamma}^{-0,22} \quad (3.14)$$

3.2.2 Inner heat transfer coefficient α_i

The inner heat transfer coefficient was calculated by the equation from the VDI Heat Atlas [14] and the important steps are stated below.

One dimensionless quantity on the inner heat transfer coefficient is the Reynolds number.

$$Re = \frac{v_{TF} * d_i}{\nu_{TF}} \quad (3.15)$$

v_{TF} is the velocity of the fluid stream, d_i the inner diameter and ν_{TF} the kinematic viscosity of the fluid. The Reynolds number declares the flow regime in the tube and is either laminar, turbulent or a mixture of both. The higher the Reynolds number the more unstable is the flow stream and therefore it will get more turbulent. Furthermore the Reynolds Number is connected to the Nusselt number which is a value for the heat transfer coefficient α and the known thermal conductivity λ .

$$Nu = \frac{\alpha_i * d_i}{\lambda_{TF}} \quad (3.16)$$

The empirical approaches to define the Nusselt number depend on flow regime and therefore Reynolds number and are calculated as followed:

Laminar flow: $Re \leq 2400$

$$Nu_{i,lam} = \sqrt[3]{3,66^3 + 0,664^3 * Pr * \left(Re * \frac{d_i}{l} \right)^{\frac{3}{2}}} \quad (3.17)$$

Transition Area: $2400 < Re < 10^5$

$$Nu_{i,trans} = \frac{\frac{\zeta}{8} * Re * Pr * f1 * f2}{1 + 12,7 * \sqrt{\frac{\zeta}{8}} * (Pr^{\frac{2}{3}} - 1)} \quad (3.18)$$

Turbulent flow: $10^5 \leq Re$

$$Nu_{i,turb} = \frac{\frac{\zeta}{8} * Re * Pr * f1 * f2}{1 + 12,7 * \sqrt{\frac{\zeta}{8}} * (Pr^{\frac{2}{3}} - 1)} \quad (3.19)$$

The Reynolds number was already mentioned. The Prandtl number can be calculated via the specific material values of the liquid.

$$Pr = \frac{\nu}{a} = \frac{\mu * c_p}{\lambda} \quad (3.20)$$

ζ is the friction coefficient inside the tube.

$$\zeta = [1,8 * \log(Re) - 1,5]^{-2} \quad (3.21)$$

The coefficients $f1$ and $f2$ are correction factors, to make the calculation more precise. While $f1$ considers the inner diameter in correlation to the length of the tube, $f2$ considers the specific values in the middle of the tube in correlation to the conditions at the inner wall of the tube.

$$f1 = 1 + \left(\frac{d_i}{l}\right)^{\frac{2}{3}} \quad (3.22)$$

$$f2 = \frac{Pr}{Pr_w} \quad (3.23)$$

The conditions at the inner wall depend on the temperature. To estimate the inner wall temperature the following equation can be used.

$$\vartheta_{Wi} = \vartheta_{mean,i} - \frac{k * d_o}{\alpha_i * d_i} * \Delta\vartheta_{mean} \quad (3.24)$$

This step is iterative as it consists of the inner heat transfer coefficient. $\Delta\vartheta_m$ is the logarithmic mean temperature. [14]

3.3 Design

The schematic representation of the test rig is shown in Figure 14. This design consists of a main chamber in which the different evaporation concepts can be integrated. The evaporated water condenses in a plate heat exchanger. Both the vessel and the plate heat exchanger are connected to a water circuit. A hot water circuit for the evaporation side in the main chamber and a cold water circuit for the condensing side of the plate heat exchanger. Below the main chamber and the condenser are the reservoirs for the evaporated water. They will be also used for determining the heat evaporation performance during the experiments (by measuring the water volume and weight). The water tank is used to store the water while the test rig is evacuated.

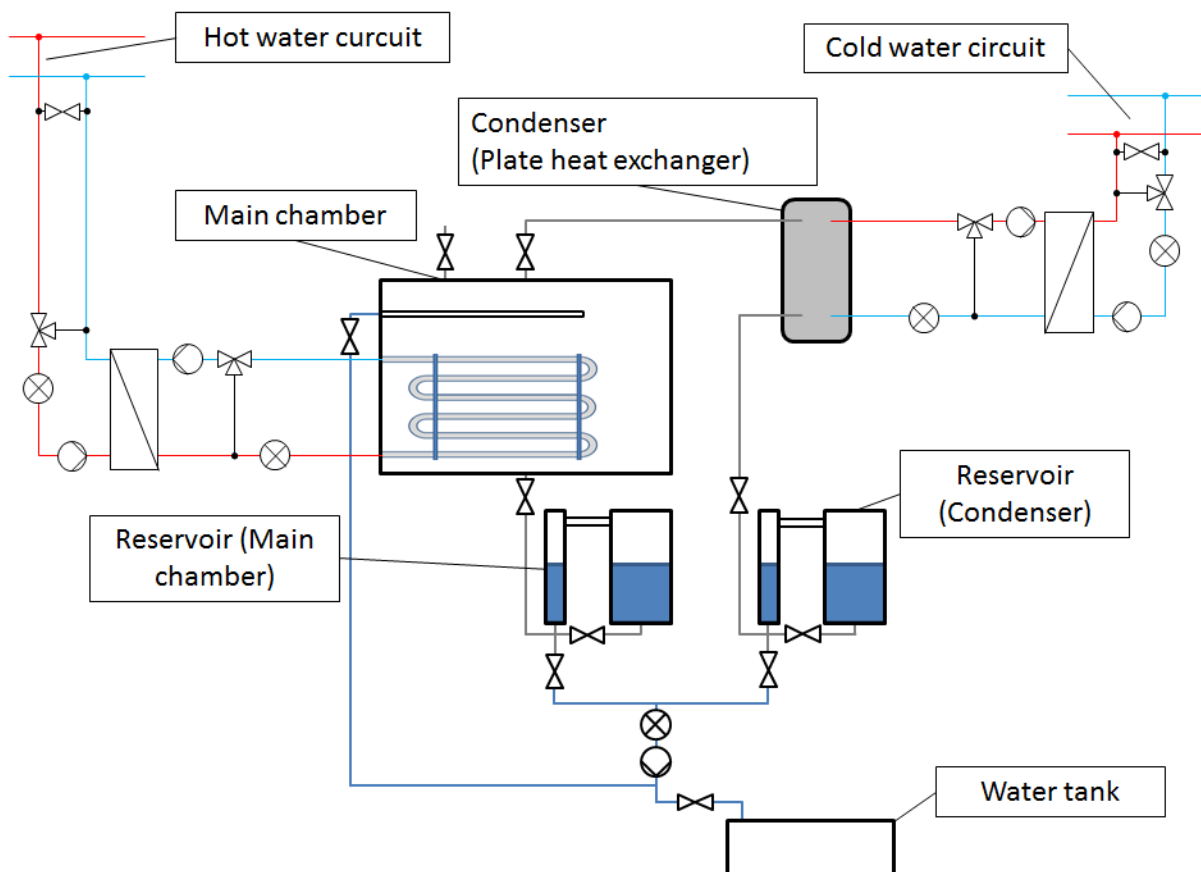


Figure 14: Schematic representation of the evaporation test facility

A detailed description of the main parts, their components and the design are given in the subsections below.

The concept was implemented and developed in FreeCAD. This program was used to design and visualize the test rig on the basis of the calculated design steps as explained in the following subsections. Concerning the software, Version 0.15 and furthermore the utilities “assembly 2”, “drawing” and “drawing dimensions” were used.

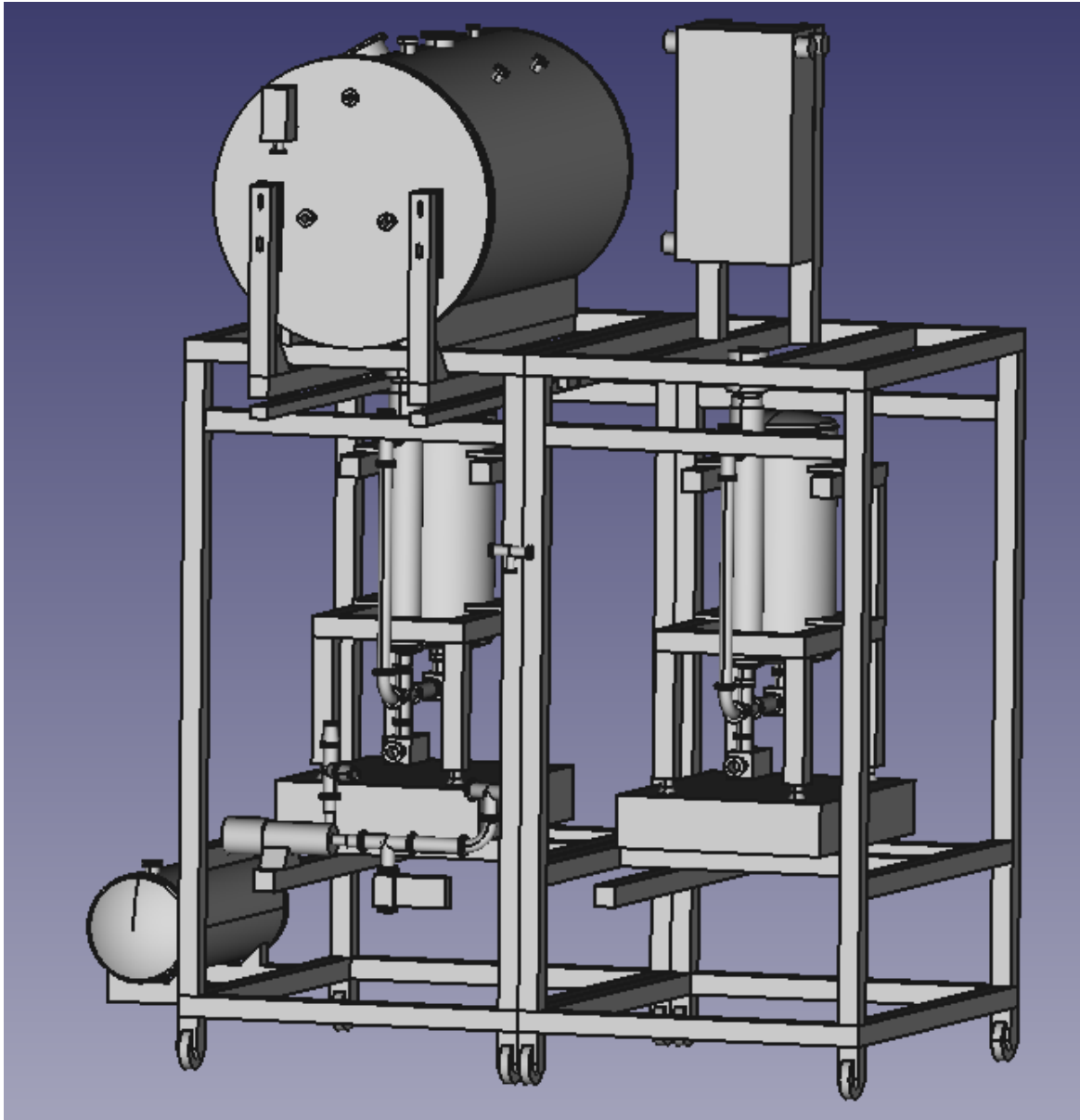


Figure 15: Test Rig visualized via FreeCAD

3.3.1 Main chamber

The main chamber consists of the heat exchanger where its evaporation power is investigated. Several heat exchanger concepts shall be possible to be investigated in this chamber, consisting of those mentioned in chapter 2. To elaborate the dimensions the falling film method has been chosen as it requires the most amount of space compared to the other concepts. The schematic concept is stated in Figure 16 and consists of the tube bundle and the distributor above the bundle. The approximation of the tube bundle and the chosen distributor design is stated in the subsections below. Finally we declared the vessel to have an inner diameter of 0.5 m and a length of 0.8 m (without taking the dished ends into account).

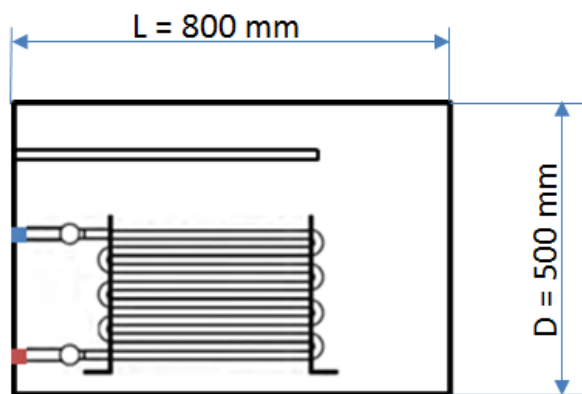


Figure 16: Schematic layout of the vessels dimension with either a small or a big tube bundle

3.3.1.1 Calculation of the heat exchanger

With assumed parameters and the given equations from 3.2.1 and 3.2.2 the scale of the heat exchanger can be approximated.

The boundary conditions are fitted to the low temperature heat source used to evaporate the water which is generally in a range of 10 – 20°C. To simplify our calculations 15°C has been chosen. As the heat flux depends on the temperature difference the evaporation side has been assumed to start with 5°C leading to 10°C for the evaporation. The material values of water were calculated with the equations of the VDI

heat atlas. Starting with the first approximation to reach roughly five kW the following initial values were defined which led to dimensions as seen below.

Table 1: Adjusted parameters: main chamber

| Fluid Falling Film | | Fluid Tube Flow | |
|---------------------|----------------------------|---------------------|---|
| T_{FF} | 10 °C | T_{TF_In} | 15 °C |
| V_{TF_In} | 0,000776 m ³ /s | T_{TF_Out} | 13 °C |
| V_{TF_evap} | 0,000155 m ³ /s | V_{TF} | 0,00033 m ³ /s |
| ρ_{FF} | 1002,9 kg/m ³ | ρ_{TF} | 1001,1 kg/m ³ |
| μ_{FF} | 0,0013 kg/ms | ν_{TF} | 1,13*10 ⁻⁶ m ² /s |
| λ_{FF} | 0,58 W/mK | λ_{TF} | 0,59 W/mK |
| $\Delta h_{v_{FF}}$ | 2478 kJ/kg | $\Delta h_{v_{TF}}$ | - kJ/kg |
| cp_{FF} | 4197 J/kgK | cp_{TF} | 4191 J/kgK |

| Tube | | Bundle | |
|----------------|----------|---------|-------|
| d_i | 12 mm | Rows | 6 - |
| d_o | 10 mm | Columns | 6 - |
| λ_{Cu} | 400 W/mK | Length | 0,4 m |
| Heat Flow | | | |
| Q | 4,7 kW | | |

For further understanding, a figure was added to the subsection four of the appendix to allocate the variables.

3.3.1.2 Distributor

The distribution of the falling film has a high impact on the efficiency. If the falling film is not fully developed before striking the tubes the heat flux can suffer due to dry areas on the first row of the tube bundle. Therefore the right path of distributing has to be found.

John G. Bustamante [15] has investigated several types of distributors based on their irrigation density Re_{Γ} . He split those distributors into two groups. The “Box Type” and the “Tube Based” distributors.

Based on his work two distributors are relevant for our conditions ($Re_{\Gamma} = 40 - 60$). The “Exit Tubes” and “Concentric: Holes, Half Tube”. For the dimensioning of our test rig the “Concentric: Holes, Half Tube” has been chosen as its maldistribution is more accurate. This concept works as shown in the following part:

The liquid enters on the top of the box and fills up a certain height of it. On the given height of the predetermined small tubes the liquid leaves through them as seen in Figure 17

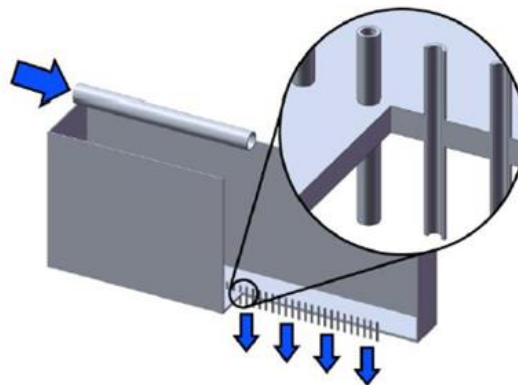


Figure 17: "Concentric: Holes, Half Tube" part of John G. Bustamante's (2014) Box-type distributor designs

The dimensions of the distributor are the same as in the work of J. G. Bustamante [15].

3.3.1.3 All connections and parts of the chamber

The vessel consists of several openings and connections displayed in Figure 18. The top left picture describes the parts which are located on the shell and the linear guidance to open the vessel.

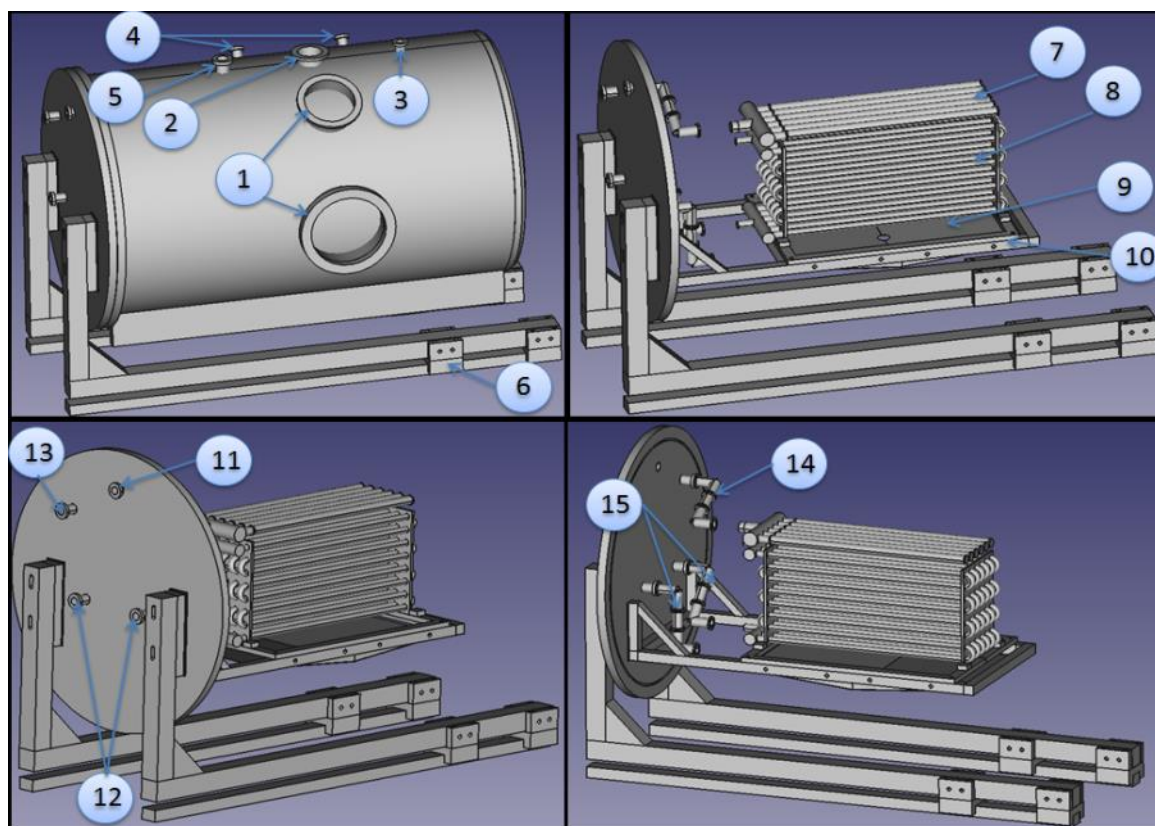


Figure 18: Connections and parts of the main chamber

There are two sight glasses (1) located on the side of the shell. They are horizontally oriented to view directly onto the heat exchanger bundle, the second to investigate the irrigation of the distributor. A big flange (2) is used to connect the two chambers with each other. It was oversized to reduce the turbulence and therefore the pressure drop of the vapour stream. A flange (3) which is used to connect electricity devices into the chamber is located next to the flange for the vapour stream flange (2). There are nine pins to supply devices, for example temperature measurement, which are not located on the moveable part of this facility. A pressure measurement device is connected to one of these two flanges (4) in order to determinate the ambient pressure and the second flange has no purpose yet. The last flange (5) on the shell is used to connect the valve for evacuation. A linear guidance (6) is intended to ensure an easy way to open and close the vessel whenever it is needed. The picture on the

top right shows the frame (10) on which the distributor (7^2), the heat exchanger bundle (8) and the drip tray (9) is attached. The two pictures on the bottom of Figure 18 show the cover of the vessel including another flange (11) for the electricity and the outer flanges (12) of the chamber for the tube and distributor stream. The same flanges are welded on the inside. While attached to them are the tubes (14;15) to connect the distributor and the heat exchanger bundle.

3.3.2 Reservoir

The reservoir collects/distributes the liquid for the evaporation process and is needed to determine the performance by measuring the change of the liquid level.

Depending on the accuracy of the liquid level indicator the dimensioning of the vessels differs. A high accuracy of the measurement system leads to a smaller vessel and therefore to a smaller observation time.

3.3.2.1 Dimensioning

The reservoir consists of three main parts as seen in Figure 19 below.

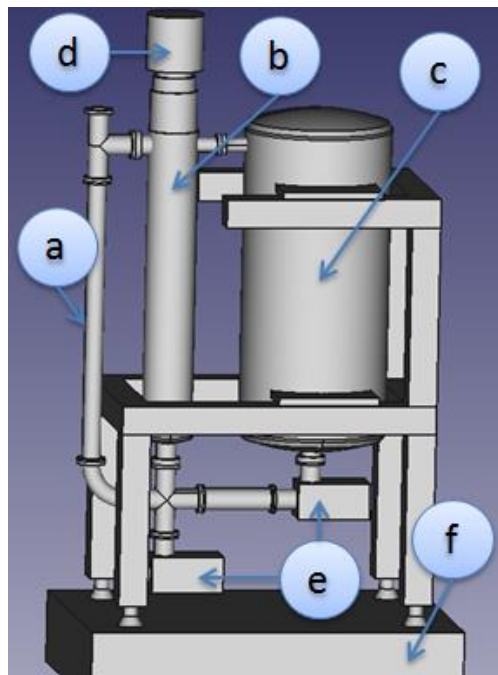


Figure 19: Layout of the Reservoir

² Sketch of the distributor, not the actual “Concentric: Holes, Half-Tube” concept was visualized in this picture

- a) The tube collects the condensate. It prevents the liquid surface in b) and c) from getting disturbed by the incoming condensate leading to a fluctuating of the floating measurement device. A connection of the condensate tube to the measurement vessel at the bottom will only harm the surface of the condensate tube which does not affect the measurement device.
- b) The measuring vessel is designed thinly to reduce the observation time as it is filled up faster by the incoming condensate.
- c) The backup vessel is used to supply the pipes and the falling film with water. Furthermore, it is used to support the measuring vessel in case the performance is so high that an insignificant small observation time would occur.
- d) Liquid level measurement device.
- e) Valves
- f) Scale

The overhead connections between the reservoirs make the vessels communicating, allowing the vapor to distribute when the tanks are getting filled during the measurement. Otherwise the pressure in those vessels would rise and distort the result.

The valves at the bottom of the reservoir are electronically controlled as they are needed during the measurement, the valve at the top of the condensate line is manually operated, as it is only used to prevent the ambient air to suppress the vacuum when the chamber is opened.

3.3.2.2 Accuracy calculation

Liquid level measurement:

The measurement system which is used to determine the liquid level is accomplished by a continuous floating device. To get a smaller vessel a magnetostrictive principle is intended. This principle usually has an accuracy of 1 mm.

An observation time of 15 minutes to 1 hour is desired. Longer experiments are rather inefficient and shorter experiments could suffer from the impact of unstable conditions at the beginning respectively at the end of the test.

The inaccuracy was tested for both subsystems. Table 2 shows the inaccuracy without the tank connected to the measurement vessel while Table 3 shows the case with the tank connected to the measurement vessel.

Table 2: Inaccuracy without the reservoir connected to the measurement vessel

| Performance [kW] | Accuracy [mm] | Diameter [m] | | |
|------------------------|---------------|------------------------|------------------|---------------|
| | | Condensate line | Measuring vessel | Backup vessel |
| 5 | 1 | 0,025 | 0,07 | 0 |
| Observation Time [min] | Volume [l] | rel. liquid level [mm] | Inaccuracy [%] | |
| 1 | 0,12 | 28 | 4% | |
| 5 | 0,60 | 138 | 1% | |
| 10 | 1,20 | 277 | 0% | |
| 15 | 1,80 | 415 | 0% | |
| 20 | 2,40 | 553 | 0% | |
| 25 | 3,00 | 691 | 0% | |
| 30 | 3,60 | 830 | 0% | |
| 35 | 4,20 | 968 | 0% | |
| 40 | 4,80 | 1106 | 0% | |
| 45 | 5,40 | 1245 | 0% | |
| 50 | 6,00 | 1383 | 0% | |
| 55 | 6,60 | 1521 | 0% | |
| 60 | 7,20 | 1659 | 0% | |
| 65 | 7,80 | 1798 | 0% | |
| 70 | 8,40 | 1936 | 0% | |
| 75 | 9,00 | 2074 | 0% | |
| 80 | 9,60 | 2212 | 0% | |
| 85 | 10,20 | 2351 | 0% | |
| 90 | 10,80 | 2489 | 0% | |

With the estimated performance the condensed volume can be calculated. The condensed volume has to be stored in the reservoir. For Table 2 the volume of the reservoir consists of the volume of the condensate line and the measuring vessel, while

Table 3 includes the tank as well. The volume of the liquid is calculated by the performance in combination with the evaporation enthalpy and the time.

$$V = t * h_v * \rho * P \quad (3.25)$$

Divided by the combined surfaces of the condensate line, measuring vessel and the backup vessel the relative liquid level is determined.

$$l_{level} = \frac{V}{d_{con} + d_{mvessel} + d_{bvessel}} \quad (3.26)$$

The liquid level results in the inaccuracy which indicates the observation time as we try to achieve an inaccuracy of less than 1%. The red marked rows define when the maximum height of the reservoir is reached.

$$Inaccuracy [\%] = \frac{Inaccuracy [mm]}{l_{level} [mm]} \quad (3.27)$$

An inaccuracy of less than 1% is reached in Table 2 between 5 and 10 minutes before the maximum height is reached.

Table 3: Inaccuracy with the reservoir connected to the measurement vessel

| Performance [kW] | Accuracy [mm] | Diameter [m] | | |
|------------------------|---------------|------------------------|------------------|----------------|
| | | Condensate line | Measuring vessel | Backup vessel |
| 5 | 1 | 0,025 | 0,07 | 0,2 |
| Observation Time [min] | Volume [l] | rel. liquid level [mm] | | Inaccuracy [%] |
| 1 | 0,12 | 3 | | 30% |
| 5 | 0,60 | 17 | | 6% |
| 10 | 1,20 | 34 | | 3% |
| 15 | 1,80 | 50 | | 2% |
| 20 | 2,40 | 67 | | 1% |
| 25 | 3,00 | 84 | | 1% |
| 30 | 3,60 | 101 | | 1% |
| 35 | 4,20 | 117 | | 1% |
| 40 | 4,80 | 134 | | 1% |
| 45 | 5,40 | 151 | | 1% |
| 50 | 6,00 | 168 | | 1% |
| 55 | 6,60 | 185 | | 1% |
| 60 | 7,20 | 201 | | 0% |
| 65 | 7,80 | 218 | | 0% |
| 70 | 8,40 | 235 | | 0% |
| 75 | 9,00 | 252 | | 0% |
| 80 | 9,60 | 269 | | 0% |
| 85 | 10,20 | 285 | | 0% |
| 90 | 10,80 | 302 | | 0% |

With the reservoir connected to the measurement vessel the observation time for about 200 mm height is 60 minutes for the same performance. However as already mentioned a high performance can decrease the observation time to a minimum where the reliability is critical. The adjusted parameters as seen in Table 2 and Table 3 are visualized Figure 20.

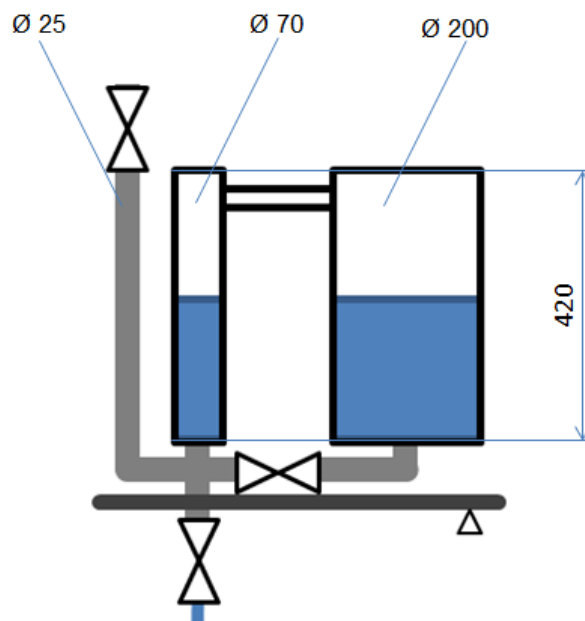


Figure 20: Dimensions of the Reservoir

Mass balance measurement:

The mass balance does not affect the height of the test rig as significantly as the liquid level measurement as its height is only 80 mm. Detailed data is stated in the subsection 3.3.6.8.

3.3.3 Plate heat exchanger

The plate heat exchanger is used to condense the evaporated fluid of the test rig. This heat exchanger chosen for our test rig is a part of a preceding project of AEE INTEC and its performance is sufficient as a condenser for the tests.

Table 4: dimensions of the plate heat exchanger

| Typ | dimensions in mm | | | | | |
|------------|---------------------|-----|-----|----|-----|----|
| | A | B | C | D | E | F |
| XB30-44/44 | 438 | 118 | 385 | 65 | 236 | 50 |

Figure 21 in combination with Table 4 give an overview of the size of the plate heat exchanger.

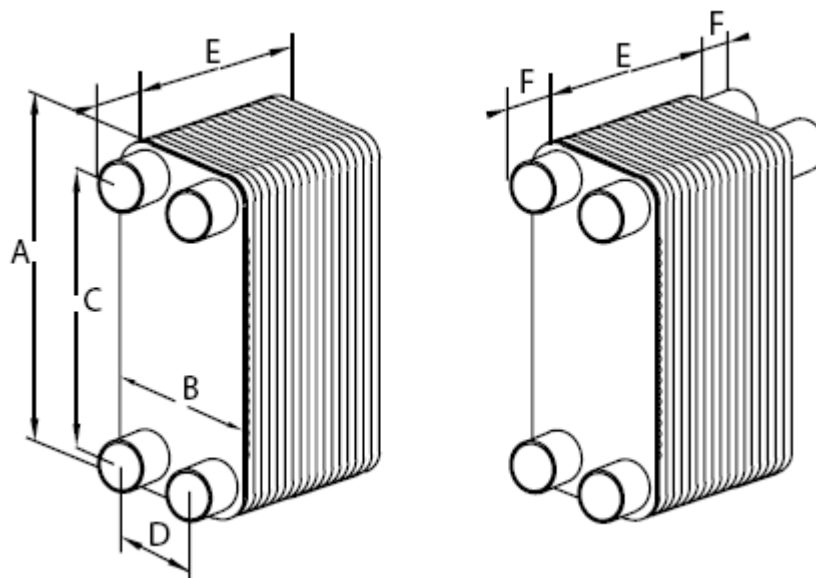


Figure 21: Design of the plate heat exchanger

3.3.4 Hot and cold water supply line

The hot and cold water circuits are provided by stations connected to the tanks of the laboratory. Those two tanks can deliver a hot water stream of 80°C and a cold water stream of 8°C. These temperatures have to be prepared to fit the conditions needed during the evaporation/condensing in this test rig via a plate heat exchanger. The schematic design was already presented in chapter 3.3. An extract of this schema focused on the supply lines is stated below.

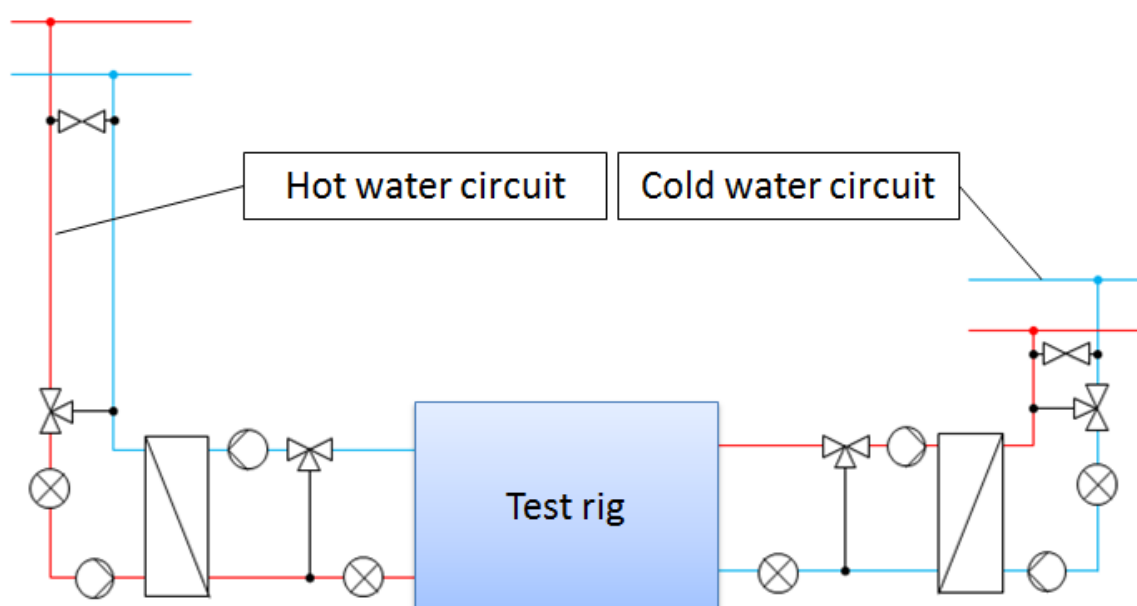


Figure 22: Hot and cold water supply line

The streams with the higher temperature in each of the circuits are coloured in red, the others are coloured in blue.

Hot water circuit:

The hot water provided by the laboratory (the two lines on the top left in Figure 22) is pumped into the plate heat exchanger where it warms up the stream flowing into the test rig. The heat meter controls the splitter responsible for the fine tuning of the streams. The valve is used to release trapped air in the circuits that are connected to the supply tanks of the laboratory.

Cold water circuit:

The cold water circuit is built in the same way as the hot water circuit. The only difference is that the colored lines have been changed as we try to cool the streams in our test rig.

Additionally there are three more modules installed per circuit which are not visualized in this schematic: A compensation tank to compensate the pressure increase/decrease during the temperature fluctuations, a manometer to check the pressure inside those circuits and a pressure relief valve for an emergency case to relief the pressure over four bar inside the circuit.

3.3.5 Heat loss calculation for insulation

In the following chapter the expected heat losses will be described. For those calculations several assumptions were made that will lead to the worst case that means the highest heat flux.

Assuming that the inner wall temperature is the same as the vapor stream and the outer wall is the same as the ambient temperature the calculation can be simplified as displayed in Figure 23.

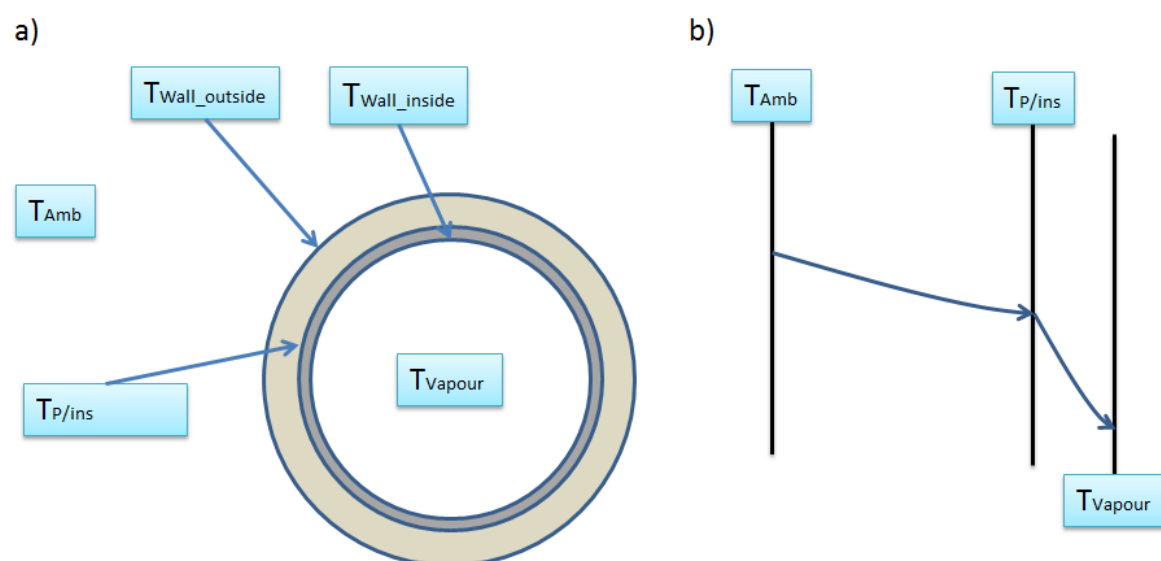


Figure 23: Heat loss calculation: a) Cross section of a vessel/pipe, b) Simplified temperature profile through the wall

By neglecting the outer and inner heat transfer coefficient the temperature difference is increasing and therefore the heat loss is increasing which is intended as the worst case is aspired.

Table 5 shows the initial values and the calculated heat loss depending on the dimensions of the vessels or pipe. The calculation and the equations for the heat loss assumption can be found in the appendix. A temperature difference between the ambient and the inner fluid was assumed to be 15°C. For the thermal conductivity, steel was chosen for the metal components and mineral wool for the insulations. The thickness, diameters and length is dictated by the design and dimensions of the components.

Table 5 is accurate when the ambient temperature is higher than the fluid temperature in the test rig. If the ambient temperature is colder than the fluid the heat flux turns outwards.

Table 5: Heat loss calculation

| Initial values | | Heat loss depending on the dimensions | | | | |
|------------------------|------------|---------------------------------------|------------|------------|-------|--------|
| T_{Amb} | 30 °C | d [m] | amount [-] | Length [m] | Q [W] | |
| $T_{Wall_outside}$ | 30 °C | Main Chamber | 0,5 | 1 | 0,8 | 57,43 |
| T_{Wall_inside} | 15 °C | Tank | 0,2 | 2 | 0,4 | 35,26 |
| T_{Vapour} | 15 °C | Measuring vessel | 0,075 | 2 | 0,4 | 13,39 |
| λ_{Steel} | 50 W/mK | Condensate line | 0,021 | 2 | 0,4 | 4,82 |
| $\lambda_{Insulation}$ | 0,045 W/mK | Big Pipe | 0,021 | - | 1 | 6,03 |
| S_{Pipe} | 0,003 m | Small Pipe | 0,012 | - | 2 | 7,47 |
| $S_{Insulation}$ | 0,01 m | | | | Sum: | 124,41 |

The heat flux of the plate heat exchanger is assumed to reach the same amount as the main chamber.

3.3.6 Measurement and Control

This chapter will characterize the upcoming measurement devices and control units. In addition a description of the sensors, valves, level indicator, mass balance, heating rod and pump as displayed in Figure 24 is declared and a more detailed information is stated in the appendix.

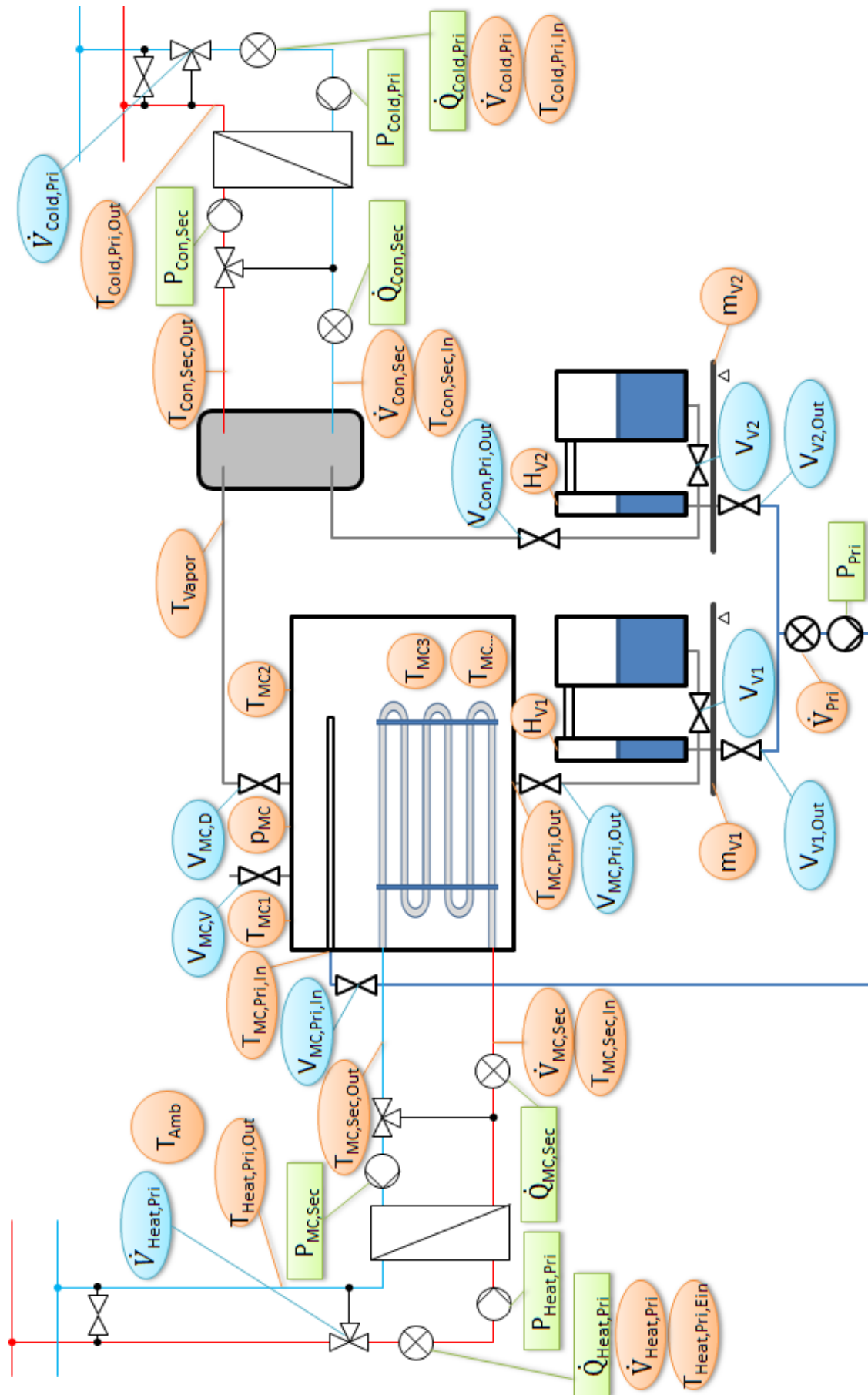


Figure 24: Schematic representation focused on "Measurement and Control"

3.3.6.1 Sensors

Two different types of sensors will be purchased for this test rig:

- Pressure sensors
- Temperature sensors

The absolute pressure transmitter used to record the pressure condition in this test rig has a range from 0 to 100 mbar with an inaccuracy of $\pm 0.05\%$, delivered by Huba Control™ (order number 680.700320). It is located on the upper side of the vessel and attached to it by Vacuum Pfeiffer™ components.



Figure 25: Pressure sensor

The temperature sensors are standard PT 100 elements with a quality class of 1/3 B DIN.

3.3.6.2 Valves

The valves in this test rig are either hand operated or pneumatic operated. The hand-operated valves are those which need to be closed when the chambers are opened, preventing the ambient air to suppress the vacuum. The pneumatic operated valves are those which need to be shifted during an experiment. Both the “Pri,Out” valves in addition to the “MC,V” are hand operated the rest are pneumatic operated valves.

The vacuum components like flanges, tubes and the valves are delivered by Vacuum Pfeiffer™.



Figure 26: Manuel valve on the left, pneumatic valve on the right

3.3.6.3 Level indicator and mass scale

As already mentioned in chapter 3.3.2 the level indicator will be magnetostrictive. The measurement device is delivered by Kobold™ and has an effective measuring range of 350 mm. The inaccuracy becomes vanishingly small after 200 mm but the remaining length is used to cover up the start respectively the end of the test where the conditions could be unsteady.



Figure 27: Head of the liquid level measurement



Figure 28: Mass measurement device

The scale has to measure the weight of the condensed water in addition to the reservoir and the framework. All of those parts combined have a weight of roughly 50 kg. The scale was rounded up to the next class which can measure up to 60 kg and is delivered by Kern™. The scale has an accuracy of 20 g.

3.3.6.4 Pump

A commercially available circulating pump is used to circulate distilled water in this test rig. To ensure vacuum tightness the selection was reduced to magnetically coupled pumps which are hermetically sealed. A simplified calculation was performed in order to estimate the head of the pump. The simplified schema is pictured in Figure 29 and Figure 31. The calculation, which is stated in the appendix, leads to the head of the two pumps as seen in Table 6 and Table 7 which can further be neglected as this small height is no challenge for any ordinary pump.

- Pump for the falling film

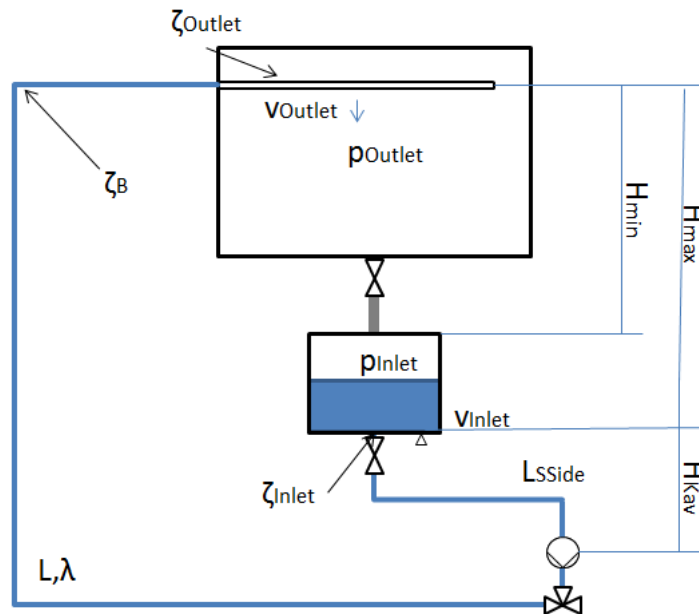


Figure 29: Simplified schema to estimate the head of the pump for the falling film

Table 6: Boundary Conditions for the head of the pump for the falling film

| Boundary Conditions: | | | | | |
|----------------------|---|------------------|--------------------|------------------|-------------------------------|
| H_{min} | 0,6 m | v_A | 0 m/s | $\zeta_{S,Side}$ | 2 pieces |
| H_{max} | 1 m | L | 2 m | g | 9,81 m/s ² |
| p_{Outlet} | 20 mbar 2000 Pa | $L_{S,Side}$ | 0,2 m | k | 0,02 mm |
| p_{Inlet} | 20 mbar 2000 Pa | λ | 0,4 | T | 20 °C |
| V | 0,35 m ³ /h 0,00010 m ³ /s | ζ_{Outlet} | 1 | v | 1,00771E-06 m ² /s |
| d | 25 mm 0,025 m | ζ_{Inlet} | 0,5 | ρ | 999,23 kg/m ³ |
| v_{Inlet} | 0 m/s | ζ_B | 0,197 10 pieces | H_{Pump} | 1,04 m |

A critical aspect for the pump will be the operation conditions near to the saturation temperature which results in cavitation. This cavitation is tolerated even though it can cause the pump to malfunction. Under these circumstances cavitation will occur and is taken into account as we do not want to build this test rig higher than needed.



Figure 30: Pump for the falling film

By neglecting the importance of the head of the pump, the size of it depends on the volumetric flow and therefore the irrigation number is needed to provide a sufficient irrigation for the heat exchanger tube bundle.

To gather some reliability for other tube bundles the pump is designed to handle 8 columns instead of the calculated 6 columns and additional 20% security which is rounded up to 10 l/min.

- Pump for the tube flow

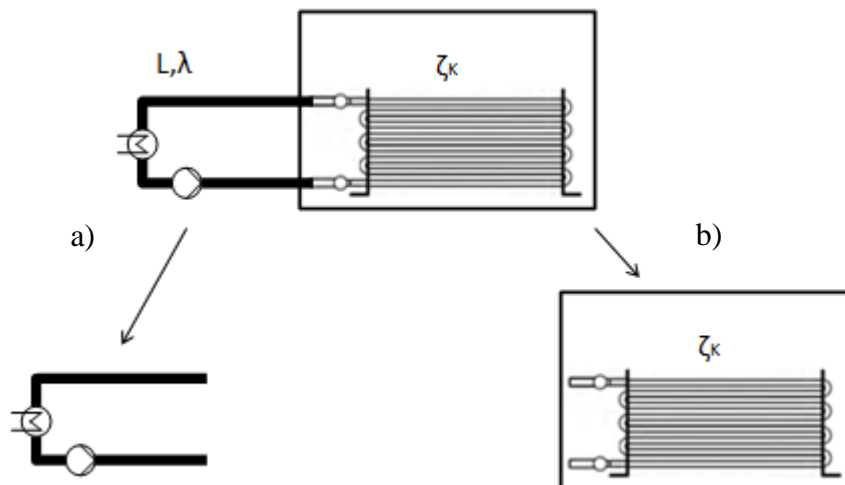


Figure 31: Simplified schema to estimate the head of the pump for the tube flow

Table 7: Boundary Conditions for the head of the pump for the tube flow

| Boundary Conditions | | | | | | |
|---------------------|-------------------------------|-------|------------------------|---------------------------|-----------|--------------|
| Initial values | | a) | | | | |
| H_{\min} | 0 m | V | 1 m ³ /h | 0,00028 m ³ /s | ζ_s | 0,197 2 Stk |
| H_{\max} | 0 m | d_1 | 25 mm | 0,025 m | | |
| p_k | 20 mbar 2000 Pa | L | 2 m | | | |
| p_v | 20 mbar 2000 Pa | b) | | | | |
| T | 20 °C | V | 0,17 m ³ /h | 0,00005 m ³ /s | ζ_s | 0,192 96 Stk |
| v | 1,00771E-06 m ² /s | d_2 | 10 mm | 0,01 m | | |
| ρ | 999,23 kg/m ³ | L | 20 m | | | |
| H_{pump} | 14,35 m | | | | | |

3.3.6.5 Volume flow measurement

A volume flow measurement device is only used in the vacuum line. The flows for the other circuits are measured with heat meters.



Figure 32: Volume flow measurement device

3.3.6.6 Heat meter

The heat meter is used to measure the volume flow and also the transferred heat for the hot and cold water circuits. The model is the MULTICAL[®] 302 from Kamstrup[™].



Figure 33: Heat Meter

3.3.6.7 Splitter

The splitter is used to split up the streams of the hot and cold water circuits. It allows a more precise adjustment of the heat flux. The splitter is made by the company BELIMO[™]



Figure 34: Splitter

3.3.6.8 Data capturing and control

This chapter specifies the modules built into the control cabin and additionally the interface of the AEE measurement input/output.

Inside the control cabin are several modules to operate the test rig shown in Figure 35 and designated and declared in Table 8.

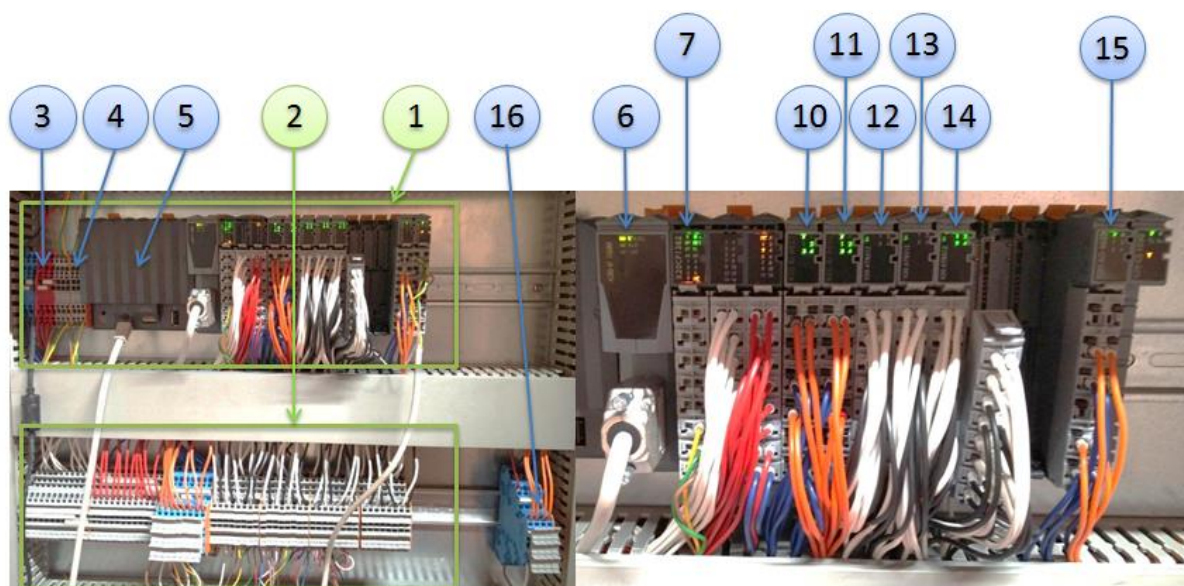


Figure 35: Determination of the modules inside the control cabinet

Table 8: Designation and Declaration of the modules of the control cabinet

| Nr. | Designation | Declaration |
|-----|-------------------------|--|
| 1 | Measurement and Control | Consisting of the modules that run the system. |
| 2 | Distribution | Interface between the control cabinet and the test rig. |
| 3 | Power Supply | |
| 4 | Mass Balance Interface | Bridge to the connection to the scale. |
| 5 | Main Board | Interface from the control cabinet to the visualisation. |
| 6 | X20IF1020 | Evaluates the second balance. |
| 7 | X20CP1382 | CPU. It is running the AEE-Measurement System and additionally consists of Input/output plugs which are used to operate magnetic valves. |
| 10 | X20AI4622 | Analog input (0 – 20 mA or 0 – 10 V). Is used to evaluate the pressure and the liquid level. |
| 11 | | |
| 12 | X20ATB312 | Input for the PT100 sensors. |
| 13 | | |
| 14 | | |
| 15 | X20AO4622 | Analog input (0 – 20 mA or 0 – 10 V). Is used to control the rpm of the pumps. |
| 16 | Pump Interface | Connection to the pumps. |

The interface is pictured in Figure 36.

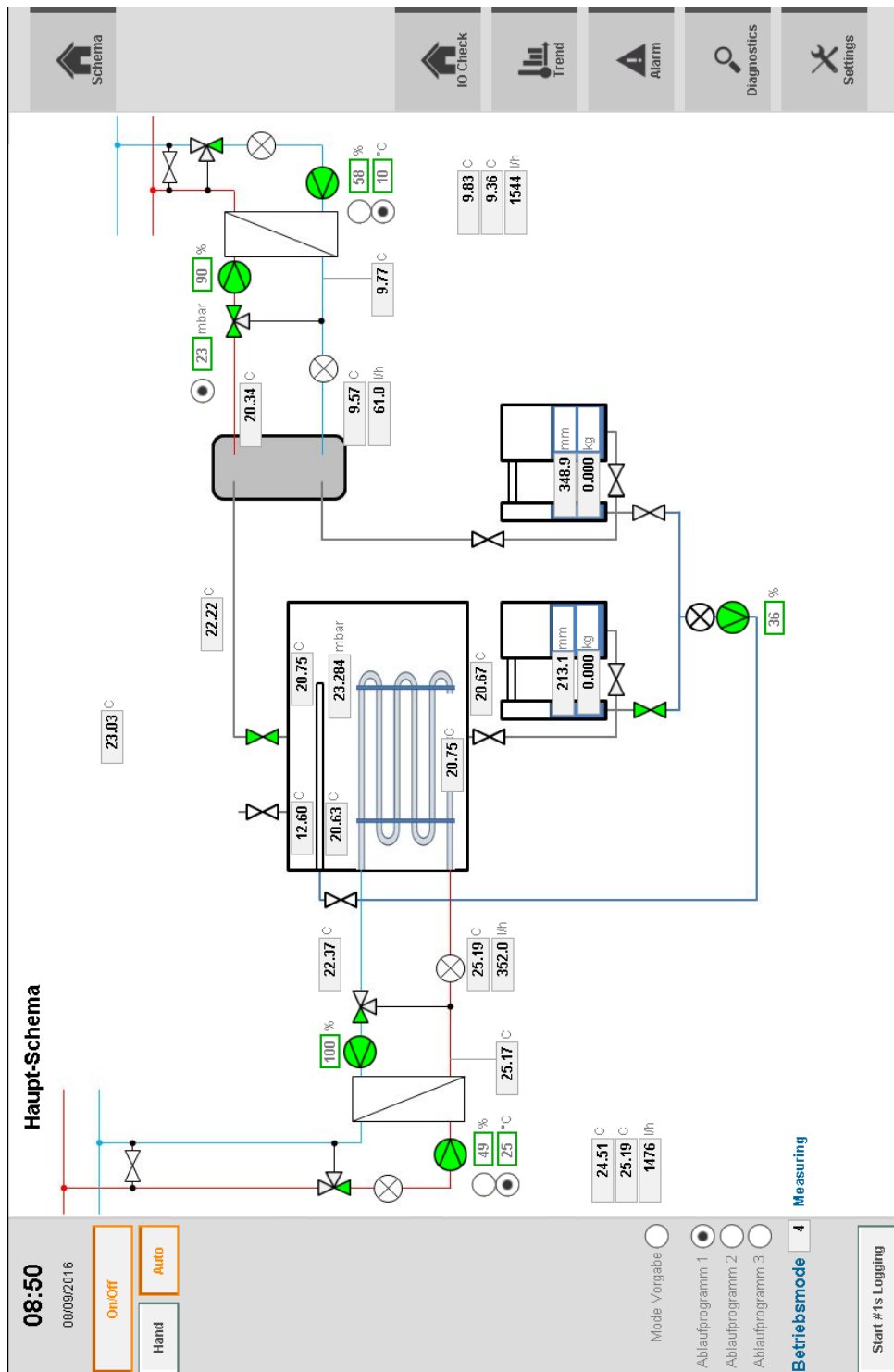


Figure 36: Interface to operate the test rig

The interface displays several values such as the status of the pumps and valves, the temperature of the PT100 sensors the height of the liquid level measurement, the weight of the reservoirs etc. Furthermore it is possible to operate the input variables for the pump and valves.

3.4 Construction of the test rig

Those previous designing steps in addition to the test rig components are constructed and combined to the following test rig as shown in Figure 37.



Figure 37: Evaporation test rig

3.5 Design for testing Condensing

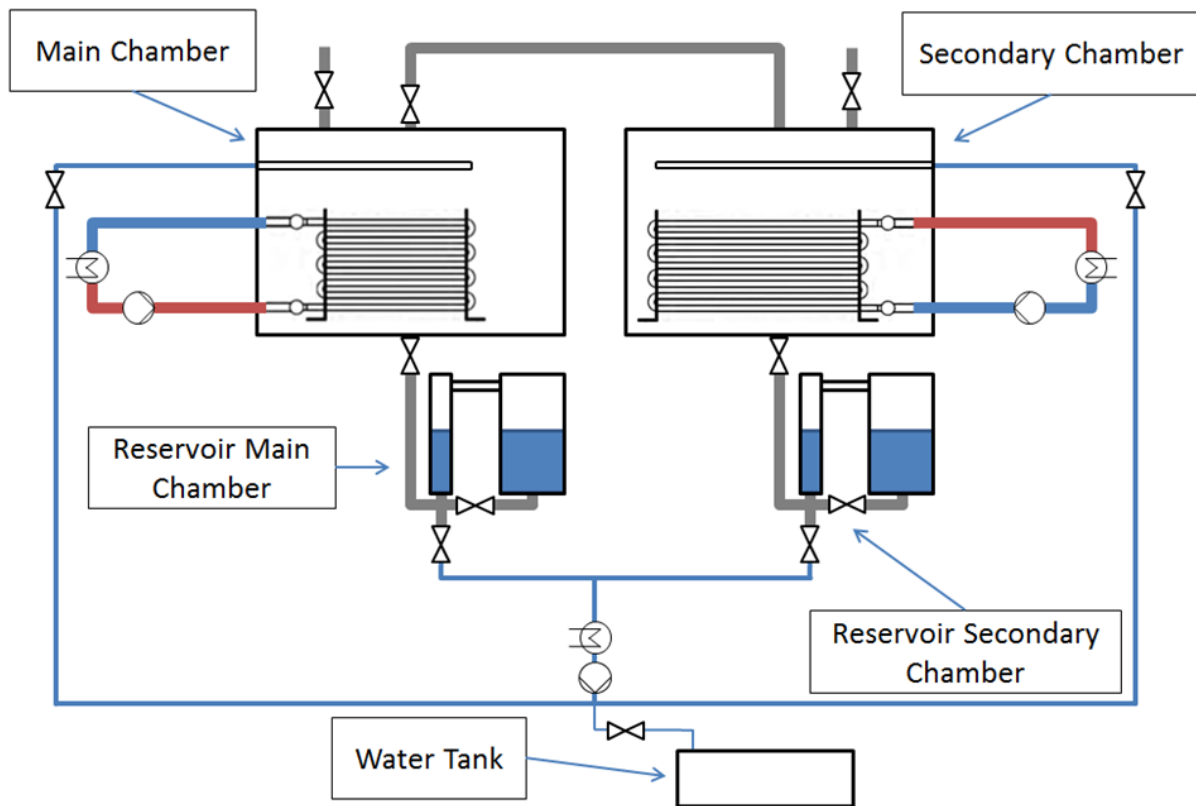


Figure 38: Test rig for evaporation and condensing with simplified heating and cooling streams

As already mentioned in the introduction this test rig will be capable of testing both the evaporation and condensing. Therefore the plate heat exchanger will be replaced by a laterally reversed main chamber, which is called the secondary chamber. The secondary chamber has to fulfill the same task as the plate heat exchanger but the condensing process can be different in relation to the concept and additionally more variables can be measured.

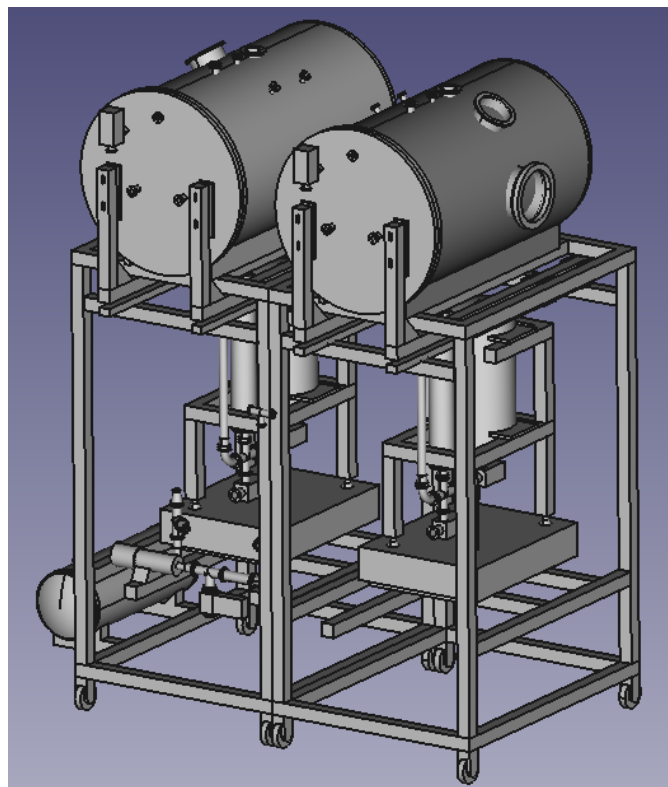


Figure 39: Design for testing condensing

4 Commissioning

During and after the construction of the test rig, different checks are necessary before it can be taken into operation. Those checks are listed in the following chapters.

4.1 Level Measurement calibration

The level measurement calibration was done for both reservoirs and also with and without the water tank.

The measurement was proceeded in 100 ml steps and further on with 250 ml steps. The 100 ml steps were measured with a volumetric flask. Those are pretty accurate due to the small ending at the top. The 250 ml steps were processed with ordinary measuring glasses. The fluid for the calibration was distilled water.

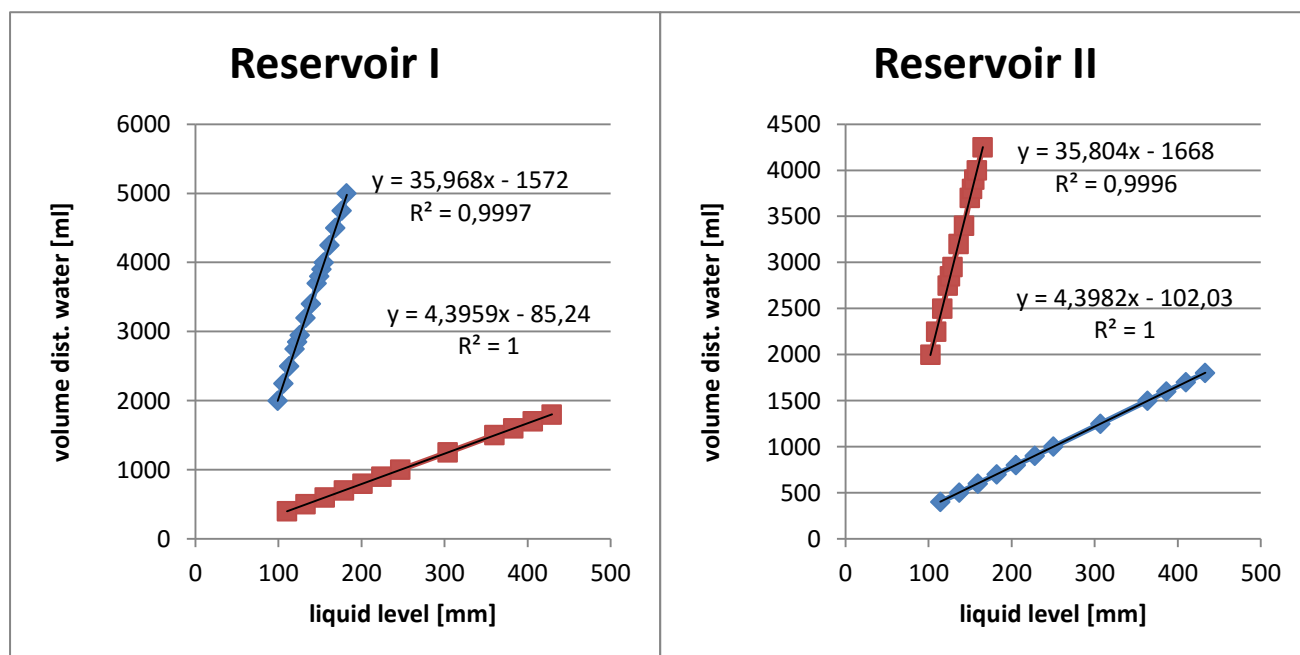


Figure 40: Function of the Volume of distilled water depending on the liquid level

The line in each figure with the lower gradient was measured without the backup vessel.

4.2 Leakage

The leakage is important as the pressure increase during the test and also the partial proportion of air distorts the measurement and therefore the validity of the experiment. In order to keep the tests relevant the leakage should be vanishingly small. The specific value that has to be reached depends on the influence of the air to the experiments and also the duration of such an experiment. In this case the influence is rather low due to the small observation time per experiment.

The leakage is defined as:
$$Leakage = \frac{mbar * l}{s}$$

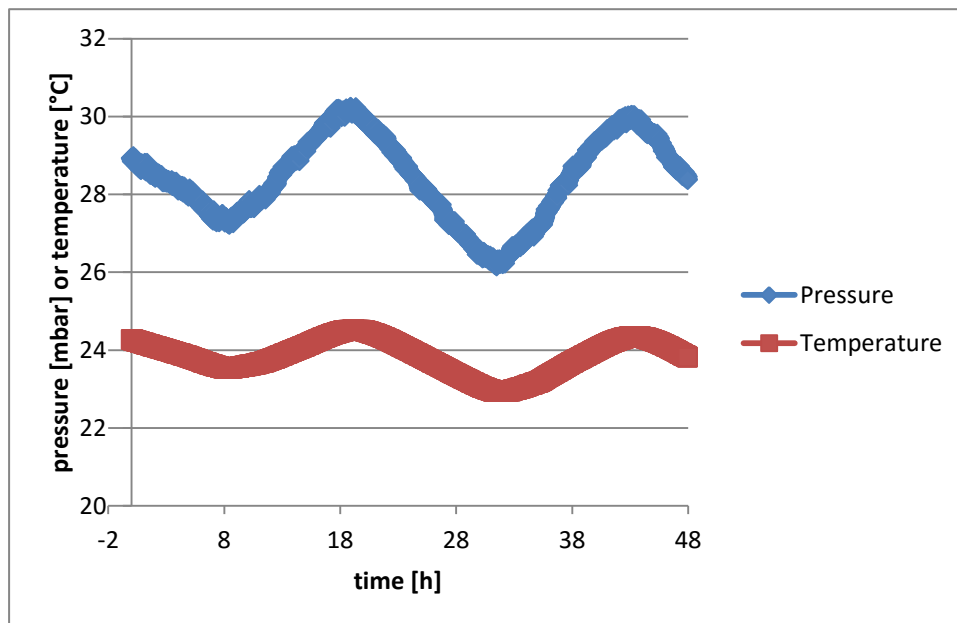


Figure 41: Leakage of the test rig depending on the temperature

In Figure 41, the pressure inside the test rig is displayed. As there is only water in it, the pressure depends on the temperature. To calculate the leakage two points have been compared with each other. One at the beginning of the leakage record and the other at the near end of the record. The second point was chosen depending on the temperature of the first one as they saturation pressure should be equal. The pressure difference for those result in the leakage of this facility.

Table 9: Leakage of the Test rig

| Date/Time | hours [h] | Pressure [mbar] | Temperature [°C] |
|------------------|-----------|-----------------|------------------|
| 06.08.2016 23:59 | 0 | 28,529 | 23,99 |
| 07.08.2016 22:52 | 46,8 | 28,705 | 23,99 |

| | |
|--------------|----------------------|
| $\Delta p =$ | 0,176 mbar |
| $V =$ | 181 l |
| Leakage = | 0,000189079 mbar*l/s |

With the Information of Table 9 the leakage has been calculated with the following equation.

$$Leakage = \frac{\Delta p * V}{\Delta t * 3600} \quad (4.1)$$

Δp is the pressure increase within the investigated time, V is the volume of the test rig, Δt is the time of investigation and the factor in the denominator changes the dependencies of the result to seconds.

The leakage is very low compared to the time of a test run but can cause a malfunction of the plate heat exchanger. The air leaking into the test rig accumulates in the plate heat exchanger as it is dragged in with the water vapour and not dragged out with the condensate. This can be noticed by the small gap between the inlet and the outlet temperature of the plate heat exchanger. If so, the air has to be pumped out so that the plate heat exchanger can work properly again. Therefore a valve was installed at the top of the plate heat exchanger.

5 Experimental procedure

Before a test can be confirmed the test rig has to be prepared to reach the desired conditions. Those steps are listed below.

5.1 Preparations

Ensure vacuum condition

To ensure vacuum conditions the water is stored completely in the water tank and further on isolated from the test rig. The connection on top of the main chamber is used to connect the vacuum pump to the system. Under vacuum conditions the valve to the vacuum pump is closed before filling the water from the water tank into the facility. The water tank is not needed for further progress.

Changing parts without releasing the vacuum in the whole facility

If during an existing vacuum parts of the main chamber need to be changed the valves to that chamber have to be closed to prevent the ambient air suppressing the vacuum. The content of this chamber can be changed and only the vacuum in this chamber has to be recovered.

5.2 Dependencies of the variables among each other

Before the automation protocol can be defined, the behavior of the variables among each other has to be clarified based on Figure 43. Furthermore the dependencies are classified in to three groups of variables, highlighted in Figure 42.

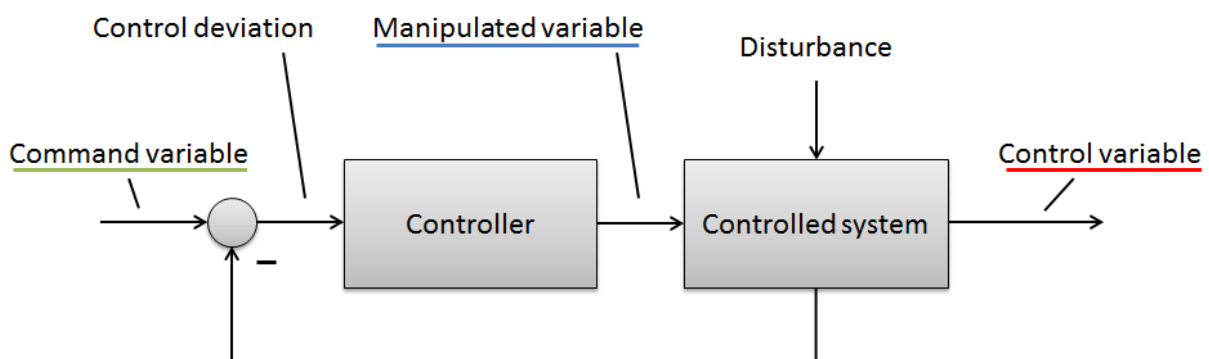


Figure 42: Control loop

Control loop

The objective of a control loop is to control a system, so that its output follows a desired control signal. The control loop monitors the output and compares its value with the reference which may be a changing value or a fixed one. The difference between the reference and the actual value is applied as a feedback to the input of the system. With the feedback the controller can compensate the difference till the desired value has been reached.

Command variables

As we are interested to achieve the heat transfer coefficient near the vacuum the ambient pressure (1) of the facility as a test is preceded has to be determined. Without inert gases the pressure equals the saturation pressure.

The pump (2) in the vacuum line provides the falling film with a given irrigation density. As it is intended to check the heat transfer coefficient of certain irrigations the volumetric flow of this pump has to be constant during a test and therefore set at the beginning.

The heating circuit (3) for the main chamber is also one of the input variables that are held constant over the observation time due to the same reason as (2).

(4) and (5) are the boundary conditions for the temperature which has to be set in order to achieve a current heat flux due to the temperature difference. In our test those will be set mainly 5°C above the saturation temperature for (4) and 5°C beneath for (5).

Manipulated variables

The manipulated variables help reaching a steady condition and also hold them during the test.

(6) controls the ambient pressure inside the main chamber (1). If the pressure and therefore the temperature is too high the cooling power increases to lower those values. (7) and (8) control the temperature coming out of the two plate heat exchangers in the hot and cold water circuits.

Control variables

The boxes highlighted in red are the controlled variables measured by different sensors. Those are needed for the manipulated variables in comparison to the command variables to reach the desired conditions.

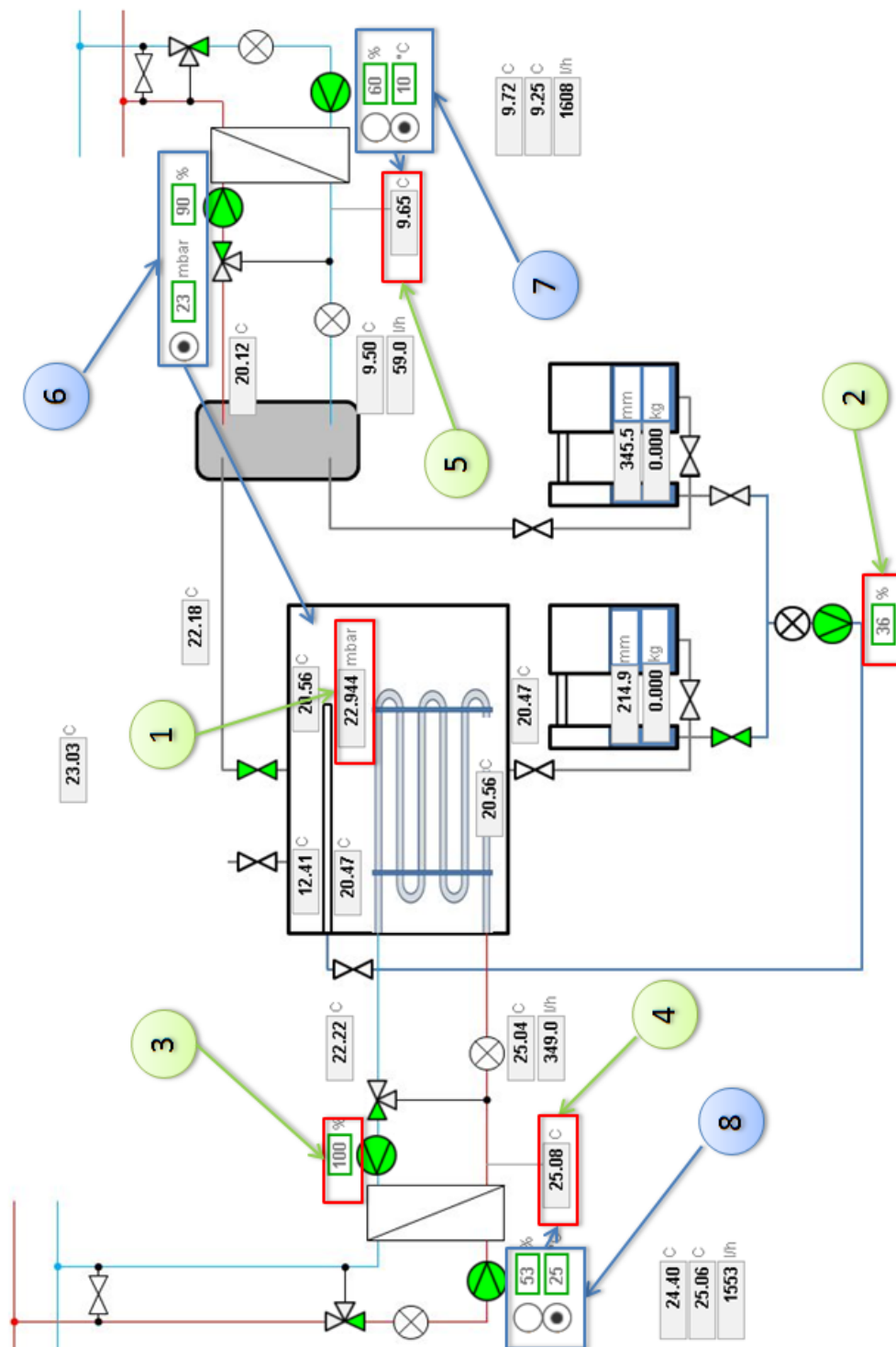


Figure 43: Dependencies of the variables among each other

5.3 Automation

To do several tests over time an automation protocol was implemented. This protocol is used to run tests without the need of a person to operate the test rig during a test.

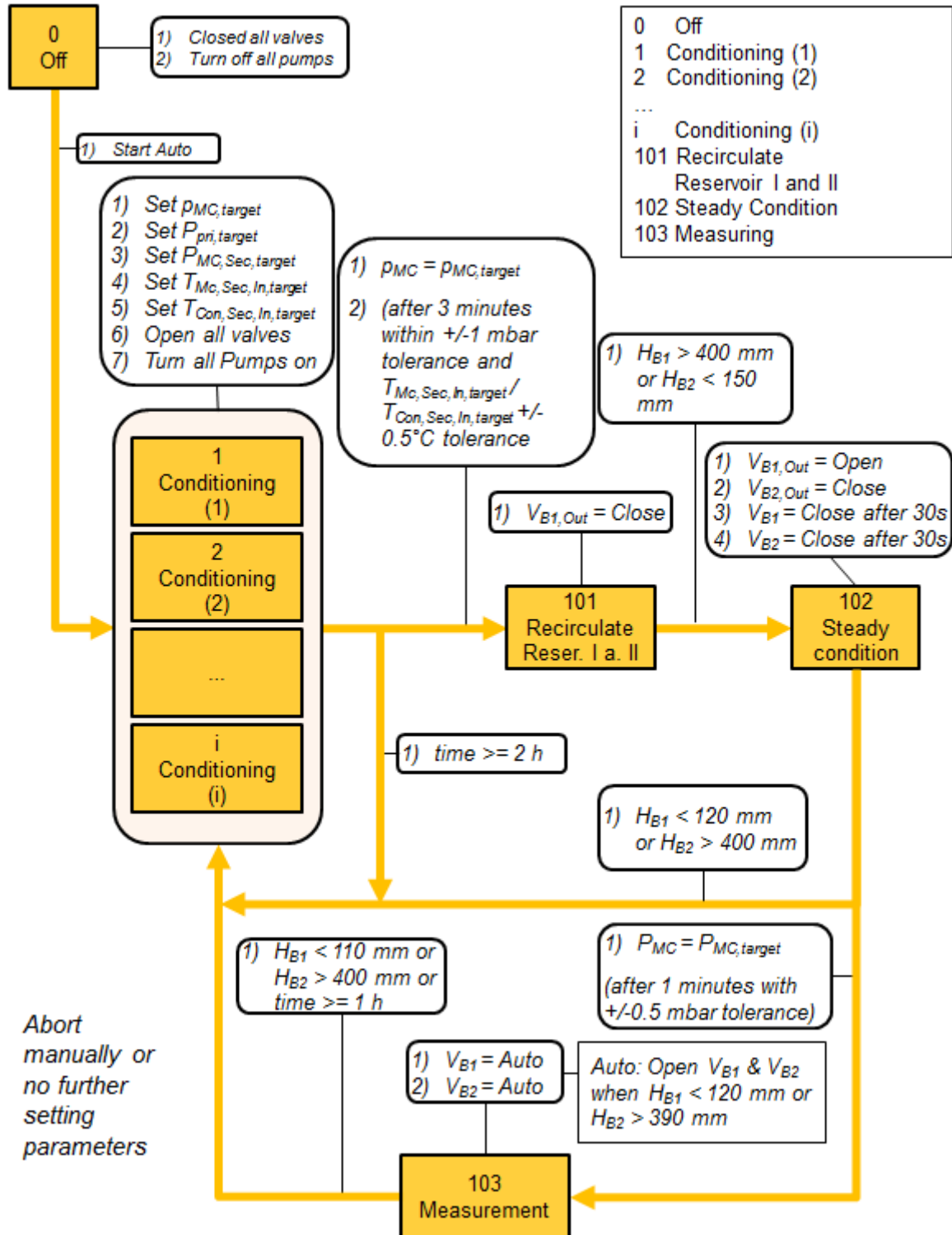


Figure 44: Automation protocol

Off

The “Off” step is reached when the preparation steps in chapter 5.1 have been performed. With the vacuum ensured, the reservoirs filled, the valves closed and the pumps switched off, the basic state where the automation protocol should be started is reached.

Conditioning

At first the water has to be prepared to reach the conditions depending on the input variables that have been defined for each conditioning step. The variables that have to be set were the “command variables” defined in the previous chapter.

The next step is initiated when the desired pressure is reached.

Recirculate Reservoir I a. II

After the conditioning the reservoirs have to be decanted. Therefore the water in the reservoir II has to be shifted into reservoir I. This step is intended to use the maximum liquid level range in both the reservoirs. The maximum and minimum height for both the reservoirs are 400 mm and 150 mm respectively, which is also set to be the initiation of the next step.

Steady Condition

This step ensures steady conditions after the recirculation. If the recirculation leads to fluctuations regarding the stability of the system this step will start conditioning again before starting the measurement.

Measurement

If steady conditions are reached the measurement can be started. When the liquid level reaches either the maximum or minimum limit inside one of the reservoirs the big tanks are connected to the measurement system. The abort criterion is when two hours have passed.

Abort Criteria

To prevent damage taken by parts of the facility several abort criteria were implemented. The pump in the vacuum line can only be activated if an output valve of one of the reservoirs is open at the same time and additionally the liquid level of the fluid inside the reservoir is above 100 mm. Furthermore the facility stops if a temperature sensor of this test rig reports a temperature beneath 5°C to prevent freezing. A overheating can be neglected as the heating source of the labour only delivers 50°C, which is far away from any critical condition.

5.4 Evaluation

By testing an evaporation concept the heat flux in this facility can be evaluated out of four different sources. The heating/cooling streams of the evaporator/condenser and the liquid level/mass change of the evaporator/condenser. The equations are similar to those in chapter 2.

Heat flux:

Evaporator stream:

$$\dot{Q}_{MC,Sec} = \dot{m}_{MC,Sec} * c_{p_{MC,Sec}} * (T_{MC,Sec,In} - T_{MC,Sec,Out}) \quad (5.1)$$

Condenser stream:

$$\dot{Q}_{Con,Sec} = \dot{m}_{Con,Sec} * c_{p_{Con,Sec}} * (T_{Con,Sec,In} - T_{Con,Sec,Out}) \quad (5.2)$$

Evaporator:

$$\dot{Q}_{MC,Pri} = \dot{m}_{MC,Pri} * \Delta h_{MC,Pri} \quad (5.3)$$

Condenser:

$$\dot{Q}_{Con,Pri} = \dot{m}_{Con,Pri} * \Delta h_{Con,Pri} \quad (5.4)$$

Those heat fluxes are calculated by the arithmetic average values over the measured time.

Additionally the heat loss of this test rig can be calculated with these results as it has to be equal to the difference between the heat flux of the heating and cooling stream.

$$\dot{Q}_{loss} = \dot{Q}_{MC,Sec} - \dot{Q}_{Con,Sec} \quad (5.5)$$

Further on the heat transfer resistance of the evaporator can be calculated as stated in chapter 3.2.

6 Experimental results

As already mentioned before, the concept that will be tested is the falling film. The experimental series only consists of the same tube bundle tested for different conditions.

6.1 Tube bundle and distributor

The tube bundle was provided by a project partner of AEE INTEC called Luvata™. It consists of three rows and five columns and is made out of plain copper tubes. The surface has not been processed. A sketch of the tube bundle is given in the appendix. The box type distributor as mentioned in the subsection 3.3 is dimensioned in the same way as the one John G. Bustamante (2014) described in his work. Figure 45 shows the tube bundle with the attached distributor on top of it already placed on the mounting of the test rig.



Figure 45: Tube bundle and distributor test arrangement

6.2 Falling film evaporation

The first test run on this test rig is explained in detail to show the proper function, while the other tests only show the conditions and results

6.2.1 First test to declare the proper function of the test rig

Conditions

The first test was performed under the conditions stated in Table 10.

Table 10: Pressure in the main chamber

| pressure check | |
|----------------|-----------|
| $p_{MC,meas}$ | 22.9 mbar |
| $p_{MC,calc}$ | 22.9 mbar |

The pressure inside the test rig was 22.9 mbar. The calculated pressure at those circumstances calculated by the mean temperature inside the test rig is 22.9 mbar.

The test was performed as described in chapter 5.3. After the conditioning and the recirculation steps were made, the measuring has been started. The exact date and time is displayed in Table 11.

Table 11: Conditions of the first test

| Conditions | | | | | | | | | |
|------------|------------------------------|----------|----------|-----------|------------|--------------|------|-----------------|------------------|
| Nr. | date/time | duration | p_{MC} | V_{Pri} | $Re\Gamma$ | $V_{MC,Sec}$ | Re | $T_{MC,Sec,In}$ | $T_{Con,Sec,In}$ |
| [-] | [D.M.Y H:MIN] | [s] | [mbar] | [%] | [-] | [%] | [-] | [°C] | [°C] |
| 1 | 9.8.16 10:57 9.8.16 11:30 | 00:33:00 | 23 | 40 | 215 | 100 | 3769 | 25 | 10 |

The data won't be stated in this thesis, only the progression of the important values are explained and pictured in this chapter. The data sheets will be deposited at the AEE INTEC.

Progressions of the test

The first figure displays the pressure inside the test rig measured by the pressure sensor attached in the main chamber. The pressure oscillates around the desired pressure. This is caused by three different control parameters interacting with each other. A deeper investigation into the control system of this test rig could lead to a smaller oscillation in this test rig.

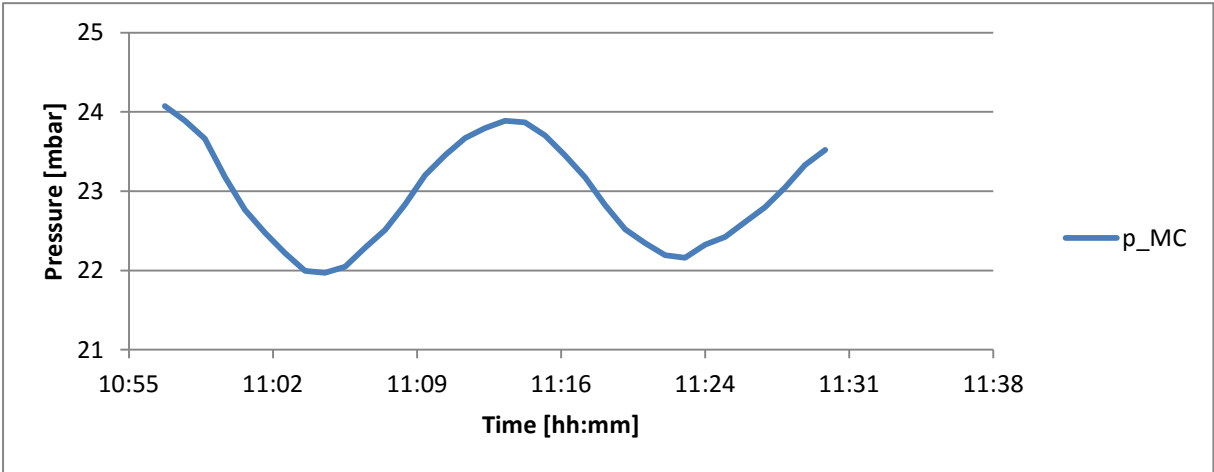


Figure 46: Pressure progression for the first test

Figure 47 displays the recorded ambient temperature, which is rising slightly during this test due to the temperatures based on the time.

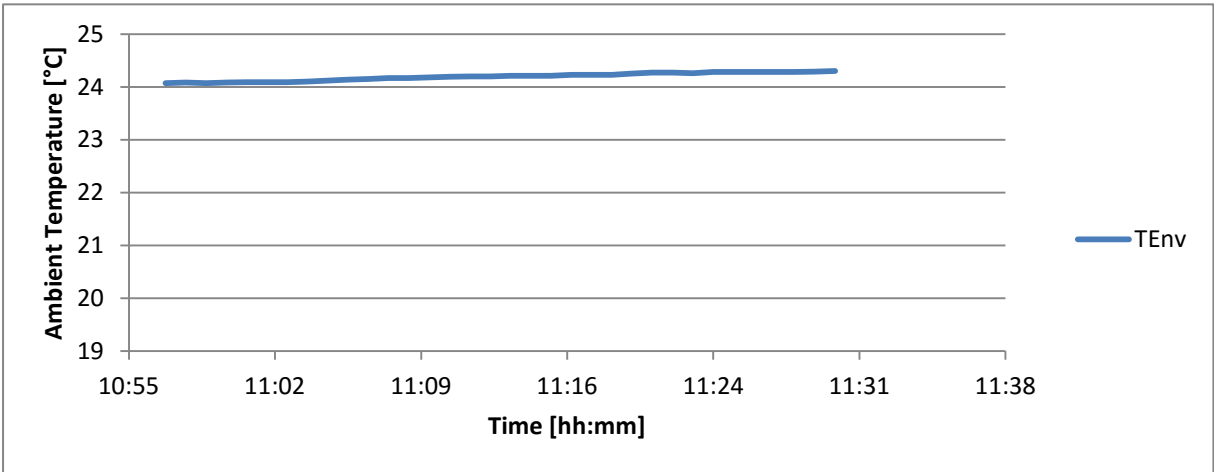


Figure 47: Ambient temperature of the first test

The temperatures inside the main chamber are stated in Figure 48. Those temperatures behave directly proportional to the pressure. The small variation is depending on their position inside the main chamber. The temperature sensor MC1 had to be cut due to its malfunction.

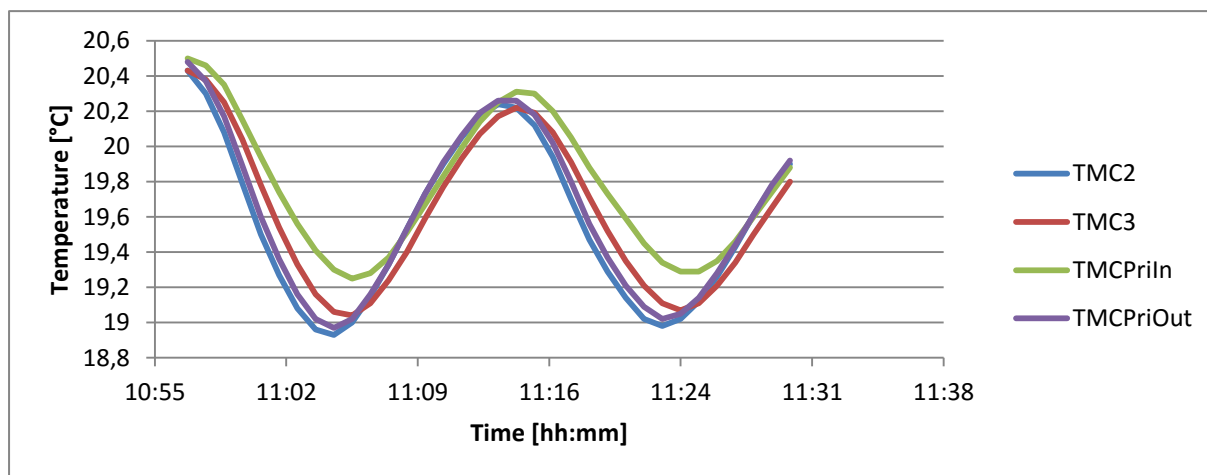


Figure 48: Temperature inside the main chamber during the first test

The liquid level in Figure 49 is needed to declare the power of the evaporator and condenser. As mentioned before, there are four possible ways to measure the power in this facility. Figure 50 displays the liquid level of evaporated respectively the condensed water.

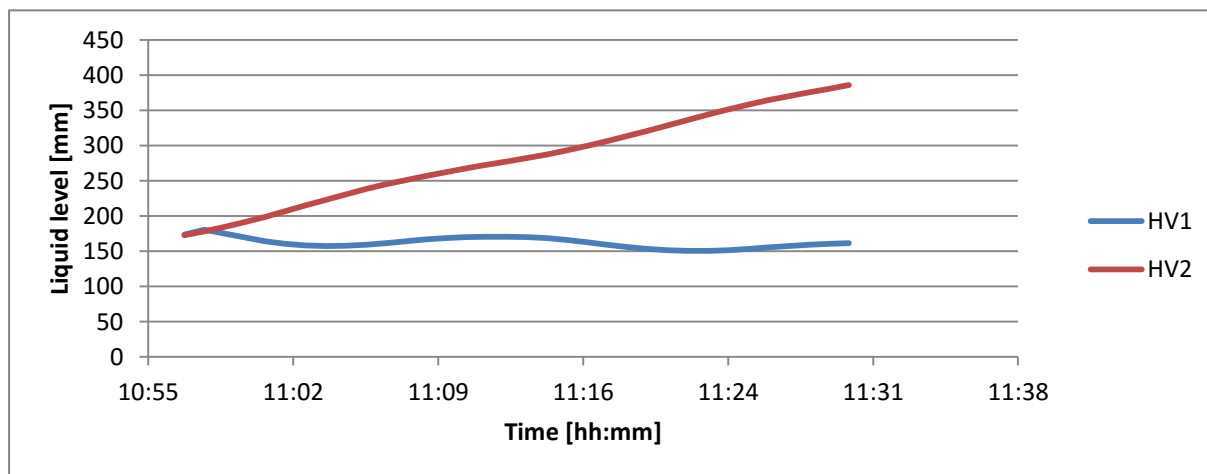


Figure 49: Liquid level curve of the first test

The unusual behavior of the liquid level in the first reservoir is caused by the circulation of the pump, parts of water not floating back into the reservoir and probably a

vapour stream in or out of the backup vessel. The vapour stream in or out of the backup vessel can be neglected by opening the valve from the backup vessel to the measurement vessel. Even then the performance does not fit the theoretical concept approached in Figure 52 at the end of this chapter. A closer inspection of this problem can be given when the scales are taken into operation. For further investigation the evaporation performance will be displayed in the results but not valuated.

Figure 50 and Figure 51 demonstrate the heating and cooling circuits into either the main chamber or the plate heat exchanger. The volumetric flow of the heating side is constant, while the flow on the cooling side is guided by the pressure inside the main chamber.

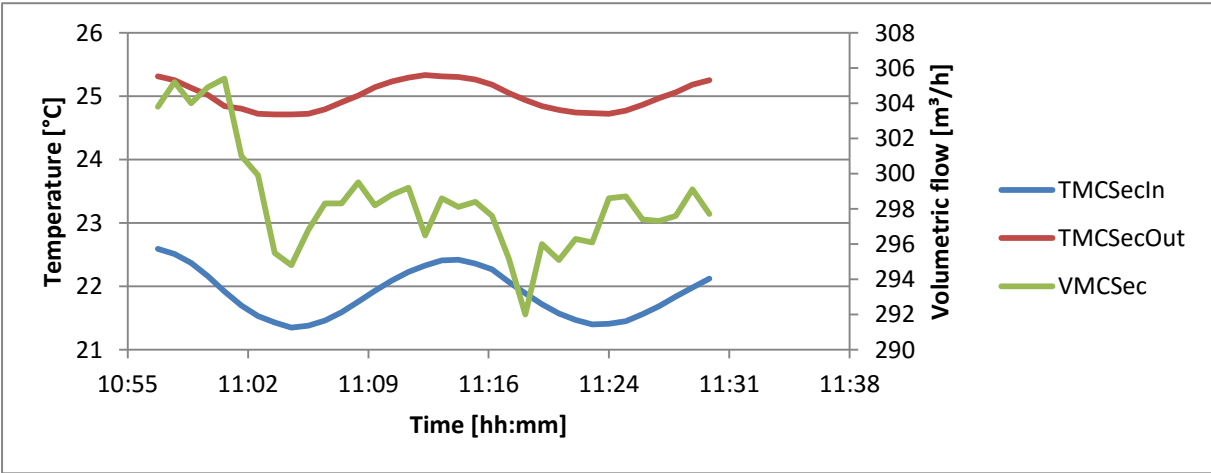


Figure 50: Temperature and volumetric flow of the heating side

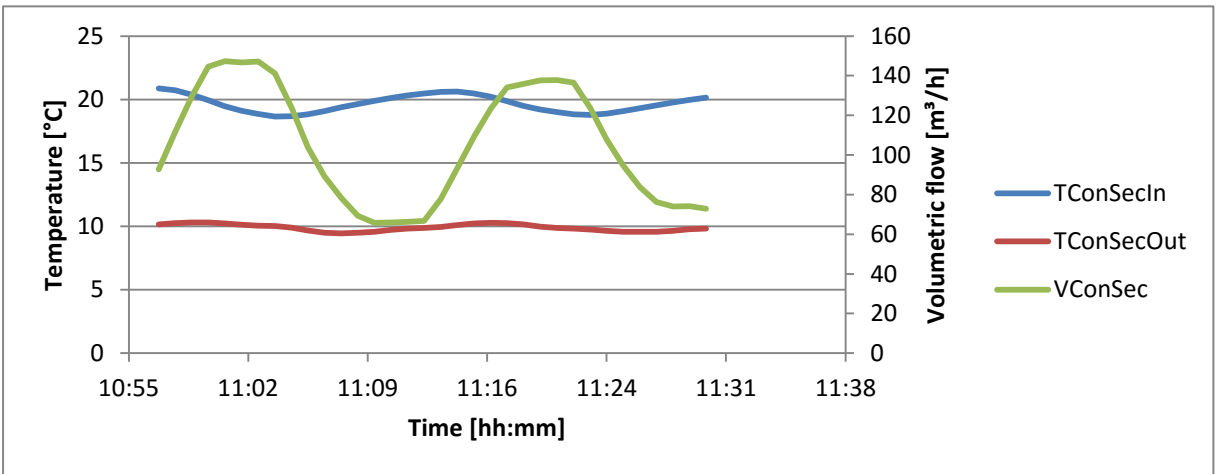


Figure 51: Temperature and volumetric flow of the cooling side

It is intended to set the pump for the heating and cooling circuit on a specific value while the mixer of the cooling circuit is guided by the pressure inside the main chamber.

Evaluation

The evaluation has been performed by the equations stated in 5.4.

Table 12: Evaluation of the evaporator and condenser

| Evaporation/Condensing | | | |
|------------------------|-----------------------|-------------------|-----------|
| fluid properties | | | |
| $T_{MC,mean}$ | 19,6 °C | | |
| ρ | 999 kg/m ³ | | |
| Δh_v | 2454 kJ/kg | | |
| Reservoir I | | Reservoir II | |
| ΔH_{V1} | 12,3 mm | ΔH_{V2} | 213,4 mm |
| ΔV_{V1} | 442,4 ml | ΔV_{V2} | 938,4 ml |
| $Q_{Res1,V}$ | 1085,0 kJ | $Q_{Res2,V}$ | 2301,3 kJ |
| $Q_{flow,Res1,V}$ | 0,548 kW | $Q_{flow,Res2,V}$ | 1,162 kW |

The conversion from the height to the volume is calculated with the results of the calibrations proceeded in chapter 4.1. It has to be distinguished whether the backup vessel is connected to the measurement vessel or not. The following equations are only correct if the backup vessel is not connected to the measurement vessel.

$$\Delta V_{B1} = 4,3959 * \Delta h_{B1} \quad (6.1)$$

$$\Delta V_{B2} = 4,3982 * \Delta h_{B2} \quad (6.2)$$

Due to the absence of the balances the results can't be cross checked, but the tests were performed more than once for each condition to neglect those uncertainties.

Table 13: Evaluation of the heating circuit for the main chamber

| Heating | | | |
|------------------------|-----------------------|---------------------------|------------------------------|
| fluid properties | | measurement | |
| $T_{\text{heat,mean}}$ | 23,4 °C | ΔT_{heat} | 3,1 K |
| ρ | 998 kg/m ³ | $V_{\text{flow,heat}}$ | 0,29852647 m ³ /h |
| c_p | 4,2 kJ/kgK | Q_{heat} | 2135,1 kJ |
| | | $Q_{\text{flow,heat}}$ | 1,078 kW |
| | | $Q_{\text{flow,heat,HM}}$ | 1,003 kW |

The flow heat with the subscripted indices HM is the value of the heat meter.

Table 14: Evaluation of the cooling circuit for the plate heat exchanger

| Cooling | | | |
|------------------------|------------------------|---------------------------|-----------------------|
| fluid properties | | measurement | |
| $T_{\text{cool,mean}}$ | 14,8 °C | ΔT_{cool} | 9,8 K |
| ρ | 1001 kg/m ³ | $V_{\text{flow,cool}}$ | 0,1 m ³ /h |
| c_p | 4,2 kJ/kgK | Q_{cool} | 2374,2 kJ |
| | | $Q_{\text{flow,cool}}$ | 1,199 kW |
| | | $Q_{\text{flow,cool,HM}}$ | 1,138 kW |

The results of each performance calculation are summed up in Table 15.

Table 15: Results of the first test

| | Performance | Unit |
|------------|-------------|------|
| Evaporator | 0,548 | kW |
| Heating | 1,078 | kW |
| Condenser | 1,162 | kW |
| Cooling | 1,199 | kW |

As mentioned before the heat flux on the evaporator side does not fit to the other three results and has to be neglected. The other results fit well to the theoretical consideration displayed in Figure 52.

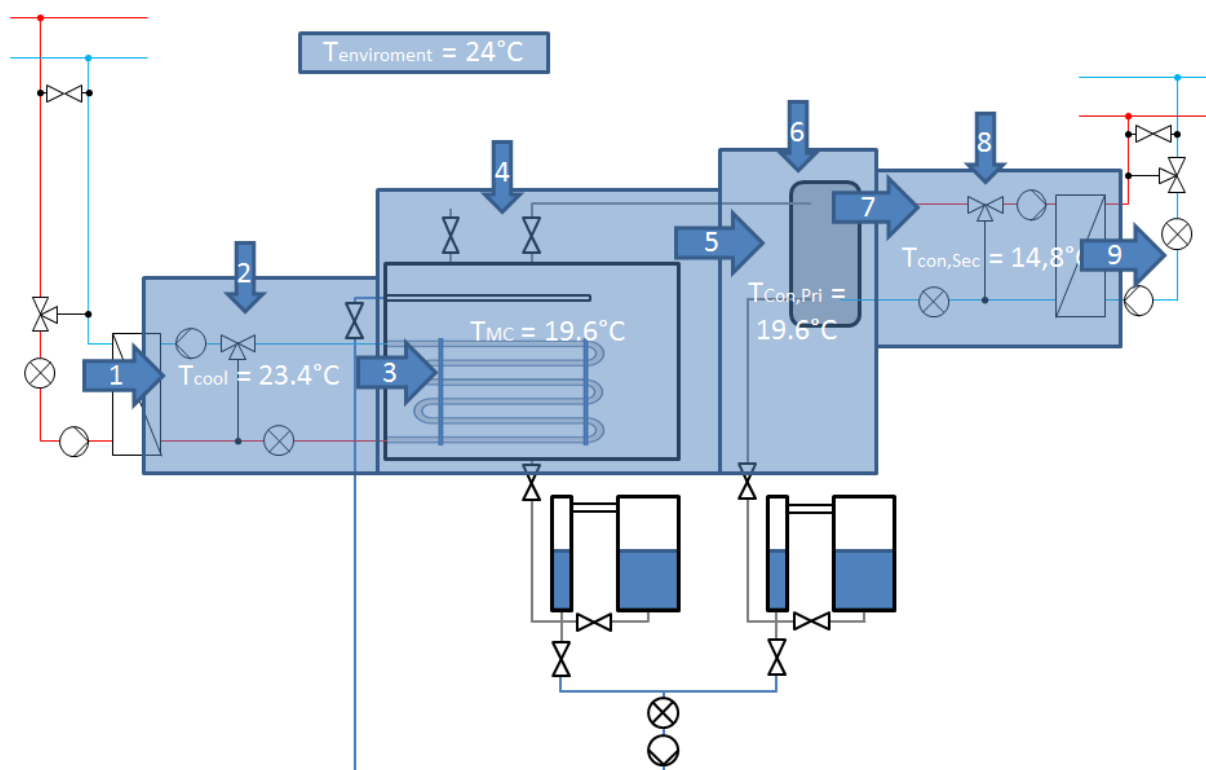


Figure 52: Heat flux of the first test

The facility was separated into four blocks. The blocks fit the categories as displayed in Table 15: Results of the first test. The temperatures in the middle of those parts state their mean temperature during the measurement.

Each block can be calculated the same way:

$$\sum Heat Flux_{In} = \sum Heat Flux_{Out} \quad (6.3)$$

Therefore the order of arrow number 1,3,5,7 and 9:

$$1 < 3 < 5 < 7 < 9 \quad (6.4)$$

If the environmental temperature drops below the mean heating stream temperature the order changes into:

$$1 > 3 < 5 < 7 < 9 \quad (6.5)$$

As the arrow number 2 changes its direction.

6.2.2 Test series

Including the test described in the previous chapter, nine different tests under different circumstances have been performed on behalf of this thesis. The volumetric flows for either the falling film or the tube flow and the pressure of the main chamber have been varied as displayed in Table 16. Each test is performed twice to decrease the insecurities.

Table 16: Varity of the test series

| Conditions | | | | | | | | | |
|------------|--------------------------------|----------|----------|-----------|------------|--------------|------|-----------------|------------------|
| Nr. | date/time | duration | p_{MC} | V_{Pri} | $Re\Gamma$ | $V_{MC,Sec}$ | Re | $T_{MC,Sec,In}$ | $T_{Con,Sec,In}$ |
| [-] | [D.M.Y H:MIN] | [s] | [mbar] | [%] | [-] | [%] | [-] | [°C] | [°C] |
| 1 | 9.8.16 10:57 9.8.16 11:30 | 00:33:00 | 23 | 40 | 215 | 100 | 3769 | 25 | 10 |
| 2 | 9.8.16 14:17 9.8.16 14:49 | 00:32:00 | 23 | 40 | 215 | 100 | 3684 | 25 | 10 |
| 3 | 9.8.16 12:01 9.8.16 12:34 | 00:33:00 | 23 | 36 | 109 | 100 | 3740 | 25 | 10 |
| 4 | 9.8.16 15:23 9.8.16 15:57 | 00:34:00 | 23 | 36 | 109 | 100 | 4141 | 25 | 10 |
| 5 | 9.8.16 13:08 9.8.16 13:42 | 00:34:00 | 23 | 40 | 215 | 80 | 3659 | 25 | 10 |
| 6 | 9.8.16 16:30 9.8.16 17:09 | 00:39:00 | 23 | 40 | 215 | 80 | 3509 | 25 | 10 |
| 7 | 10.8.16 7:40 10.8.16 8:15 | 00:35:00 | 17 | 40 | 187 | 100 | 4389 | 20 | 10 |
| 8 | 10.8.16 10:55 10.8.16 11:42 | 00:47:00 | 17 | 40 | 187 | 100 | 3966 | 20 | 10 |
| 9 | 10.8.16 8:43 10.8.16 9:24 | 00:41:00 | 17 | 36 | 83 | 100 | 4419 | 20 | 10 |
| 10 | 10.8.16 12:05 10.8.16 12:48 | 00:43:00 | 17 | 36 | 83 | 100 | 4375 | 20 | 10 |
| 11 | 10.8.16 9:50 10.8.16 10:47 | 00:57:00 | 17 | 40 | 187 | 80 | 3108 | 20 | 10 |
| 12 | 10.8.16 13:14 10.8.16 14:03 | 00:49:00 | 17 | 40 | 187 | 80 | 3036 | 20 | 10 |
| 13 | 10.8.16 15:04 10.8.16 16:11 | 01:07:00 | 12 | 40 | 169 | 100 | 3683 | 15 | 9 |
| 14 | 10.8.16 18:34 10.8.16 19:05 | 00:31:00 | 12 | 40 | 169 | 100 | 2979 | 15 | 9 |
| 15 | 10.8.16 17:06 | 00:24:00 | 12 | 36 | 76 | 100 | 3595 | 15 | 9 |

| | | | | | | | | | |
|----|---------------|----------|----|----|-----|-----|------|----|---|
| | 10.8.16 17:30 | | | | | | | | |
| 16 | 10.8.16 19:12 | 00:34:00 | 12 | 36 | 76 | 100 | 3514 | 15 | 9 |
| | 10.8.16 19:46 | | | | | | | | |
| 17 | 10.8.16 18:00 | 00:24:00 | 12 | 40 | 169 | 80 | 2843 | 15 | 9 |
| | 10.8.16 18:24 | | | | | | | | |
| 18 | 10.8.16 19:56 | 00:47:00 | 12 | 40 | 169 | 80 | 2860 | 15 | 9 |
| | 10.8.16 20:43 | | | | | | | | |

The duration varies on the starting and end point set by the user. The tests were performed by two different pressures and also for two different volume flows for either the falling film or the tube flow. The temperatures of the hot water circuit into the test rig were set to be 5°C above the saturation temperature depending on the pressure inside the main chamber. The cold water circuit is set to be 10°C for the test nr. 1 -12 respectively 9°C for the test nr. 13 – 18.

The tests were evaluated like the one described in chapter 6.2.1. The wetting of the falling film was quit the same throughout the whole test series and pictured in Figure 53



Figure 53: Wetting of the tubes caused by the falling film

As displayed in Figure 53 the tubes are not fully wetted. Also the irrigation is not constant over the length and columns of tubes. These circumstances deteriorate the heat transfer. Improvements that can be made are listed in chapter 2.1.3.

Test Nr.1 and 2:

Table 17: Test conditions: $p_{MC} = 23 \text{ mbar}$, $V_{Pri} = 40\%$ and $V_{MC,Sec} = 100\%$

| Conditions | | | | | | | | | |
|------------------|------------------------------|----------|----------|-----------|------------------|--------------|------|-----------------|------------------|
| Nr. | date/time | duration | p_{MC} | V_{Pri} | Re_{Γ} | $V_{MC,Sec}$ | Re | $T_{MC,Sec,In}$ | $T_{Con,Sec,In}$ |
| [-] | [D.M.Y H:MIN] | [s] | [mbar] | [%] | [-] | [%] | [-] | [°C] | [°C] |
| 1 | 9.8.16 10:57 9.8.16 11:30 | 00:33:00 | 23 | 40 | 215 | 100 | 3769 | 25 | 10 |
| 2 | 9.8.16 14:17 9.8.16 14:49 | 00:32:00 | 23 | 40 | 215 | 100 | 3684 | 25 | 10 |
| Results | | | | | | | | | |
| Nr. 1 | | | | | Nr. 2 | | | | |
| Power [kW] | | | | | Power [kW] | | | | |
| Evaporator 0,548 | | | | | Evaporator 0,644 | | | | |
| Heating 1,078 | | | | | Heating 1,144 | | | | |
| Condenser 1,162 | | | | | Condenser 1,185 | | | | |
| Cooling 1,199 | | | | | Cooling 1,213 | | | | |

Test Nr. 3 and 4:Table 18: Test conditions: $p_{MC} = 23 \text{ mbar}$, $V_{Pri} = 36\%$ and $V_{MC,Sec} = 100\%$

| Conditions | | | | | | | | | |
|------------|---------------|----------|----------|-----------|---------------|--------------|------|-----------------|------------------|
| Nr. | date/time | duration | p_{MC} | V_{Pri} | Re_{Γ} | $V_{MC,Sec}$ | Re | $T_{MC,Sec,In}$ | $T_{Con,Sec,In}$ |
| [-] | [D.M.Y H:MIN] | [s] | [mbar] | [%] | [-] | [%] | [-] | [°C] | [°C] |
| 3 | 9.8.16 12:01 | 00:33:00 | 23 | 36 | 109 | 100 | 3740 | 25 | 10 |
| | 9.8.16 12:34 | | | | | | | | |
| 4 | 9.8.16 15:23 | 00:34:00 | 23 | 36 | 109 | 100 | 4141 | 25 | 10 |
| | 9.8.16 15:57 | | | | | | | | |
| Results | | | | | | | | | |
| Nr. 3 | | | | | Nr. 4 | | | | |
| | | | Power | | | | | Power | |
| | | | [kW] | | | | | [kW] | |
| Evaporator | | | 0,347 | | Evaporator | | | 0,343 | |
| Heating | | | 1,135 | | Heating | | | 1,136 | |
| Condenser | | | 1,193 | | Condenser | | | 1,157 | |
| Cooling | | | 1,220 | | Cooling | | | 1,198 | |

Test Nr. 5 und 6:Table 19: Test conditions: $p_{MC} = 23 \text{ mbar}$, $V_{Pri} = 40\%$ and $V_{MC,Sec} = 80\%$

| Conditions | | | | | | | | | |
|------------|---------------|----------|----------|-----------|---------------|--------------|------|-----------------|------------------|
| Nr. | date/time | duration | p_{MC} | V_{Pri} | Re_{Γ} | $V_{MC,Sec}$ | Re | $T_{MC,Sec,In}$ | $T_{Con,Sec,In}$ |
| [-] | [D.M.Y H:MIN] | [s] | [mbar] | [%] | [-] | [%] | [-] | [°C] | [°C] |
| 5 | 9.8.16 13:08 | 00:34:00 | 23 | 40 | 215 | 80 | 3659 | 25 | 10 |
| | 9.8.16 13:42 | | | | | | | | |
| 6 | 9.8.16 16:30 | 00:39:00 | 23 | 40 | 215 | 80 | 3509 | 25 | 10 |
| | 9.8.16 17:09 | | | | | | | | |
| Results | | | | | | | | | |
| Nr. 5 | | | | | Nr. 6 | | | | |
| | | | Power | | | | | Power | |
| | | | [kW] | | | | | [kW] | |
| Evaporator | | | 1,431 | | Evaporator | | | 0,950 | |
| Heating | | | 1,084 | | Heating | | | 0,966 | |
| Condenser | | | 1,120 | | Condenser | | | 0,990 | |
| Cooling | | | 1,152 | | Cooling | | | 1,015 | |

Test Nr. 7 und 8:Table 20: Test conditions: $p_{MC} = 17 \text{ mbar}$, $V_{Pri} = 40\%$ and $V_{MC,Sec} = 100\%$

| Conditions | | | | | | | | | |
|------------|--------------------------------|----------|----------|-----------|---------------|--------------|------|-----------------|------------------|
| Nr. | date/time | duration | p_{MC} | V_{Pri} | Re_{Γ} | $V_{MC,Sec}$ | Re | $T_{MC,Sec,In}$ | $T_{Con,Sec,In}$ |
| [-] | [D.M.Y H:MIN] | [s] | [mbar] | [%] | [-] | [%] | [-] | [°C] | [°C] |
| 7 | 10.8.16 7:43 10.8.16 8:15 | 00:32:00 | 17 | 40 | 187 | 100 | 4388 | 20 | 10 |
| 8 | 10.8.16 11:05 10.8.16 11:42 | 00:37:00 | 17 | 40 | 187 | 100 | 3904 | 20 | 10 |
| Results | | | | | | | | | |
| Nr. 7 | | | | | Nr. 8 | | | | |
| Power | | | | | Power | | | | |
| [kW] | | | | | [kW] | | | | |
| Evaporator | | | | | Evaporator | | | | |
| 0,817 | | | | | 0,619 | | | | |
| Heating | | | | | Heating | | | | |
| 0,873 | | | | | 0,778 | | | | |
| Condenser | | | | | Condenser | | | | |
| 0,936 | | | | | 0,828 | | | | |
| Cooling | | | | | Cooling | | | | |
| 0,998 | | | | | 0,858 | | | | |

Test Nr. 9 und 10:Table 21: Test conditions: $p_{MC} = 17 \text{ mbar}$, $V_{Pri} = 36\%$ and $V_{MC,Sec} = 100\%$

| Conditions | | | | | | | | | |
|------------|--------------------------------|----------|----------|-----------|---------------|--------------|------|-----------------|------------------|
| Nr. | date/time | duration | p_{MC} | V_{Pri} | Re_{Γ} | $V_{MC,Sec}$ | Re | $T_{MC,Sec,In}$ | $T_{Con,Sec,In}$ |
| [-] | [D.M.Y H:MIN] | [s] | [mbar] | [%] | [-] | [%] | [-] | [°C] | [°C] |
| 9 | 10.8.16 8:43 10.8.16 9:24 | 00:41:00 | 17 | 36 | 83 | 100 | 4419 | 20 | 10 |
| 10 | 10.8.16 12:05 10.8.16 12:48 | 00:43:00 | 17 | 36 | 83 | 100 | 4375 | 20 | 10 |
| Results | | | | | | | | | |
| Nr. 9 | | | | | Nr. 10 | | | | |
| Power | | | | | Power | | | | |
| [kW] | | | | | [kW] | | | | |
| Evaporator | | | | | Evaporator | | | | |
| 0,263 | | | | | 0,251 | | | | |
| Heating | | | | | Heating | | | | |
| 0,889 | | | | | 0,808 | | | | |
| Condenser | | | | | Condenser | | | | |
| 0,949 | | | | | 0,859 | | | | |
| Cooling | | | | | Cooling | | | | |
| 0,975 | | | | | 0,881 | | | | |

Test Nr. 11 und 12:Table 22: Test conditions: $p_{MC} = 17 \text{ mbar}$, $V_{Pri} = 40\%$ and $V_{MC,Sec} = 80\%$

| Conditions | | | | | | | | | |
|------------|--------------------------------|----------|----------|-----------|---------------|--------------|------|-----------------|------------------|
| Nr. | date/time | duration | p_{MC} | V_{Pri} | Re_{Γ} | $V_{MC,Sec}$ | Re | $T_{MC,Sec,In}$ | $T_{Con,Sec,In}$ |
| [-] | [D.M.Y H:MIN] | [s] | [mbar] | [%] | [-] | [%] | [-] | [°C] | [°C] |
| 11 | 10.8.16 9:55 10.8.16 10:47 | 00:52:00 | 17 | 40 | 187 | 80 | 3111 | 20 | 10 |
| 12 | 10.8.16 13:14 10.8.16 14:03 | 00:49:00 | 17 | 40 | 187 | 80 | 3036 | 20 | 10 |
| Results | | | | | | | | | |
| Nr. 1 | | | | | Nr. 2 | | | | |
| Power | | | | | Power | | | | |
| [kW] | | | | | [kW] | | | | |
| Evaporator | | | | | Evaporator | | | | |
| 0,514 | | | | | 0,497 | | | | |
| Heating | | | | | Heating | | | | |
| 0,627 | | | | | 0,598 | | | | |
| Condenser | | | | | Condenser | | | | |
| 0,675 | | | | | 0,656 | | | | |
| Cooling | | | | | Cooling | | | | |
| 0,690 | | | | | 0,684 | | | | |

Test Nr. 13 und 14:Table 23: Test conditions: $p_{MC} = 12 \text{ mbar}$, $V_{Pri} = 40\%$ and $V_{MC,Sec} = 100\%$

| Conditions | | | | | | | | | |
|------------|--------------------------------|----------|----------|-----------|---------------|--------------|------|-----------------|------------------|
| Nr. | date/time | duration | p_{MC} | V_{Pri} | Re_{Γ} | $V_{MC,Sec}$ | Re | $T_{MC,Sec,In}$ | $T_{Con,Sec,In}$ |
| [-] | [D.M.Y H:MIN] | [s] | [mbar] | [%] | [-] | [%] | [-] | [°C] | [°C] |
| 13 | 10.8.16 15:04 10.8.16 16:11 | 01:07:00 | 12 | 40 | 169 | 100 | 3683 | 15 | 9 |
| 14 | 10.8.16 18:34 10.8.16 19:05 | 00:31:00 | 12 | 40 | 169 | 100 | 2979 | 15 | 9 |
| Results | | | | | | | | | |
| Nr. 13 | | | | | Nr. 14 | | | | |
| Power | | | | | Power | | | | |
| [kW] | | | | | [kW] | | | | |
| Evaporator | | | | | Evaporator | | | | |
| 0,111 | | | | | 0,133 | | | | |
| Heating | | | | | Heating | | | | |
| 0,770 | | | | | 0,543 | | | | |
| Condenser | | | | | Condenser | | | | |
| 0,889 | | | | | 0,650 | | | | |
| Cooling | | | | | Cooling | | | | |
| 0,985 | | | | | 0,686 | | | | |

Test Nr. 15 und 16:Table 24: Test conditions: $p_{MC} = 12 \text{ mbar}$, $V_{Pri} = 36\%$ and $V_{MC,Sec} = 100\%$

| Conditions | | | | | | | | | |
|------------|---------------|----------|----------|-----------|---------------|--------------|------|-----------------|------------------|
| Nr. | date/time | duration | p_{MC} | V_{Pri} | Re_{Γ} | $V_{MC,Sec}$ | Re | $T_{MC,Sec,In}$ | $T_{Con,Sec,In}$ |
| [-] | [D.M.Y H:MIN] | [s] | [mbar] | [%] | [-] | [%] | [-] | [°C] | [°C] |
| 15 | 10.8.16 17:06 | 00:24:00 | 12 | 36 | 76 | 100 | 3595 | 15 | 9 |
| | 10.8.16 17:30 | | | | | | | | |
| 16 | 10.8.16 19:12 | 00:34:00 | 12 | 36 | 76 | 100 | 3514 | 15 | 9 |
| | 10.8.16 19:46 | | | | | | | | |
| Results | | | | | | | | | |
| Nr. 15 | | | | | Nr. 16 | | | | |
| Power | | | | | Power | | | | |
| [kW] | | | | | [kW] | | | | |
| Evaporator | | | | | Evaporator | | | | |
| 0,210 | | | | | 0,163 | | | | |
| Heating | | | | | Heating | | | | |
| 0,622 | | | | | 0,615 | | | | |
| Condenser | | | | | Condenser | | | | |
| 0,734 | | | | | 0,658 | | | | |
| Cooling | | | | | Cooling | | | | |
| 0,758 | | | | | 0,749 | | | | |

Test Nr. 17 und 18:Table 25: Test conditions: $p_{MC} = 12 \text{ mbar}$, $V_{Pri} = 40\%$ and $V_{MC,Sec} = 80\%$

| Conditions | | | | | | | | | |
|------------|---------------|----------|----------|-----------|---------------|--------------|------|-----------------|------------------|
| Nr. | date/time | duration | p_{MC} | V_{Pri} | Re_{Γ} | $V_{MC,Sec}$ | Re | $T_{MC,Sec,In}$ | $T_{Con,Sec,In}$ |
| [-] | [D.M.Y H:MIN] | [s] | [mbar] | [%] | [-] | [%] | [-] | [°C] | [°C] |
| 17 | 10.8.16 18:00 | 00:24:00 | 12 | 40 | 169 | 80 | 2843 | 15 | 9 |
| | 10.8.16 18:24 | | | | | | | | |
| 18 | 10.8.16 20:07 | 00:36:00 | 12 | 40 | 169 | 80 | 2870 | 15 | 9 |
| | 10.8.16 20:43 | | | | | | | | |
| Results | | | | | | | | | |
| Nr. 17 | | | | | Nr. 18 | | | | |
| Power | | | | | Power | | | | |
| [kW] | | | | | [kW] | | | | |
| Evaporator | | | | | Evaporator | | | | |
| 0,105 | | | | | 0,096 | | | | |
| Heating | | | | | Heating | | | | |
| 0,532 | | | | | 0,517 | | | | |
| Condenser | | | | | Condenser | | | | |
| 0,653 | | | | | 0,603 | | | | |
| Cooling | | | | | Cooling | | | | |
| 0,692 | | | | | 0,635 | | | | |

All these results have the same error in common: the evaporation performance will be neglected for the further investigation.

6.3 Evaluation

For the evaluation the mean value of the condenser of each test with the same conditions will be taken.

Comparison on the basis of the pressure:

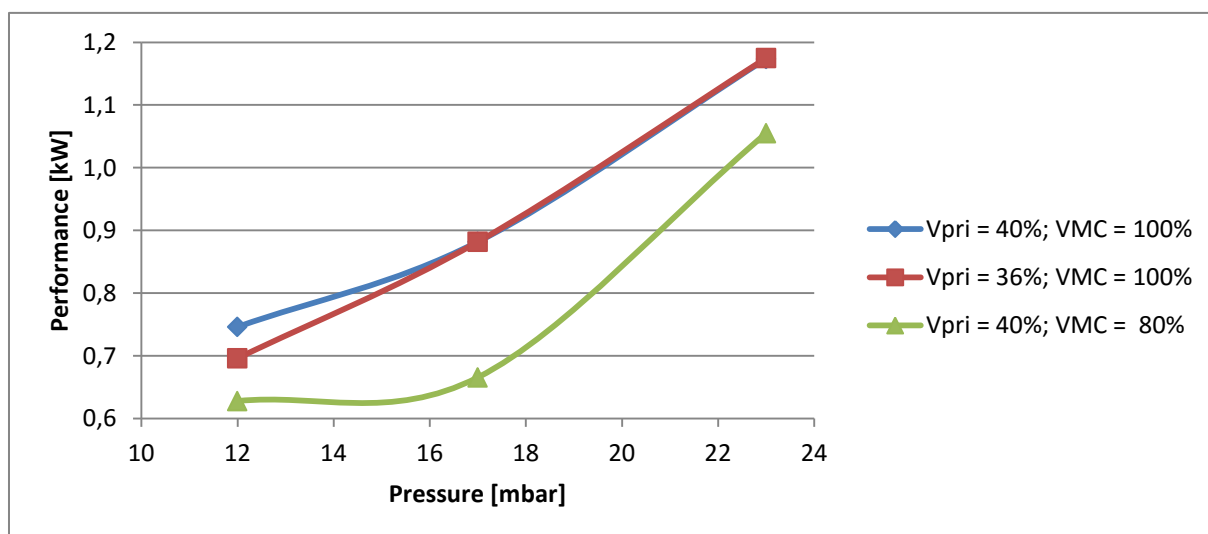


Figure 54: Performance of the evaporator based on the ambient pressure

The performance decreases with the decrease of the ambient pressure.

Comparison on the basis to the irrigation:

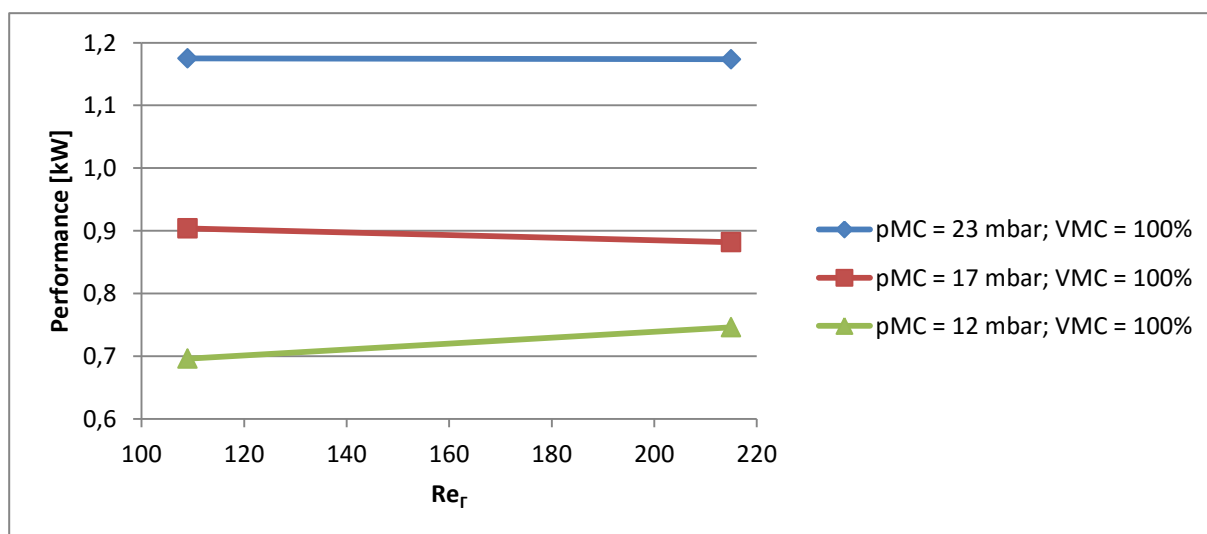


Figure 55: Performance of the evaporator based on the irrigation density

It seems that the influence of the irrigation density can be neglected as for both the irrigations the falling film couldn't moisten the tubes completely.

Comparison on the basis to the tube flow:

It turned out that the pump for the tube flow does not work properly as the volume flow differs too much when either adjusted for 100% or 80% of the power. Even so a hint on the performance for either the 100% or the 80% can be given as seen in Figure 56.

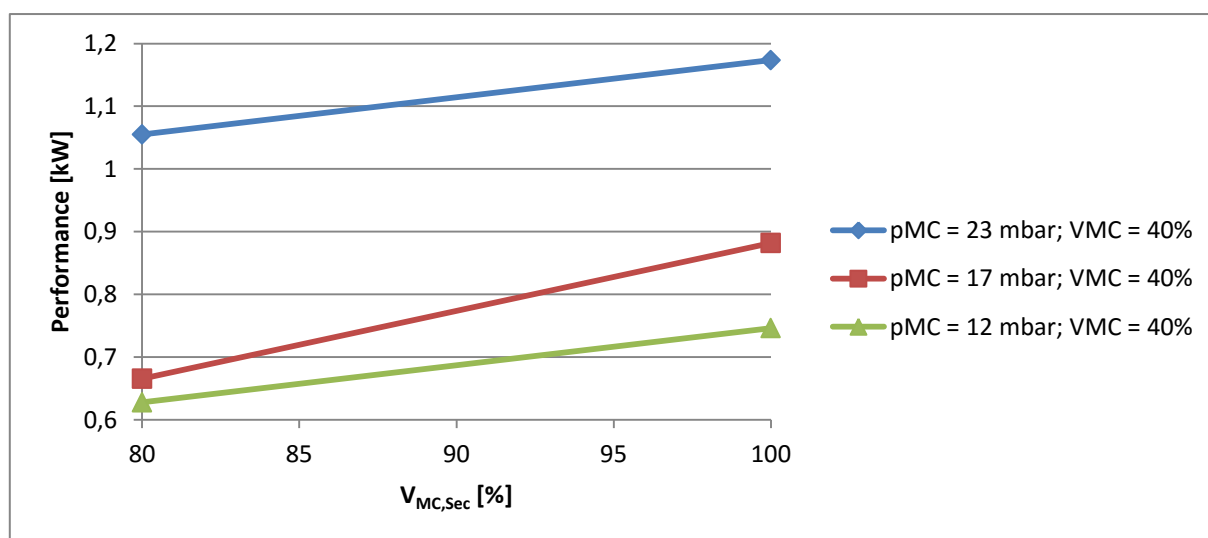


Figure 56: Performance of the evaporator based on the tube flow

6.4 Comparison of the theoretical calculation to the experiment

This chapter will compare the theoretical approach by Lorenz and Yung used to define the dimensions for the main chamber to the experimental results, investigated by the tests performed within this thesis.

As the investigated tube bundle and the circumstances differ from the calculation in chapter 3, a new approach for the theoretical heat flux has to be derived.

The tube bundle specifications are stated in Table 26.

Table 26: Tube bundle specifications

| Tube | | Bundle | |
|----------------|----------|---------|-------|
| d_i | 12,7 mm | Rows | 3 - |
| d_o | 11,5 mm | Columns | 8 - |
| λ_{Cu} | 400 W/mK | Length | 0,4 m |

The heat fluxes for the different test circumstances have been calculated similar to the one derived for the proportions of the main chamber. Furthermore the Nusselt Number and the heat transfer resistance have been added for a better comparison. The results of the theoretical calculation and the experimental analysis are summarized in Table 27 which is stated in the appendix.

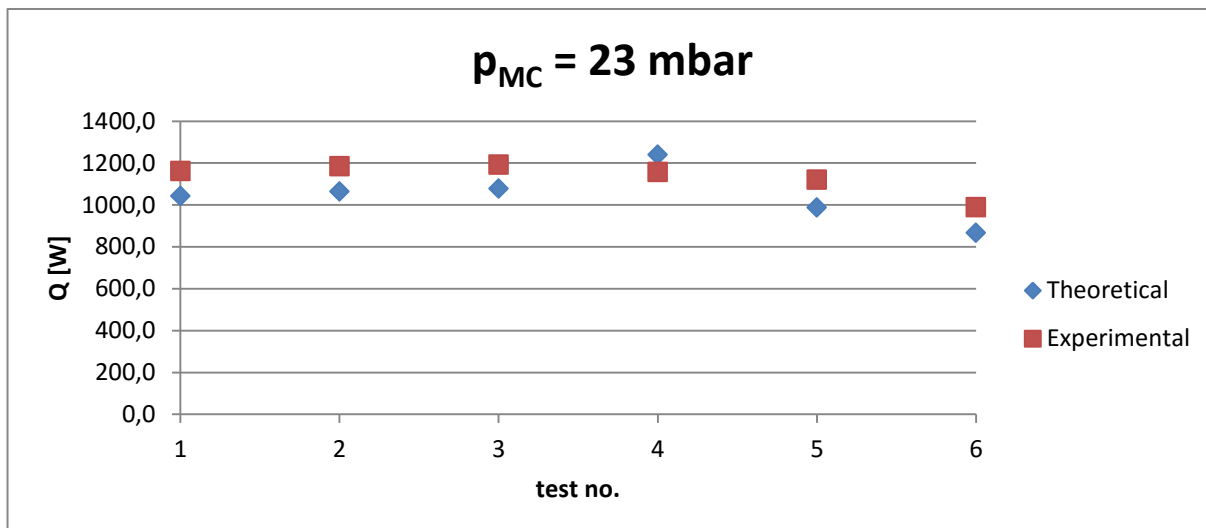


Figure 57: Theoretical and Experimental heat flux at 23 mbar

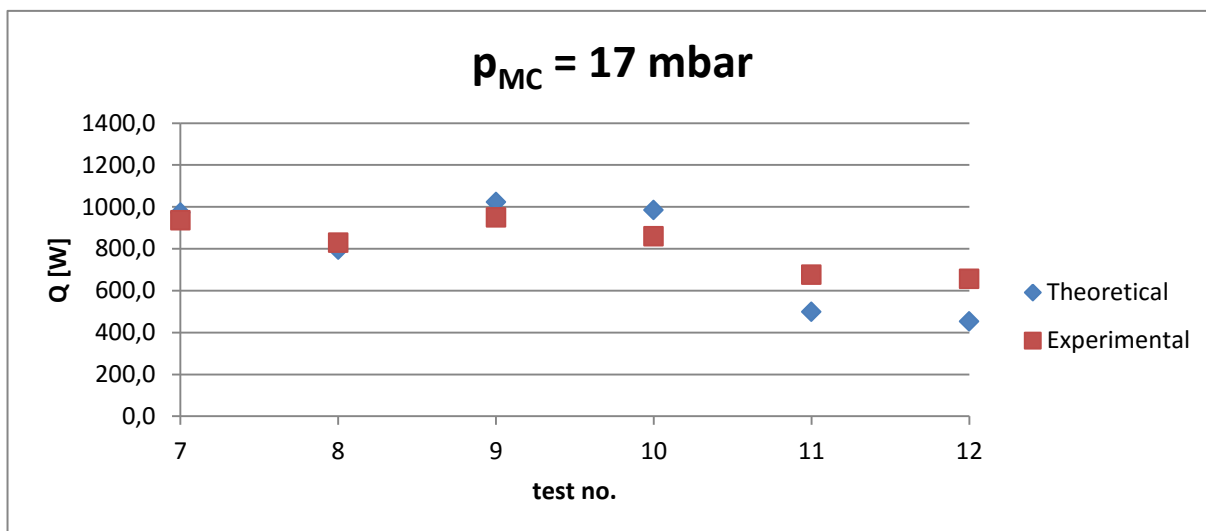


Figure 58: Theoretical and Experimental heat flux at 17 mbar

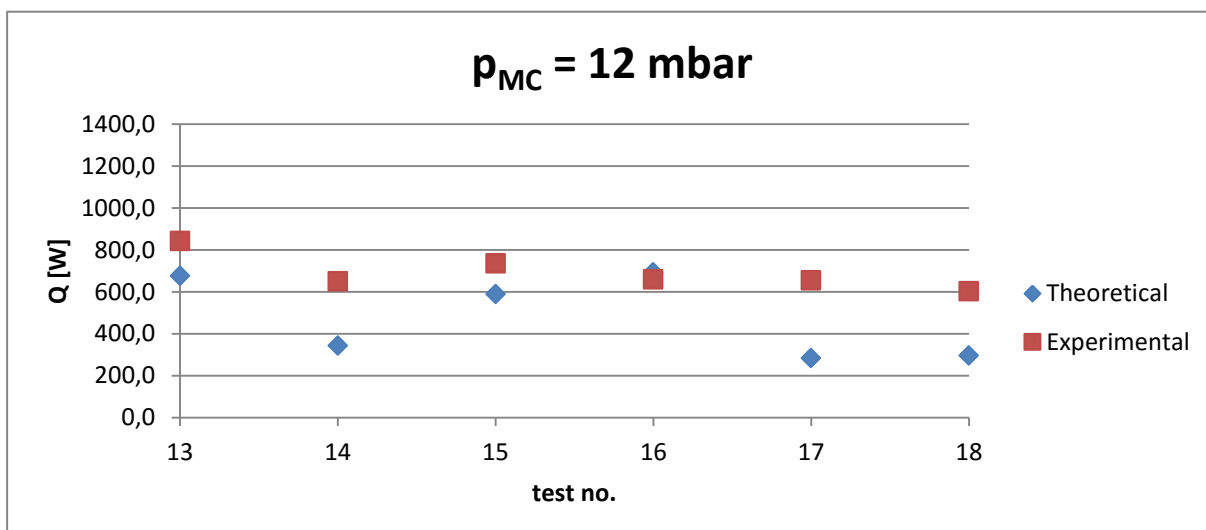


Figure 59: Theoretical and Experimental heat flux at 12 mbar

Figure 57 – 59 displays the theoretical derived results compared to the results of the experiments. As seen does the theoretical approach fit well for those conditions even if the circumstances do not match those where Lorenz and Yung defined it. Also the theoretical heat flux decreases by the decreasing pressure conditions as a result of the changing material values included in this approach.

There are just two uncertainties that cannot be calculated theoretical. First the dry spots for the falling film (displayed in Figure 53) and second the turbulence inside the tubes caused by the distribution at the beginning and the bends throughout the tube bundle.

Both those aspects cause the theoretical calculation to vary from the experimental data's. As the distributor and the bends promote the turbulence inside the tube bundle the inner heat transfer coefficient and therefore the heat flux should be higher compared to the theoretical one. The influence caused by the turbulence can be shown on the basis of the Nusselt Number recorded in Table 27 and displayed in Figure 60.

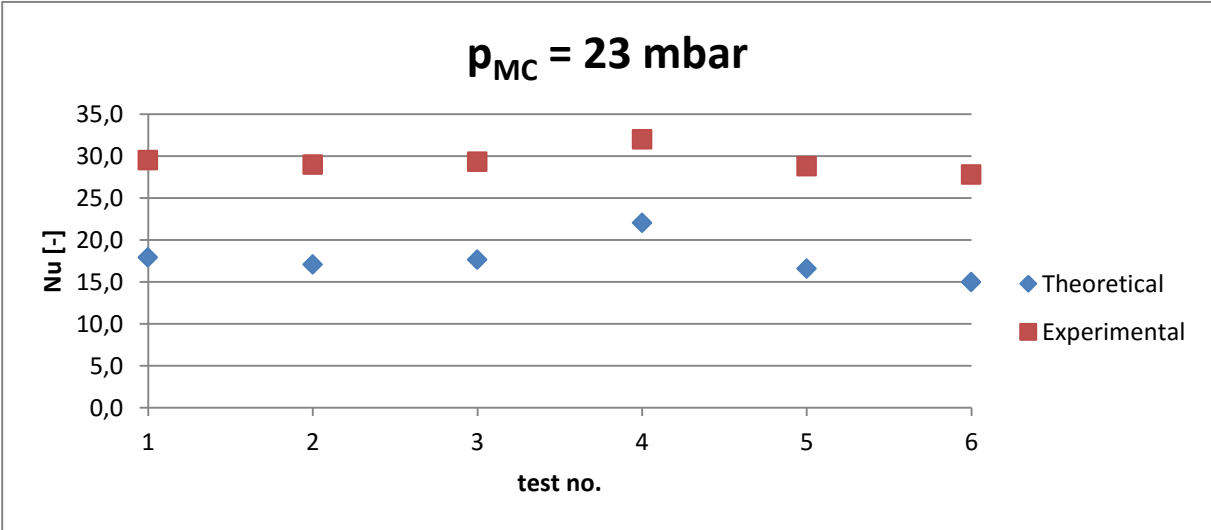


Figure 60: Theoretical and Experimental Nusselt Number at 23 mbar

In contrast the dry spots decrease the outer heat transfer coefficient during the experiment compared to the theoretical calculation as displayed in Figure 61. The dry spots do not contribute to the surface area available for the evaporation.

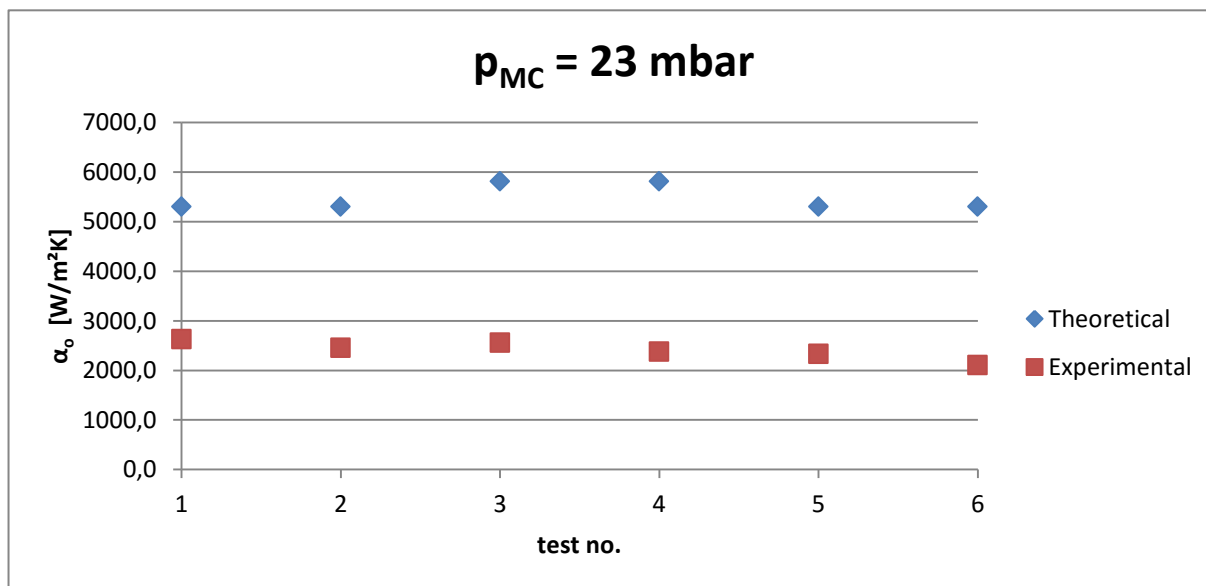


Figure 61 Theoretical and Experimental outer heat transfer coefficient at 23 mbar:

Both those discrepancies cannot be calculated theoretically causing the theoretical approach to have these two insecurities. But their impact can be decreased as followed:

The higher the turbulence inside the tube bundle the smaller the impact of the distributor and the bends. The conditions of the tube flow performed in this thesis resulted theoretically in the transition area between the laminar flow and the turbulent flow. This means that even the slightest distraction has a significant impact on the flow regime and therefore the inner heat transfer coefficient.

The dry spots can be avoided by altering the surface of the tubes. The tube bundle in those tests was made out of plane copper tubes. The steps to improve the wetting of the tubes surface can for example be to roughen up the surface or adding a structure onto the tube. A more detailed description to encourage the wetting is listed in chapter 2.1.3.

7 Summary

The purpose of this master thesis is to take a facility to test evaporation concepts at low pressure conditions into operation. On the basis of the derived theoretical foundations a concept has been chosen which led to the dimensions of this test rig. The evaporation concept and all the consisting parts were implemented in FreeCAD program on which the orders were performed. After assembling the parts the test rig has been started up and the measurement and control was adjusted. Besides the manual operation an automation protocol was implemented which runs test for dictated conditions. At the end tests consisting on the falling film principle were performed to proof the functionality of this facility. The tests demonstrated the functionality and showed possibilities to improve this facility. Changing the pumps in the hot and cold water circuit to provide a constant volume flow and fine tuning of the control unit to decrease the fluctuation during the measurements will lead to a more precise measurement. Even if the tests show unsteadiness caused by the previous mentioned issues the tendencies of the different conditions could have been approximated. As in the decrease of the pressure conditions or the tube flow inside the tube bundle also decreases the performance of the evaporator. At last the tests performed within this master thesis were compared to the theoretical approach used to define the dimensions of this facility. This leads to the conclusion that the theoretical approach fits quiet well to the real behavior if the uncertainties described at last are taken into account.

8 Appendix

8.1 Measurement and control

8.1.1 Sensors

| Description | Function | Measurement targets |
|----------------------|--|---|
| T_{Amb} | Indicator for the dissipation. | Environmental temperature |
| $T_{MC1/MC2/MC}$ | Records the temperature of the vapour. In combination with the pressure of the vessel results in the saturation pressure or indicates a sub cooled/superheated boiling Or indicates inert gases in the system | Operation conditions |
| T_{MC3} | Records the temperature of the liquid water while testing the pool boiling or capillary evaporation. It is not needed for the liquid falling film evaporation. | Water temperature in the vessel (pool boiling, capillary evaporation) |
| $T_{MC...}$ | Some more connections are implemented in order to further investigation | Backup connections for temperature sensors |
| p_{MC} | Records the pressure of the water vapour. | Operation conditions |
| $T_{MC,Pri,In}$ | Temperature measurement of the primary stream into the distributor or the pool if pool boiling its investigated. With $T_{MC,Pri,Out}$ the heat flow can be established if the water is overheated/sub cooled This temperature is also needed to vary the performance of the heating rod. => Preconditioning to reach the saturation vapour pressure. | Evaporator/Condenser heat flux $Q = f(m, \Delta T, h_v, h)$ |
| $T_{MC,Pri,Out}$ | The temperature at the bottom of the vessel is needed to determine the temperature of the condensate. | Evaporator/Condenser heat flux $Q = f(m, \Delta T, h_v, h)$ |
| $T_{MC,Sec,Out/In}$ | Temperature difference is needed to determine the evaporator heat flux | Evaporator heat flux $Q = f(m, \Delta T, h_v, h)$ |
| $T_{Con,Sec,Out/In}$ | Temperature difference is needed to determine the condenser heat flux | Condenser heat flux $Q = f(m, \Delta T, h_v, h)$ |
| T_{Vapor} | Temperature of the vapour stream | As it should be saturation temperature it can be used to allocate the pressure drop between the main chamber and the plate heat exchanger |

| | | |
|------------------------------|---|---------------|
| $T_{\text{Heat,Pri,Out/In}}$ | Regulation of the heating stream from the labor | Heating power |
| $T_{\text{Cool,Pri,Out/In}}$ | Regulation of the cooling stream from the labor | Cooling power |

8.1.2 Valves

| Description | Function | Valve position |
|-------------------------------------|---|---|
| $V_{\text{MC,V}}$ | Is used to connect the vacuum pump to the system. | Is opened while a vacuum is created |
| $V_{\text{MC,D}}$ | Separates the evaporator of the condenser | Closing $V_{\text{MC,V}}$, $V_{\text{Pri,MK,Ein}}$ and $V_{\text{Pri,MK,Aus}}$ before opening the main chamber prevents the whole setup from losing the vacuum |
| $V_{\text{MC,Pri,In}}$ | Locks the inflow to the vessel. | The chamber which does not evaporate has its valve closed while the evaporating chamber has its valve opened. |
| $V_{\text{MC,Pri,Out/Con,Pri,Out}}$ | Locks the inflow to the reservoir. | see $V_{\text{MC,V}}$ |
| $V_{\text{V1/V2}}$ | Separates the tank and the measurement vessel. | Is opened to increase the observation time. small heat flux => valve closed big heat flux => valve opened |
| $V_{\text{V1,Out/V2,Out}}$ | Blocks off the reservoir from the primary cycle. | Depends on the operation conditions: Unsteady: both opened Steady: the valve beneath the condensing vessel gets closed |

8.1.3 Level Indicator and mass balance

| Description | Function | Measurement targets |
|--------------------|--|--|
| $H_{\text{V1/V2}}$ | Level indicator to dedicate the condensed/evaporated volume. | Evaporator/Condenser heat flux $Q = f(m, \Delta T, h_v, h)$ |
| $m_{\text{R1/R2}}$ | Weight measuring of the condensed/evaporated mass of water. | Evaporator/Condenser heat flux $Q = f(m, \Delta T, h_v, h)$ |

8.1.4 Heat meter

| Description | Function | Energy demand |
|----------------------|---|--|
| $\dot{Q}_{MC,Sec}$ | Controls the temperature of the liquid stream into the investigated heat exchanger. | operation conditions |
| $\dot{Q}_{Con,Sec}$ | Controls the temperature of the liquid into the plate heat exchanger. | Operation conditions |
| $\dot{V}_{MC,Sec}$ | Volume flow inside the tubes. Controls the fluid stream and also the pattern of the stream. | Evaporator/Condenser heat flux $Q = f(m, \Delta T, hv, h)$ inner heat transfer coefficient $\alpha_i = f(Re)$ |
| $\dot{V}_{Con,Sec}$ | Volume flow inside the tubes. Controls the fluid stream and also the pattern of the stream. | Evaporator/Condenser heat flux $Q = f(m, \Delta T, hv, h)$ inner heat transfer coefficient $\alpha_i = f(Re)$ |
| $\dot{V}_{Heat,Pri}$ | Measures the flow into the plate heat exchangers for the heating step. | Operation conditions |
| $\dot{Q}_{Heat,Pri}$ | Heat flux of the heating side of the laboratory. | |
| $\dot{V}_{Cold,Pri}$ | Measures the flow into the plate heat exchangers for the heating step. | Operation conditions |
| $\dot{Q}_{Cold,Pri}$ | Heat flux of the cooling side of the laboratory. | |

8.1.5 Splitter

| Description | Function |
|----------------------|--|
| $\dot{V}_{Heat,Pri}$ | Regulates the flow circulating in the hot water supply side |
| $\dot{V}_{Cold,Pri}$ | Regulates the flow circulating in the cold water supply side |





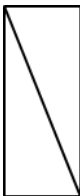
8.1.6 Pump

| Description | Function | Target |
|----------------|--|---|
| P_{pri} | Regulation of the liquid flow. | Irrigation density for the falling film Liquid level of the pool for pool boiling or capillary evaporation |
| $P_{MC,Sec}$ | Regulation of the liquid flow into the main chamber. | Heat flux regulation |
| $P_{Con,Sec}$ | Regulation of the liquid flow into the plate heat exchanger. | Heat flux and pressure regulation |
| $P_{Heat,Pri}$ | Regulation of the liquid flow into the plate heat exchanger. | Heat flux and pressure regulation |
| $P_{Cold,Pri}$ | Regulation of the liquid flow into the plate heat exchanger. | Heat flux and pressure regulation |

8.2 Symbol directory

| Symbol | Unit | designation |
|------------------------------|--------------------|---------------------------|
| ϑ | °C | temperature |
| \dot{m} | kg/s | mass flow |
| m | kg | mass |
| q | W/m ² | heat flux density |
| δ | m | boundary layer |
| \dot{Q} | W | heat flux |
| c_p | J/kgK | heat capacity |
| T | K | absolute Temperature |
| k | W/m ² K | heat transfer resistance |
| α | W/m ² K | heat transfer coefficient |
| A | m ² | surface |
| Re | - | Reynolds |
| Nu | . | Nusselt |
| Pr | - | Prandtl |
| Re_r | - | irrigation density |
| Γ | kg/ms | irrigation |
| n | - | number |
| ρ | kg/m ³ | density |
| μ | kg/ms | dynamic viscosity |
| ν | m ² /s | static viscosity |
| λ | W/mK | thermal conductivity |
| Δh_v | kJ/kg | evaporation enthalpy |
| P | W | performance |
| \dot{V} | m ³ /s | volume flow |
| H | m | height |
| Superscripted Indices | | designation |
| krit | | critical |
| W | | wall |
| FF | | falling film |
| TF | | tube flow |

| | |
|-------|-------------------------|
| evap | evaporate |
| In | inlet |
| Out | outlet |
| i | inside |
| o | outside |
| In | logarithmic |
| dev | developing region |
| lam | laminar |
| trans | transition area |
| turb | turbulent |
| In | natural logarithmic |
| sec | secondary |
| mean | mean value |
| nb | nucleate boiling |
| dev | convective film heating |
| l | liquid |
| Wi | wall inner temperature |
| Cu | copper |
| MC | main chamber |
| Cond | condenser |
| Pri | primary |
| Sec | secondary |
| Res | reservoir |
| B | bend |
| S | suction |
| meas | measured |
| calc | calculated |
| HM | heat meter |

| Graphical symbol | designation |
|---|--------------------------------------|
|  | pump |
|  | heat meter / volume flow measurement |
|  | splitter |
|  | valve |
|  | plate heat exchanger |

8.3 List of Equations

8.3.1 Heat loss calculation

$$k_{Steel} = \left(\frac{(2 * s_p + d)}{2 * \lambda_{Steel}} * \ln \frac{(2 * s_p + d)}{d} \right)^{-1} \quad (7.3.1.1)$$

$$k_{ins} = \left(\frac{(2 * s_p + d + 2 * s_{ins})}{2 * \lambda_{ins}} * \ln \frac{(2 * s_p + d + 2 * s_{ins})}{d + 2 * s_p} \right)^{-1} \quad (7.3.1.2)$$

$$T_{P/ins} = \frac{k_{Steel} * A_p * T_{vapour} + k_{ins} * A_{ins} * T_{Amb}}{k_{Steel} * A_p + k_{ins} * A_{ins}} \quad (7.3.1.3)$$

$$Q = k_{Steel} * A_p * (T_{P/ins} - T_{vapour}) \quad (7.3.1.4)$$

8.3.2 Pump calculation

$$H_A = H_{Pressure} + H_{Velocity} + H_{max} + H_L \quad (7.3.2.1)$$

$$H_{Pressure} = \frac{p_{Outlet} - p_{Inlet}}{\rho * g} \quad (7.3.2.2)$$

$$H_{Geschw} = \frac{v_{Outlet}^2 - v_{Inlet}^2}{\rho * g} \quad (7.3.2.3)$$

$$H_L = H_{L,Velocity} + H_{L,Bend} + H_{L,In/Out} \quad (7.3.2.4)$$

$$H_{V,Velocity} = \lambda * \frac{L}{d} * \frac{v^2}{2 * g} \quad (7.3.2.4)$$

$$H_{V,Bend} = p_{CS} * \zeta_{Bend} * \frac{v^2}{2 * g} \quad (7.3.2.4)$$

$$H_{V,In/Out} = (\zeta_{In} + \zeta_{Out}) * \frac{v^2}{2 * a} \quad (7.3.2.4)$$

$$H_{cav} = NPSH_{Facility} - \frac{p_{Outlet} - p_{Inlet}}{\rho * g} - H_{A,max,SSide} \quad (7.3.2.4)$$

$$H_{A,max,SSide} = \frac{L_{SSide}}{L} * H_{L,Velocity} + \frac{n_{SSide}}{n} * H_{V,Bend} + \zeta_E * \frac{v^2}{2 * g} \quad (7.3.2.5)$$

8.4 Allocation of the variables to determine the performance

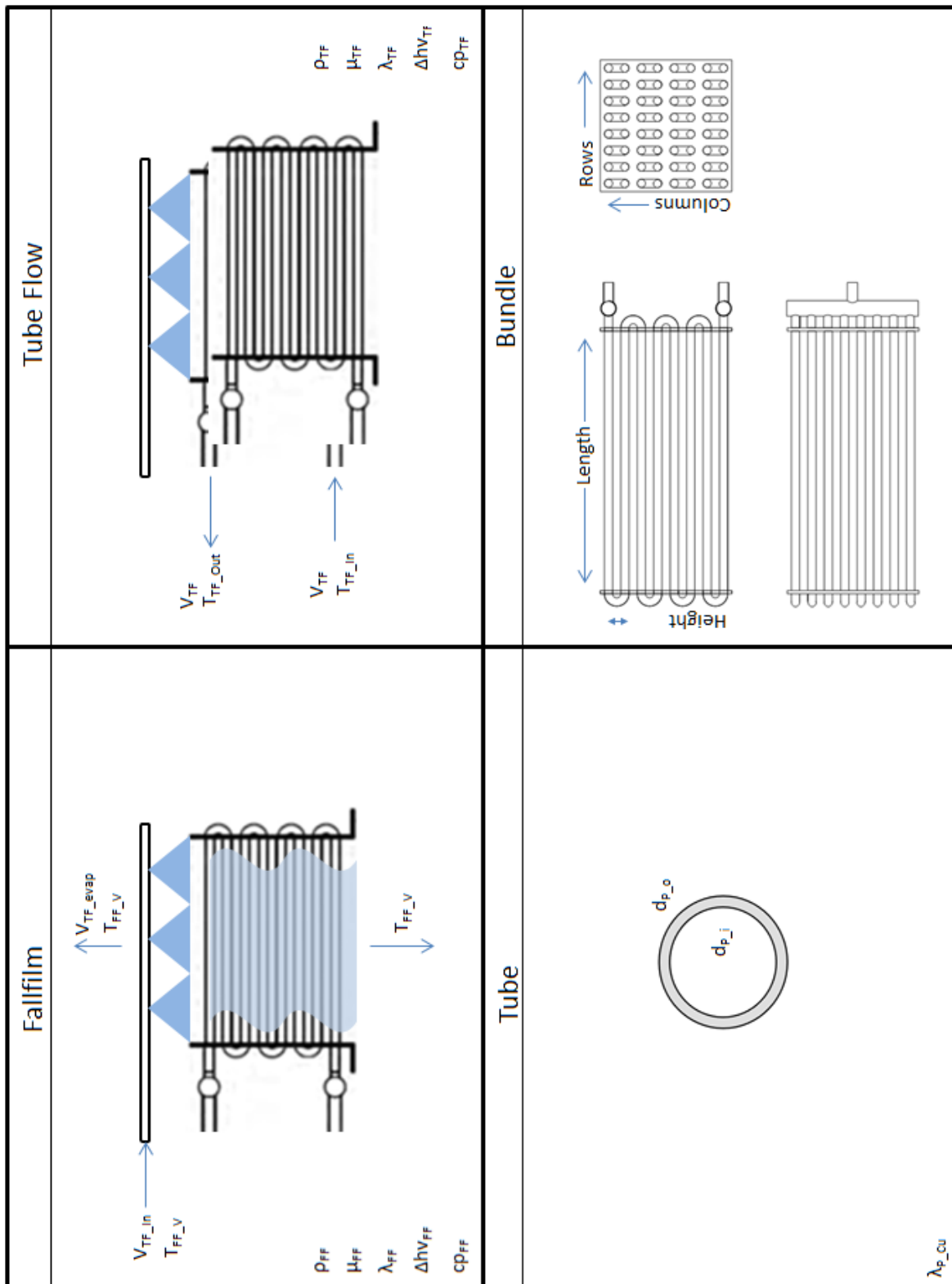


Figure 62: Adjusted parameters design

8.5 Illustrations of the several test rig components

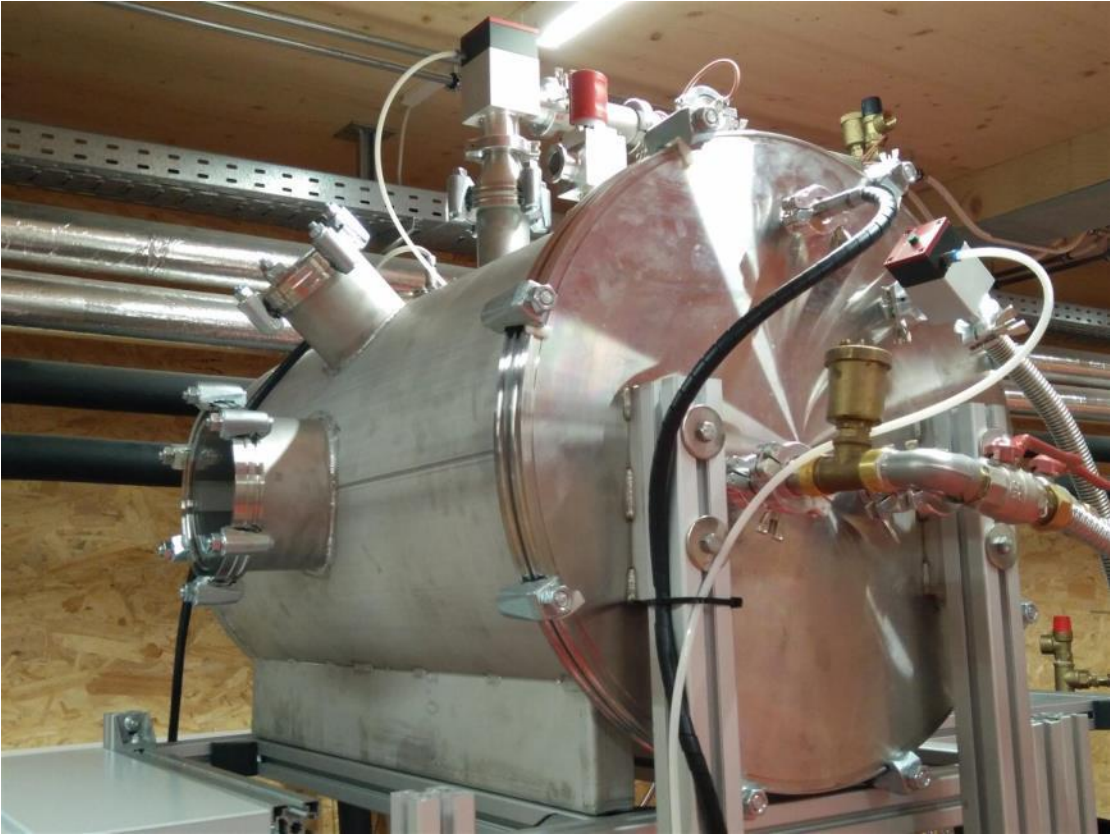


Figure 63: Main chamber

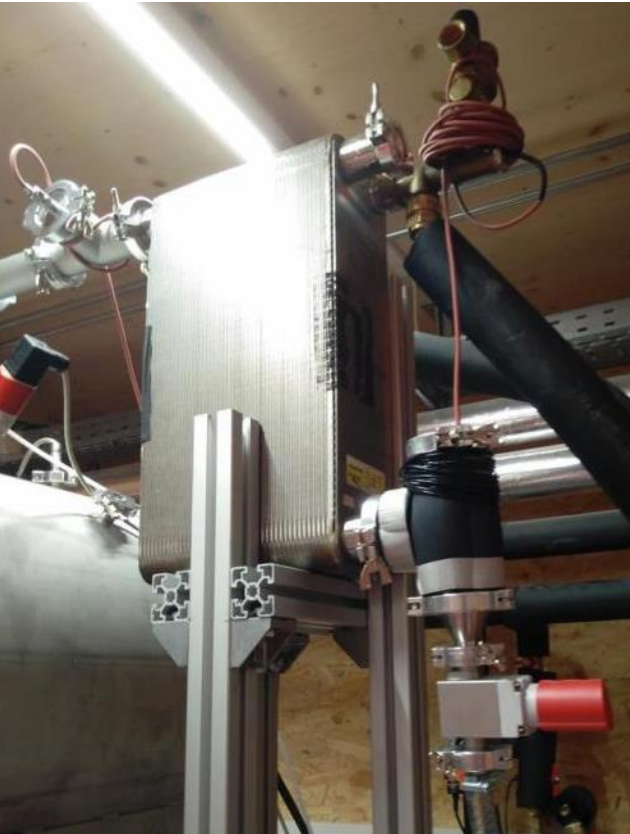


Figure 64: Plate heat exchanger on the left and Reservoir II on the right side of this figure (Reservoir I is built identical)

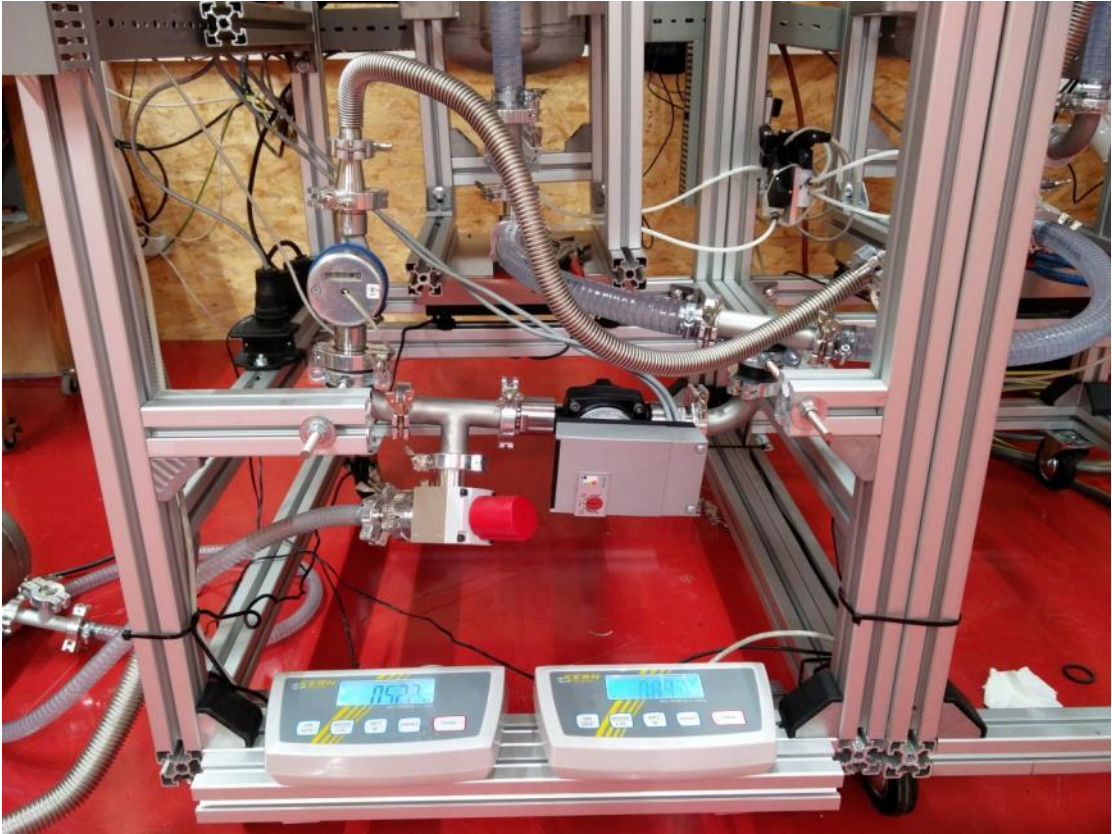


Figure 65: Connection to the chamber and the water tank



Figure 66: Hot and cold water circuit, on the right side connected to the test rig, on the left side connected to the labor

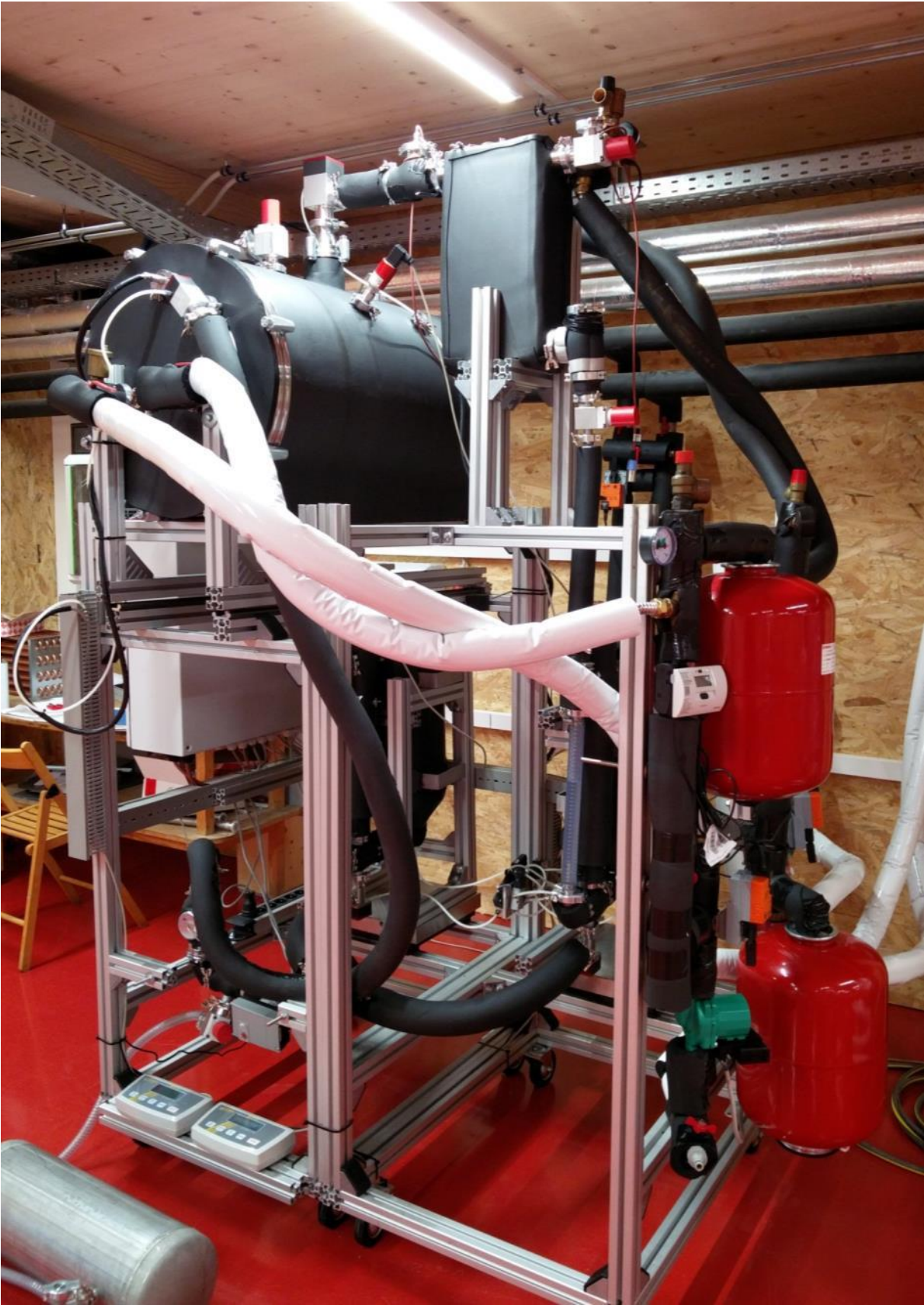


Figure 67: Insulated test rig

8.6 Dimensioning of the tube bundle

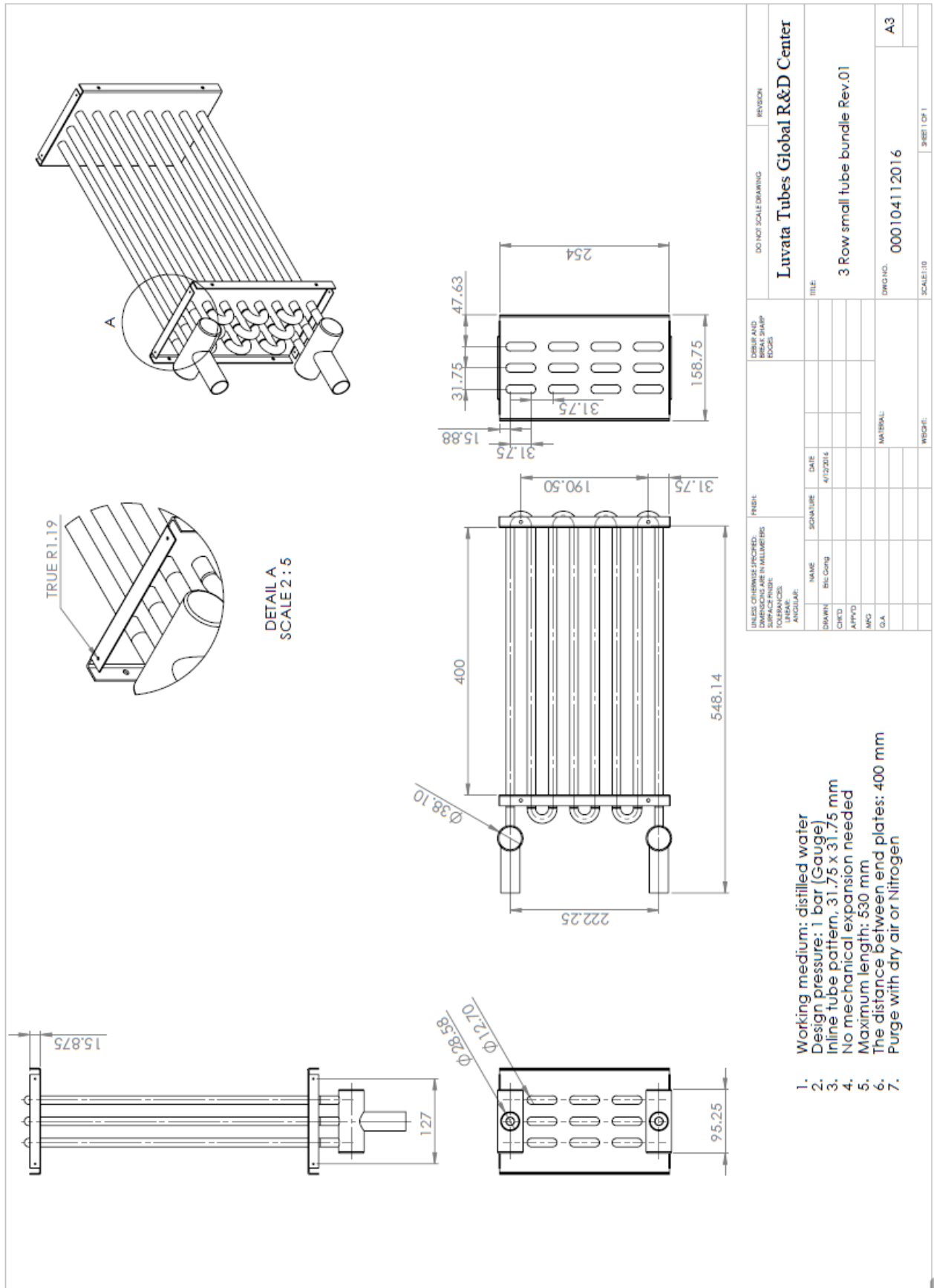


Figure 68: Sketch of the distributor provided by Luvata™

8.7 Comparison of the theoretical calculations to the experimental evaluated tests

Table 27: Comparison of the theoretical calculations to the experimental evaluated tests

| Test Nr. [-] | Conditions | | | Theoretical | | | | | Experimental | | | | |
|-----------------|---------------|-------------|----------------|------------------------------------|-----------|------------------------------------|---------------------------|----------|------------------------------------|-----------|------------------------------------|---------------------------|----------|
| | pMC [mbar] | Vpri [%] | VMC,Sec [%] | α_i [W/m ² K] | Nu [-] | α_o [W/m ² K] | k [W/m ² K] | Q [W] | α_i [W/m ² K] | Nu [-] | α_o [W/m ² K] | k [W/m ² K] | Q [W] |
| 1 | 23 | 40 | 100 | 945 | 17,9 | 5305,9 | 735,9 | 1042,2 | 1513,7 | 29,5 | 2630,0 | 899,8 | 1162,25 |
| 2 | 23 | 40 | 100 | 901 | 17,1 | 5305,9 | 706,4 | 1063,4 | 1486,8 | 29,0 | 2457,7 | 868,7 | 1185,1 |
| 3 | 23 | 36 | 100 | 931 | 17,6 | 5814,1 | 735,5 | 1077,7 | 1504,9 | 29,3 | 2563,7 | 888,5 | 1192,6 |
| 4 | 23 | 36 | 100 | 1163 | 22,0 | 5814,1 | 890,2 | 1240,1 | 1640,7 | 32,0 | 2383,1 | 913,8 | 1157,3 |
| 5 | 23 | 40 | 80 | 875 | 16,6 | 5305,9 | 688,9 | 986,8 | 1476,9 | 28,8 | 2334,2 | 849,1 | 1120,5 |
| 6 | 23 | 40 | 80 | 790 | 15,0 | 5305,9 | 629,7 | 866,2 | 1425,0 | 27,8 | 2107,0 | 799,3 | 989,6 |
| 7 | 17 | 40 | 100 | 1292,1 | 24,9 | 5191,9 | 953,4 | 971,9 | 1799,7 | 35,1 | 2062,1 | 909,0 | 935,8 |
| 8 | 17 | 40 | 100 | 1011,5 | 19,5 | 5191,9 | 777,6 | 795,1 | 1632,0 | 31,8 | 1830,4 | 816,6 | 827,9 |
| 9 | 17 | 36 | 100 | 1315,2 | 25,3 | 5780,5 | 985,9 | 1021,9 | 1812,4 | 35,3 | 2125,9 | 924,8 | 949,0 |
| 10 | 17 | 36 | 100 | 1292,7 | 24,9 | 5780,5 | 972,0 | 983,9 | 1798,9 | 35,1 | 1953,3 | 887,0 | 858,6 |
| 11 | 17 | 40 | 80 | 535,3 | 10,3 | 5191,9 | 443,0 | 498,8 | 1350,0 | 26,3 | 1559,7 | 684,6 | 675,1 |
| 12 | 17 | 40 | 80 | 487,3 | 9,4 | 5191,9 | 406,4 | 452,2 | 1322,9 | 25,8 | 1561,6 | 677,2 | 656,0 |
| 13 | 12 | 40 | 100 | 804,3 | 15,7 | 4995,6 | 635,0 | 675,0 | 1580,0 | 30,8 | 1959,8 | 825,9 | 842,3 |
| 14 | 12 | 40 | 100 | 434,9 | 8,5 | 4995,6 | 364,8 | 343,0 | 1366,4 | 26,6 | 1654,6 | 707,1 | 649,9 |
| 15 | 12 | 36 | 100 | 836,1 | 16,3 | 5633,5 | 666,7 | 588,2 | 1602,3 | 31,2 | 1846,3 | 811,4 | 734,3 |
| 16 | 12 | 36 | 100 | 1042,2 | 20,4 | 5633,5 | 807,3 | 691,3 | 1571,2 | 30,6 | 1471,2 | 722,5 | 657,8 |
| 17 | 12 | 40 | 80 | 342,3 | 6,7 | 4995,6 | 291,7 | 283,1 | 1314,3 | 25,6 | 1732,2 | 704,6 | 653,3 |
| 18 | 12 | 40 | 80 | 361,1 | 7,1 | 4995,6 | 306,8 | 295,6 | 1325,0 | 25,8 | 1488,3 | 663,6 | 602,5 |

8.8 Image Index

| | |
|--|----|
| Figure 1: Desorption (charging) process of a closed sorption storage system [3] | 2 |
| Figure 2: Adsorption (discharging) process of a closed sorption heat storage system [3] | 3 |
| Figure 3: Scheme of evaporator and condenser [3]..... | 3 |
| Figure 4: Evaporation heat flux of water at 1 bar pressure [4], edited by Author | 6 |
| Figure 5: Bubble growth with liquid and vapor jets following the bubble departure ($P_v = 1.2 \text{ kPa}$, $T_l = 10 \text{ }^\circ\text{C}$, $h_l = 200 \text{ mm}$, $q = 22.6 \text{ W/cm}^2$). [5], edited by Author | 7 |
| Figure 6: Example of a micro area with a seed inside | 7 |
| Figure 7: Capillary-assisted evaporation principle [8], edited by Author | 8 |
| Figure 8: The schematic of capillary-assisted evaporation along a circumferential rectangular micro-groove and the extended meniscus: (a) l -directional cross-section, and (b) the extended meniscus. [8], simplified by Author | 9 |
| Figure 9: Wetting of a surface about the water surface [9] | 10 |
| Figure 10: Falling film tube bundle..... | 10 |
| Figure 11: Falling-film flow modes: (a) droplet mode, (b) droplet-jet mode, (c) inline jet mode, (d) staggered jet mode, (e) jet-sheet mode, and (f) sheet mode [10]..... | 12 |
| Figure 12: Experimental setup and the enhanced tubes. (a) fins on Turbo-CAB tubes, (b) Turbo-CAB-19 fpi, and (c) Korodense. [13]..... | 13 |
| Figure 13: Heat transfer coefficients of different tube types on the basis of [13] | 13 |
| Figure 14: Schematic representation of the evaporation test facility..... | 20 |
| Figure 15: Test Rig visualized via FreeCAD | 21 |
| Figure 16: Schematic layout of the vessels dimension with either a small or a big tube bundle..... | 22 |
| Figure 17: "Concentric: Holes, Half Tube" part of John G. Bustamante's (2014) Box-type distributor designs..... | 24 |
| Figure 18: Connections and parts of the main chamber | 25 |
| Figure 19: Layout of the Reservoir | 26 |
| Figure 20: Dimensions of the Reservoir | 30 |
| Figure 21: Design of the plate heat exchanger | 31 |
| Figure 22: Hot and cold water supply line..... | 32 |
| Figure 23: Heat loss calculation: a) Cross section of a vessel/pipe, b) Simplified temperature profile through the wall | 33 |
| Figure 24: Schematic representation focused on "Measurement and Control"..... | 35 |
| Figure 25: Pressure sensor | 36 |
| Figure 26: Manuel valve on the left, pneumatic valve on the right | 36 |
| Figure 27: Head of the liquid level measurement | 37 |
| Figure 28: Mass measurement device..... | 37 |
| Figure 29: Simplified schema to estimate the head of the pump for the falling film ... | 38 |
| Figure 30: Pump for the falling film | 38 |
| Figure 31: Simplified schema to estimate the head of the pump for the tube flow..... | 39 |
| Figure 32: Volume flow measurement device..... | 40 |
| Figure 33: Heat Meter..... | 40 |
| Figure 34: Splitter | 40 |
| Figure 35: Determination of the modules inside the control cabin | 41 |
| Figure 36: Interface to operate the test rig..... | 42 |
| Figure 37: Evaporation test rig..... | 43 |
| Figure 38: Test rig for evaporation and condensing with simplified heating and cooling streams | 44 |
| Figure 39: Design for testing condensing | 44 |

| | |
|---|----|
| Figure 40: Function of the Volume of distilled water depending on the liquid level.... | 45 |
| Figure 41: Leakage of the test rig depending on the temperature | 46 |
| Figure 42: Control loop | 48 |
| Figure 43: Dependencies of the variables among each other..... | 50 |
| Figure 44: Automation protocol..... | 51 |
| Figure 45: Tube bundle and distributor test arrangement..... | 55 |
| Figure 46: Pressure progression for the first test..... | 57 |
| Figure 47: Ambient temperature of the first test..... | 57 |
| Figure 48: Temperature inside the main chamber during the first test..... | 58 |
| Figure 49: Liquid level curve of the first test | 58 |
| Figure 50: Temperature and volumetric flow of the heating side | 59 |
| Figure 51: Temperature and volumetric flow of the cooling side..... | 59 |
| Figure 52: Heat flux of the first test..... | 62 |
| Figure 53: Wetting of the tubes caused by the falling film | 64 |
| Figure 54: Performance of the evaporator based on the ambient pressure..... | 70 |
| Figure 55: Performance of the evaporator based on the irrigation density | 70 |
| Figure 56: Performance of the evaporator based on the tube flow | 71 |
| Figure 57: Theoretical and Experimental heat flux at 23 mbar | 73 |
| Figure 58: Theoretical and Experimental heat flux at 17 mbar | 73 |
| Figure 59: Theoretical and Experimental heat flux at 12 mbar | 73 |
| Figure 60: Theoretical and Experimental Nusselt Number at 23 mbar | 74 |
| Figure 61 Theoretical and Experimental outer heat transfer coefficient at 23 mbar:.. | 75 |
| Figure 62: Adjusted parameters design | 85 |
| Figure 63: Main chamber..... | 86 |
| Figure 64: Plate heat exchanger on the left and Reservoir II on the right side of this figure (Reservoir I is built identical)..... | 86 |
| Figure 65: Connection to the chamber and the water tank | 87 |
| Figure 66: Hot and cold water circuit, on the right side connected to the test rig, on the left side connected to the labor | 87 |
| Figure 67: Insulated test rig | 88 |
| Figure 68: Sketch of the distributor provided by Luvata™ | 89 |

8.9 List of Tables

| | |
|--|----|
| Table 1: Adjusted parameters: main chamber | 23 |
| Table 2: Inaccuracy without the reservoir connected to the measurement vessel..... | 28 |
| Table 3: Inaccuracy with the reservoir connected to the measurement vessel..... | 29 |
| Table 4: dimensions of the plate heat exchanger | 31 |
| Table 5: Heat loss calculation..... | 34 |
| Table 6: Boundary Conditions for the head of the pump for the falling film | 38 |
| Table 7: Boundary Conditions for the head of the pump for the tube flow | 39 |
| Table 8: Designation and Declaration of the modules of the control cabinet | 41 |
| Table 9: Leakage of the Test rig | 47 |
| Table 10: Pressure in the main chamber | 56 |
| Table 11: Conditions of the first test | 56 |
| Table 12: Evaluation of the evaporator and condenser | 60 |
| Table 13: Evaluation of the heating circuit for the main chamber | 61 |
| Table 14: Evaluation of the cooling circuit for the plate heat exchanger | 61 |
| Table 15: Results of the first test | 61 |
| Table 16: Varity of the test series | 63 |
| Table 17: Test conditions: $p_{MC} = 23$ mbar, $V_{Pri} = 40\%$ and $V_{MC,Sec} = 100\%$ | 65 |
| Table 18: Test conditions: $p_{MC} = 23$ mbar, $V_{Pri} = 36\%$ and $V_{MC,Sec} = 100\%$ | 66 |
| Table 19: Test conditions: $p_{MC} = 23$ mbar, $V_{Pri} = 40\%$ and $V_{MC,Sec} = 80\%$ | 66 |
| Table 20: Test conditions: $p_{MC} = 17$ mbar, $V_{Pri} = 40\%$ and $V_{MC,Sec} = 100\%$ | 67 |
| Table 21: Test conditions: $p_{MC} = 17$ mbar, $V_{Pri} = 36\%$ and $V_{MC,Sec} = 100\%$ | 67 |
| Table 22: Test conditions: $p_{MC} = 17$ mbar, $V_{Pri} = 40\%$ and $V_{MC,Sec} = 80\%$ | 68 |
| Table 23: Test conditions: $p_{MC} = 12$ mbar, $V_{Pri} = 40\%$ and $V_{MC,Sec} = 100\%$ | 68 |
| Table 24: Test conditions: $p_{MC} = 12$ mbar, $V_{Pri} = 36\%$ and $V_{MC,Sec} = 100\%$ | 69 |
| Table 25: Test conditions: $p_{MC} = 12$ mbar, $V_{Pri} = 40\%$ and $V_{MC,Sec} = 80\%$ | 69 |
| Table 26: Tube bundle specifications | 72 |
| Table 27: Comparison of the theoretical calculations to the experimental evaluated tests..... | 90 |

8.10 Bibliography

- [1] A. Hauer, "Thermal Energy Storage," ETSAP - IRENA, 2013.
- [2] N. Yu, L.W. Wang, "Sorption Thermal Storage for Solar Energy," Elsevier, Shanghai, 2013.
- [3] R. Köll, "Development of a Seasonal Solar Heat Sorption Storage System for Space Heating and Domestic Hot Water," FH Joanneum University of Applied Science, Kapfenberg, 2015.
- [4] P. von Böckh, T. Wetzels, Wärmeübertragung - Grundlagen und Praxi, Berlin Heidelberg: Springer-Verlag, 2014.
- [5] F. Giraud, R. Rullière, C. Toubanc, M. Clausse, J. Bonjour, "Experimental evidence of a new regime for boiling of water at subatmospheric pressure," Elsevier, Lyon, 2014.
- [6] F. Giraud, "Vaporization of water at subatmospheric pressure," Lyon, 2015.
- [7] M. A. Chan, C. R. Yap, K. C. Ng, "Pool boiling heat transfer of water on finned surfaces at near vacuum pressures," Department of Mechanical Engineering, Singapore, 2010.
- [8] Z. Z. Xia, G. Z. Yang, R. Z. Wang, "Experimental investigation of capillary-assisted evaporation on the outside surface of horizontal tubes," Elsevier, Shanghai, 2008.
- [9] F. Lanzareth, "Modellgestützte Entwicklung von Adsorptionswärmepumpen," Technische Hochschule Aachen, Aachen, 2013.
- [10] X. Hu, A. M. Jacobi, "The Intertube Falling Film: Part 1 - Flow Characteristics, Mode Transitions and Hysteresis," Journal of Heat Transfer, Urbana, 1995.
- [11] G. Ribatski, A. M. Jacobi, "Falling-film evaporation on horizontal tubes - a critical review," Elsevier, Lausanne, 2004.
- [12] Wolverine Tube, Inc., Engineering Data Book III, Lausanne: Wolverine Tube, Inc., 2006.
- [13] Wei Li, Xiao-Yu Wu, Zhong Luo, Ralph L. Webb, "Falling water film evaporation on newly-designed enhanced tube bundles," Elsevier, Shanghai, 2010.
- [14] VDI e V, VDI Wärmeatlas, Berlin Heidelberg: Springer-Verlag, 2013.
- [15] J. G. Bustamante, "Falling-Film evaporation over horizontal rectangular Tubes," Georgia Institute of Technology, Georgia, 2014.